High-Burnup Demonstration: Thermal Modeling of TN-32B Vacuum Drying and ISFSI Transients

Spent Fuel and Waste Disposition

Prepared for
US Department of Energy
Spent Fuel and Waste Science and Technology

Pacific Northwest National Laboratory
JA Fort
DJ Richmond
BJ Jensen
SR Suffield

September 20, 2019
SFWD-SFWST-M2SF-19PN010203027
PNNL-29058

SUMMARY

This report fulfills the deliverable for milestone M2SF-19PN010203027.

This report describes thermal modeling done for the High-Burnup Spent Fuel Data Project that is being performed by the U.S. Department of Energy's Spent Fuel and Waste Science and Technology research and development program. The purpose of this project is to investigate the performance of high-burnup spent nuclear fuel in dry storage. Part of this project is a demonstration test being performed with a storage module in the North Anna Nuclear Power Station's Independent Spent Fuel Storage Installation (ISFSI). The storage module selected for this demonstration is an Orano TN-32B High-Burnup cask which has been loaded with fuel assemblies from the North Anna spent fuel pool. The main goals of this test are to provide confirmatory data for model validation and potential improvement; support license renewals and new licenses for ISFSIs; and to support transportation licensing for high-burnup spent nuclear fuel (EPRI 2014). This report describes results of transient simulations to model the fuel cladding temperature increases following loading in the pool and transfer to the decontamination bay. The helium blowdown and vacuum drying processes are examined with several models. Simulations are also described for response of the TN-32B cask to changes in ambient temperature and wind in its present location at the North Anna ISFSI. The modeling and results described in this report are initial attempts at accurately predicting temperature transients during vacuum drying. Because of the general lack of data and experience with realistic modeling, significant assumptions needed to be made. Assumptions regarding helium-steam properties and gap modeling are two examples described in this report. Furthermore, this modeling is not intended to be a conservative safety analysis. In this study, temperature results above or below the measured value are considered equally acceptable. The goal of this work is to assess the initial modeling attempts and assumptions so that they may be refined in the future as more data and experience becomes available.

Simulations were performed with COBRA-SFS and STAR-CCM+ to try to reproduce the fuel assembly thermocouple measurements during the blowdowns and vacuum drying transient. The COBRA-SFS model was most accurate in this effort. It used the measured cask surface temperatures as a boundary condition. An example of the COBRA-SFS model results is shown in Figure S.1 for Assembly 14. This assembly is located near the center of the basket and consistently gives the highest temperatures of the seven instrumented assemblies. The COBRA-SFS model predictions for Assembly 14 are less accurate at 6.5 and 10 hours into the blowdown and vacuum drying transient but are within 10°C at all other times shown in Figure S.1. Two STAR-CCM+ models were used for this effort, the one from the Demo Round Robin which used a porous media representation for the fuel assemblies and the surrounding fluid and a detailed model developed for this study which represented the fuel assemblies explicitly. The detailed model did a better job of matching the axial temperature profiles than did the porous media representation. Both STAR-CCM+ models matched the change in peak cladding temperature (PCT) during vacuum drying better than the COBRA-SFS model, although predicted temperatures were lower than measured. Of the two models, the detailed model was closer to matching the measurements. This result is illustrated in Figure S.2. Both STAR-CCM+ models used the measured ambient temperature in the decontamination bay in boundary conditions that modeled the convection and thermal radiation heat transfer from the cask surface.

The STAR-CCM+ models did well in matching the cask surface temperature measurements. The porous model was compared to measurements made near the time the cask was drained. Surface temperatures near the top of the cask were most accurately represented, within 1°C, while the model overpredicted measurements at the lower elevations by up to 14°C. Comparisons for the porous model with another set of measurements at one week into the test were more consistent, still within 1°C near the top of the cask, but within 5°C for all other elevations. The detailed model used a more approximate treatment of the cask up to the point it was drained, but the comparisons with surface measurements were still within 5°C. The detailed model was also compared with measurements at 5.5 hours after vacuum drying and helium

backfill. The model overpredicted surface temperatures there by 7 to 9°C. Finally, the steady-state solution for the detailed model was compared with measurements after the cask reached thermal equilibrium and agreement was within 3°C at all locations.

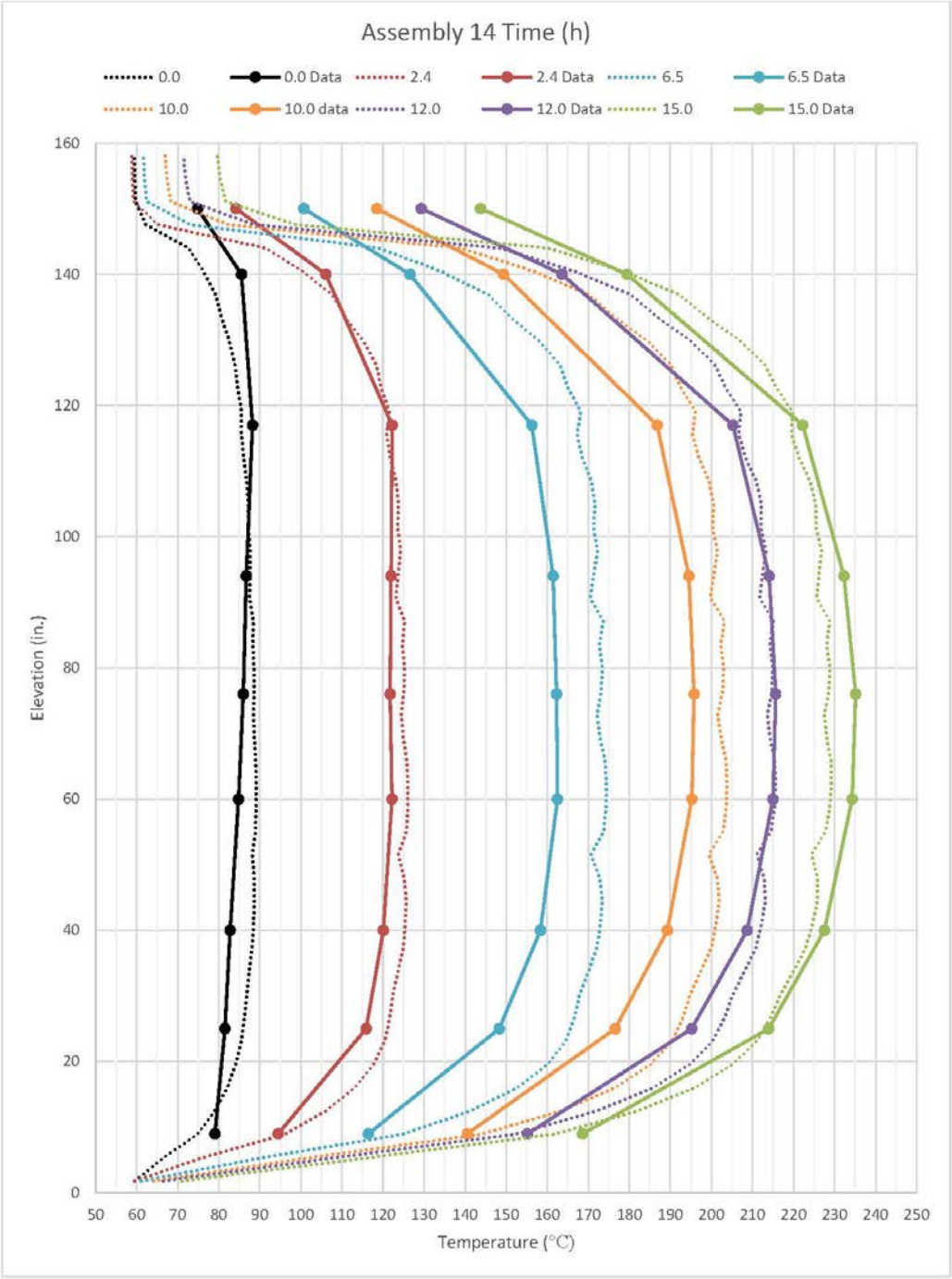

Figure S.1. COBRA-SFS simulation compared to thermocouple data through time, Assembly 14 (elevation shown relative to cask cavity, solid lines are measured data, dotted lines are model results)

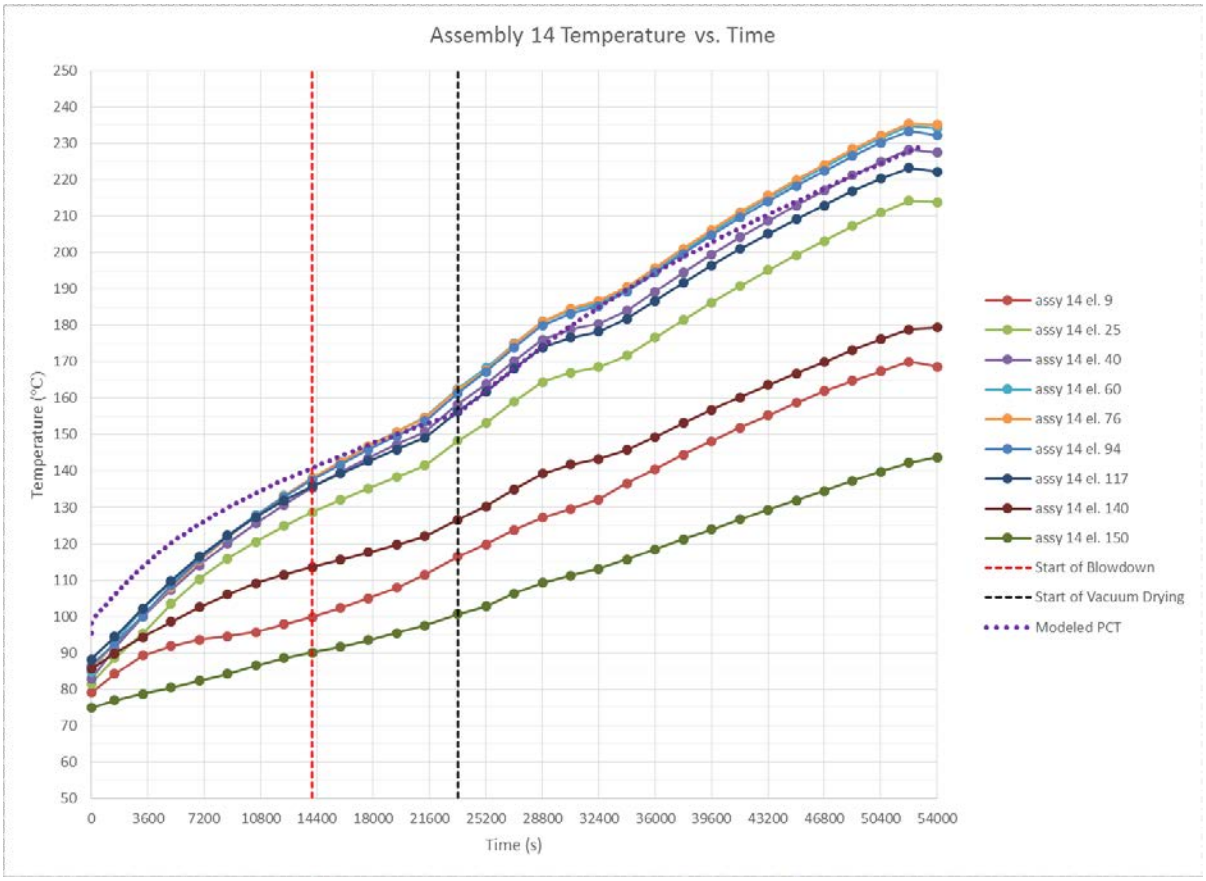

Figure S.2. STAR-CCM+ detailed model peak clad temperature during blowdowns and vacuum drying

COBRA-SFS simulations ended with completion of the vacuum drying transient. The STAR-CCM+ simulations were continued further. The STAR-CCM+ porous model results for fuel temperatures were compared with measurements mid-way through the two-week test. Results were within 15°C for Assembly 2, which is in the outer portion of the basket, and within 30°C for Assembly 14. The STAR-CCM+ detailed model was compared at four hours following the helium backfill. The temperature profile for Assembly 2 was within 2 to 3°C of the measured values. The predictions at this time for Assembly 14 were within 7°C, except for the uppermost measurement point. Steady-state model predictions were compared to measurements at mid test. They agreed very well at measurement points in the uppermost section of the assembly, but the model over predicted measured values at the rest of the measurement positions by up to 10°C. The STAR-CCM+ detailed model post-vacuum drying fuel temperature results for Assembly 14 are shown in Figure S.3.

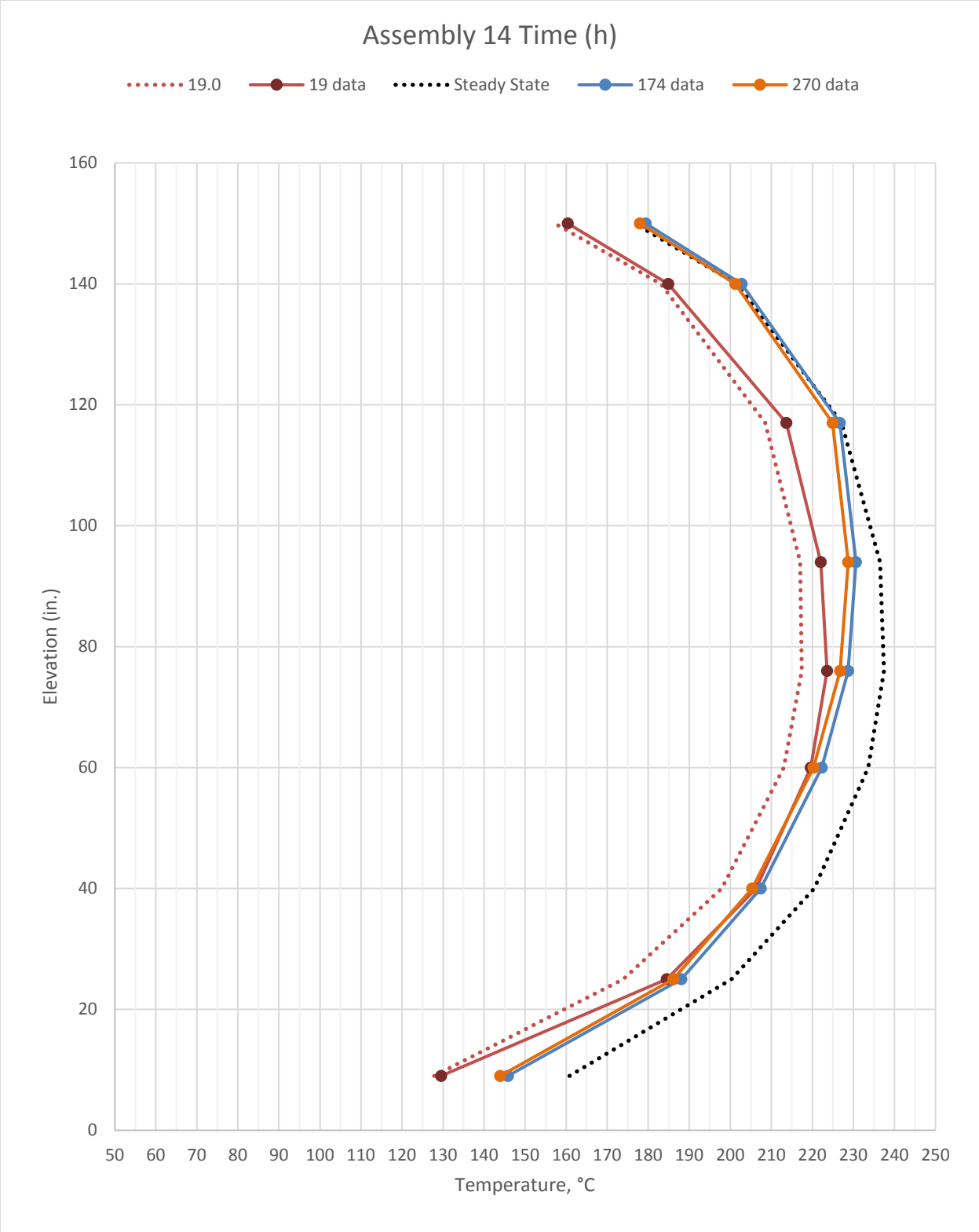

Figure S.3. Comparison of STAR-CCM+ detailed model results with measurements – after completion of drying – Assembly 14

The TN-32B cask is now located in the North Anna ISFSI and fuel temperatures are being continuously measured. Using these measurements for comparison, a second set of simulations was performed predicting fuel temperature changes in response to changing ambient conditions. Results are presented for two cases, representing two different time periods which have very different ambient conditions. Case 1 was for conditions between 1/5/2018 and 1/16/2018. Case 2 was between 3/1/2018 and 3/5/2018. This second case is illustrated in Figure S.4. COBRA-SFS and STAR-CCM+ models are used for both cases. Each model was the best estimate storage condition model used in planning the High Burnup Demonstration test. In comparing model results to measurements, wind was found to have a significant influence on changes in fuel temperatures. Changes to the models to incorporate wind effects in the boundary condition were successful. Figure S.5 shows the result for Case 2, which, as shown in Figure S.4, featured a strong wind event along with a modest ambient temperature change. Although the temperature magnitudes are overpredicted by as much as 15°C, the trends agree well. If wind is not accounted for in the model, the fuel temperatures change very little.

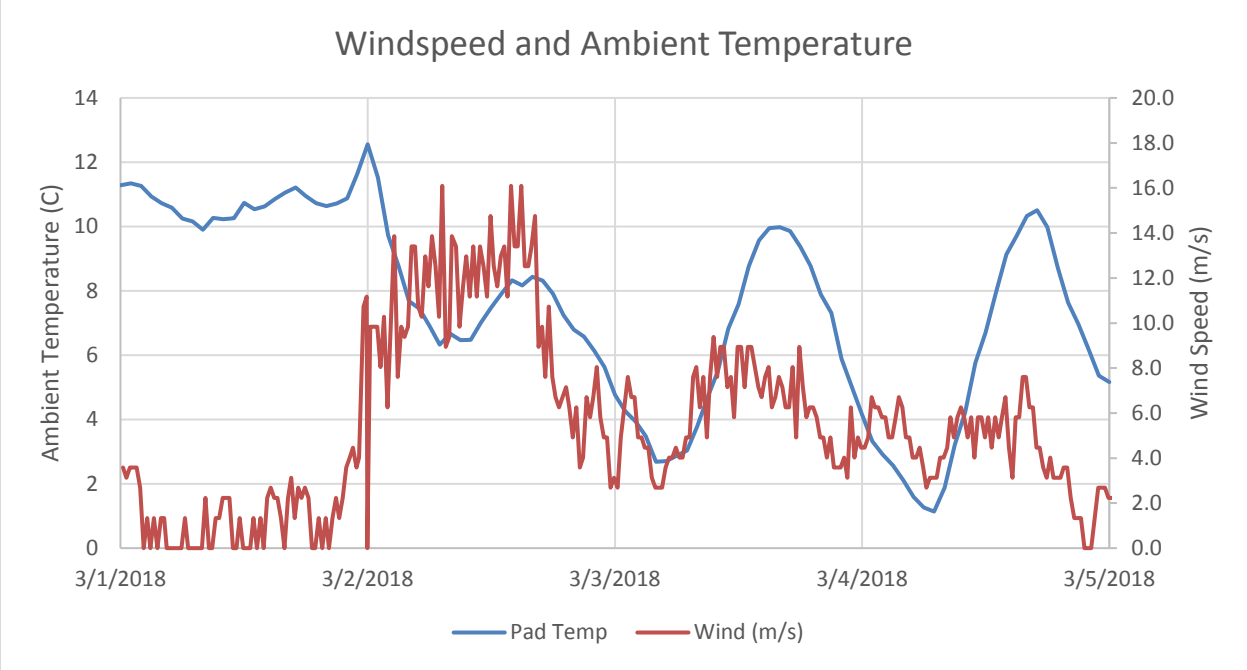

Figure S.4. Windspeed and Ambient temperature from March 1st to March 5th

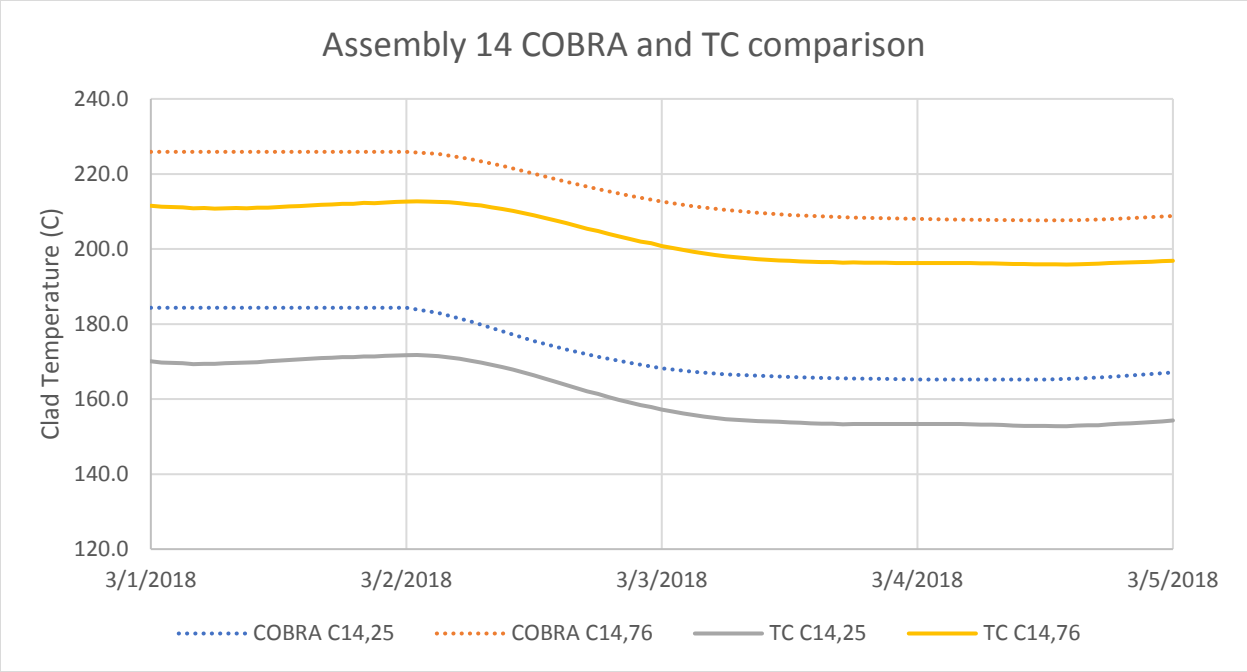

Figure S.5. COBRA-SFS model with wind and thermocouple results for Assembly 14

ACKNOWLEDGEMENTS

PNNL wishes to thank EPRI for coordinating the High-Burnup Demonstration at North Anna, and in particular Keith Waldrop. We appreciate the continued participation of Dominion Energy and the cask temperature data they are providing.

The authors would like to thank Colleen Winters for helping us achieve a clearly written and well-formatted report and Christopher Grant for a comprehensive review and many helpful suggestions.

This page is intentionally left blank.

CONTENTS

LIST OF FIGURES

LIST OF TABLES

This page is intentionally left blank.

ACRONYMS

CFD	computational fluid dynamics
DOE	U.S. Department of Energy
EPRI	Electric Power Research Institute
FAA	Federal Aviation Administration
FSAR	Final Safety Analysis Report
IR	infrared
ISFSI	independent spent fuel storage installation
NOAA	National Oceanic and Atmospheric Administration
NRC	Nuclear Regulatory Commission
ORNL	Oak Ridge National Laboratory
PCT	peak cladding temperature
PNNL	Pacific Northwest National Laboratory
PWR	pressurized water reactor
SNF	spent nuclear fuel
SNL	Sandia National Laboratories
TC	thermocouple
UFSAR	Updated Final Safety Analysis Report

This page is intentionally left blank.

HIGH-BURNUP DEMONSTRATION: THERMAL MODELING OF TN-32B VACUUM DRYING AND ISFSI TRANSIENTS

1. INTRODUCTION

The Spent Fuel and Waste Science and Technology research and development program of the U.S. Department of Energy (DOE) is conducting a high-burnup fuel demonstration at the North Anna Nuclear Power Station's Independent Spent Fuel Storage Installation (ISFSI). The storage system selected for this demonstration is a TN-32B cask. The main goals of this test are to provide confirmatory data for model validation and potential improvement, to support license renewals and new licenses for ISFSIs, and to support transportation licensing for high-burnup spent nuclear fuel (EPRI 2014). The focus of the High-Burnup Spent Fuel Data Project (aka Demonstration project) is the performance of the high-burnup fuel.

A description of thermal modeling support of this project from planning to execution is provided in Fort, et al. (2019). The current report describes follow-on work to model the loading and vacuum drying transient along with transient analysis of storage conditions. The modeling and results described in this report are initial attempts at accurately predicting temperature transients during vacuum drying. Because of the general lack of data and experience with realistic modeling, some significant assumptions needed to be made. Assumptions regarding helium-steam properties and gap modeling are two examples described in this report. Furthermore, this modeling is not intended to be a conservative safety analysis. In this study, temperature results above or below the measured value are considered equally acceptable. The goal of this work is to assess the initial modeling attempts and assumptions so that they may be refined in the future as more data and experience becomes available.

Section 2 lists the reference data that were used either as model inputs or for comparison with model predictions. Sections 3 through 5 describe COBRA-SFS modeling and results for the loading and vacuum drying transients. Sections 6 and 7 describe the same for STAR-CCM+ modeling. Section 8 describes models and results for the cask thermal transients on the ISFSI pad. Finally, Section 9 presents conclusions and recommendations from this work.

This page is intentionally left blank.

2. REFERENCE DATA

There are several datasets of interest to the present study. These include the measurements associated with the initial loading of the cask and monitoring in the decontamination bay while it reached equilibrium temperature (this has been referred to as the two-week “thermal soak”). This group of data includes the ambient temperatures in the room, the cask surface temperatures, and the fuel temperatures. There are also measurements associated with the long-term monitoring of the cask once placed in the ISFSI. Primarily this is the fuel temperature, but ambient conditions are also of interest. Outside ambient temperatures were provided by Dominion for the site, but wind speed data was also of interest and was obtained from a nearby monitoring station. These reference datasets are described briefly in this section.

It is important to distinguish between which of these datasets are used as model inputs and which are used for comparison with model outputs. The ambient information, whether in the decontamination bay or outside on the pad, is used as a model input in the form of boundary conditions. The objective of the models is to predict fuel temperature, so that dataset is used in comparisons with model results to assess accuracy of the models. The cask surface temperature measurements fall into both categories, depending on the model. For the COBRA-SFS model of the cask loading and vacuum drying process, the cask surface temperatures are used directly as the boundary condition, and thus are model inputs. For the STAR-CCM+ models of the cask during this time in the decontamination bay, the ambient temperature is used in the boundary condition and the cask surface temperature is one of the outputs of the model. In that case then, the cask surface measurements are also used to assess the accuracy of the model.

2.1 Thermocouple Lances

Thermocouple lances were installed following loading of the TN-32B demonstration cask. Individual thermocouple lances were installed in a guide tube in each of seven different assemblies. These positions are shown schematically on a map of the TN-32B basket in Figure 2.1. The axial thermocouple locations relative to the base of the cask are listed in Table 2.1. An example of measured temperatures from a thermocouple lance are shown for the hottest assembly (basket cell 14) in Figure 2.2. Time zero in this figure is when the cask draining is complete and recording of thermocouple lance date is initiated. Uncertainties for these fuel temperature measurements have been estimated between 1.7-2.11°C (Waldrop et al. 2019) depending on the magnitude of the value measured. Although this uncertainty is not negligible it is relatively small compared to the effect of unknowns in model input parameters. For this reason and for clarity, measurement uncertainty is not listed in this report.

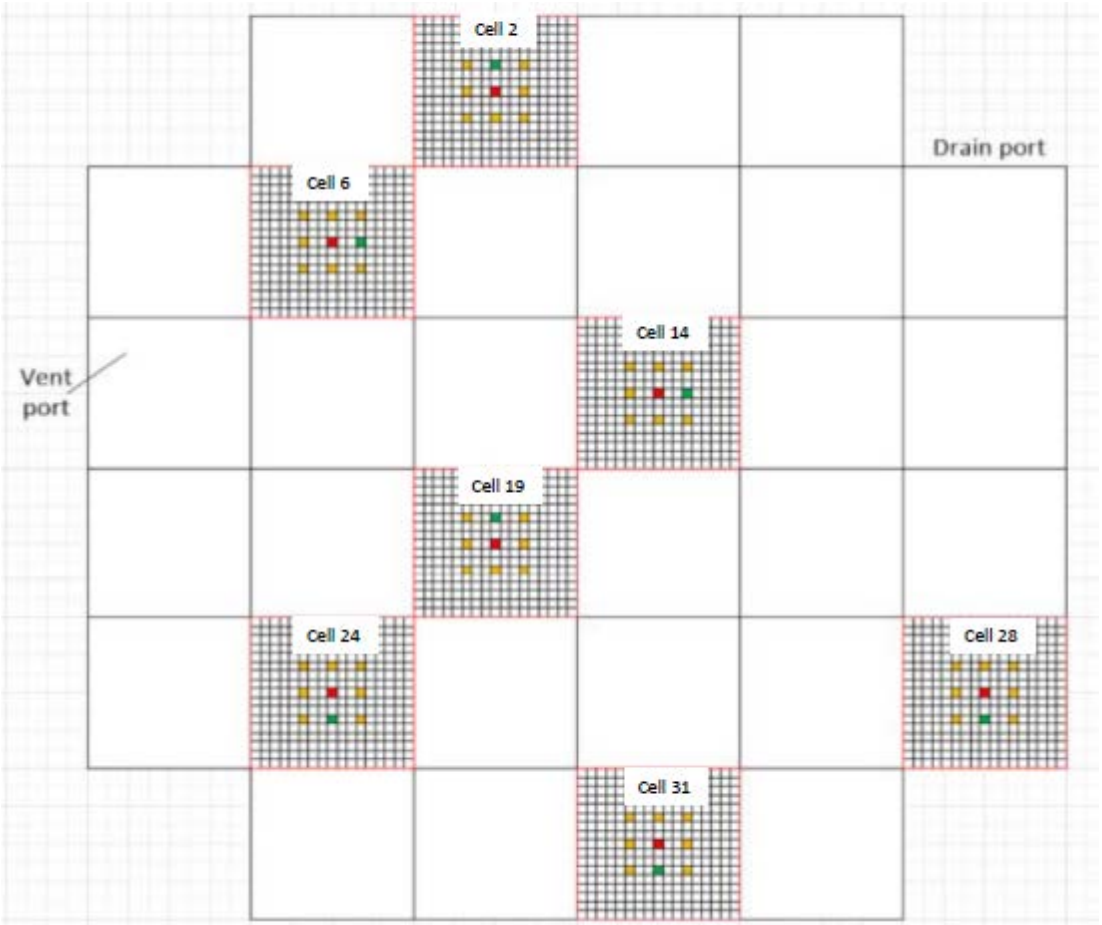

Figure 2.1. Thermocouple lance insertion locations (shown in green) in selected assemblies

Table 2.1. Thermocouple locations (EPRI, 2019)

Label	Distance from Bottom of Cavity (in.)
TC9	150
TC8	140
TC7	117
TC6	94
TC5	76
TC4	60
TC3	40
TC2	25
TC1	9

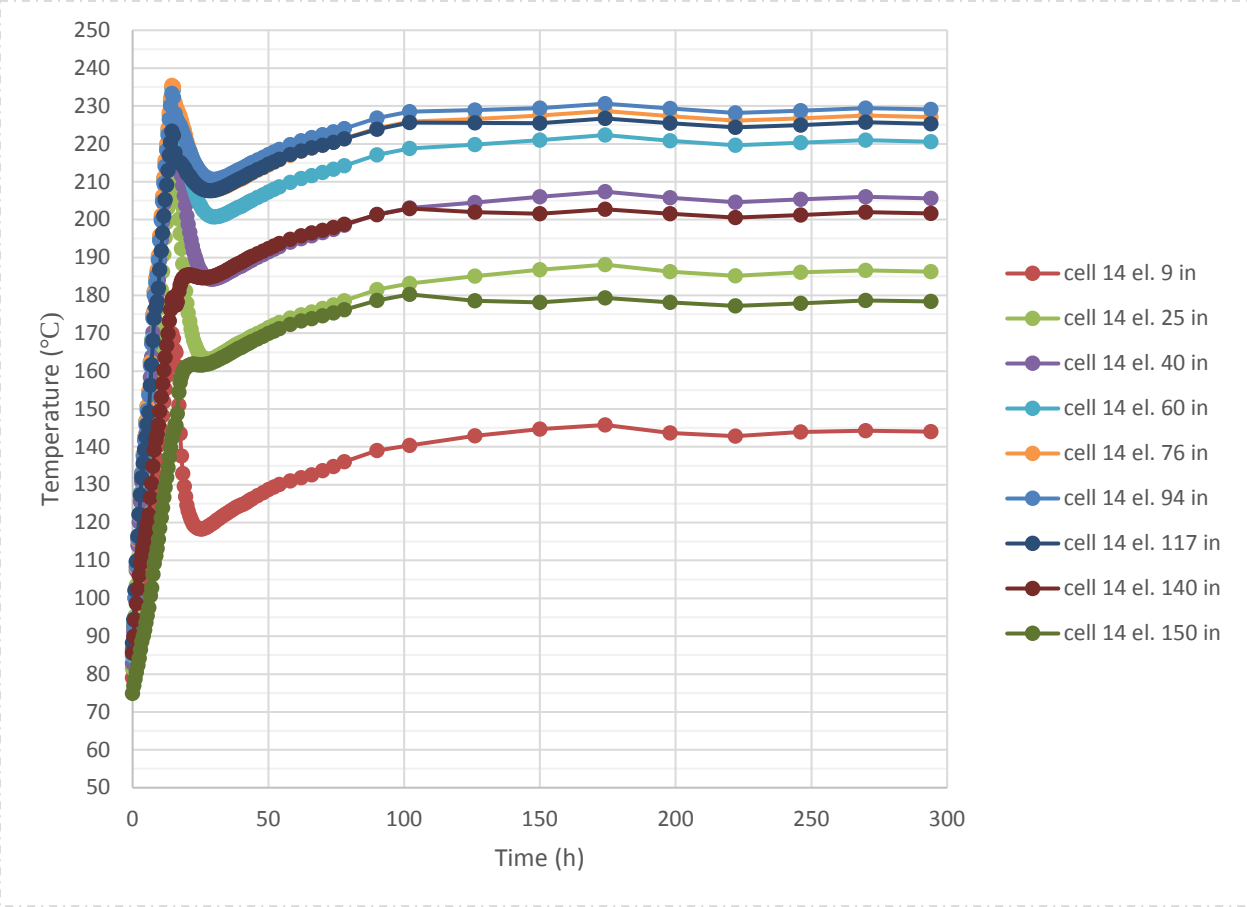

Figure 2.2. Temperatures versus time, cell 14

2.2 Cask Surface Temperatures

Cask surface temperatures were obtained with an infrared (IR) measurement at labeled positions on one quadrant of the cask. These measurement positions and the measured data can be found at the High-Burnup Test Data website (EPRI, 2019). These measurement locations are shown in red in Figure 2.3.

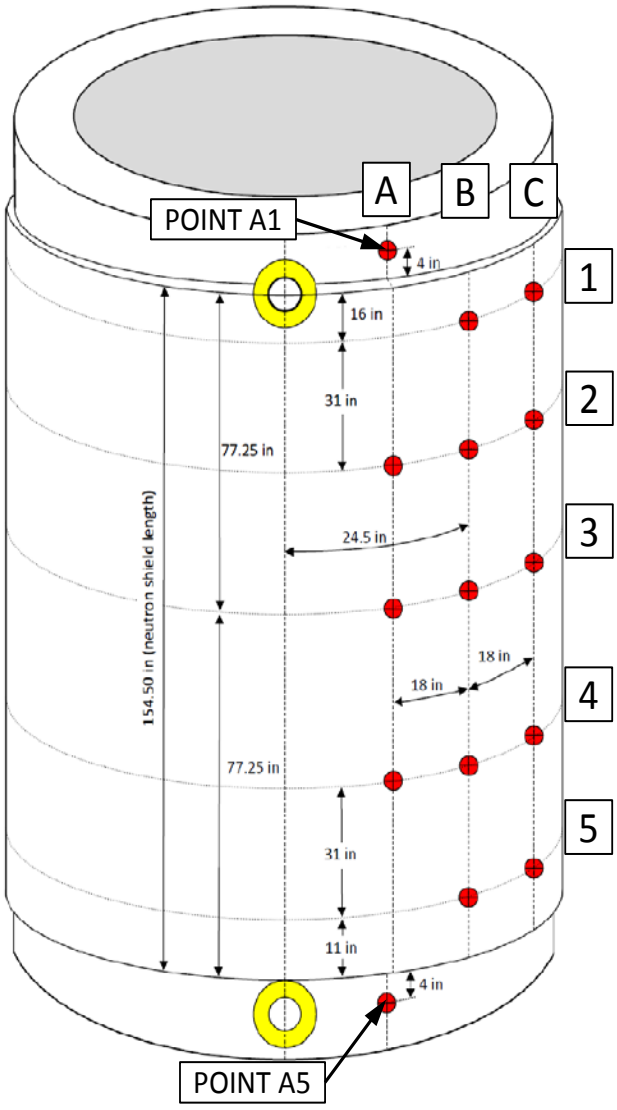

Figure 2.3. Cask surface measurement locations (EPRI, 2019)

2.3 Decontamination Bay Ambient Temperatures

During the two-week test with the cask in the decontamination bay, temperatures were measured in the space above the working platform and also in the more restricted space below the working platform. The majority of the cask was below the working platform. The geometry of this test space is described along with the thermocouple locations in Fort, et al. (2019). Measured ambient temperatures for the period of the two-week test are shown in Figure 2.3 where the "Ambient thermocouple" plot is for thermocouple

temperature measurements below the work platform near the axial midpoint of the cask. “Logger 1” and “Logger 2” are for thermocouples above the work platform near the data loggers used for the test.

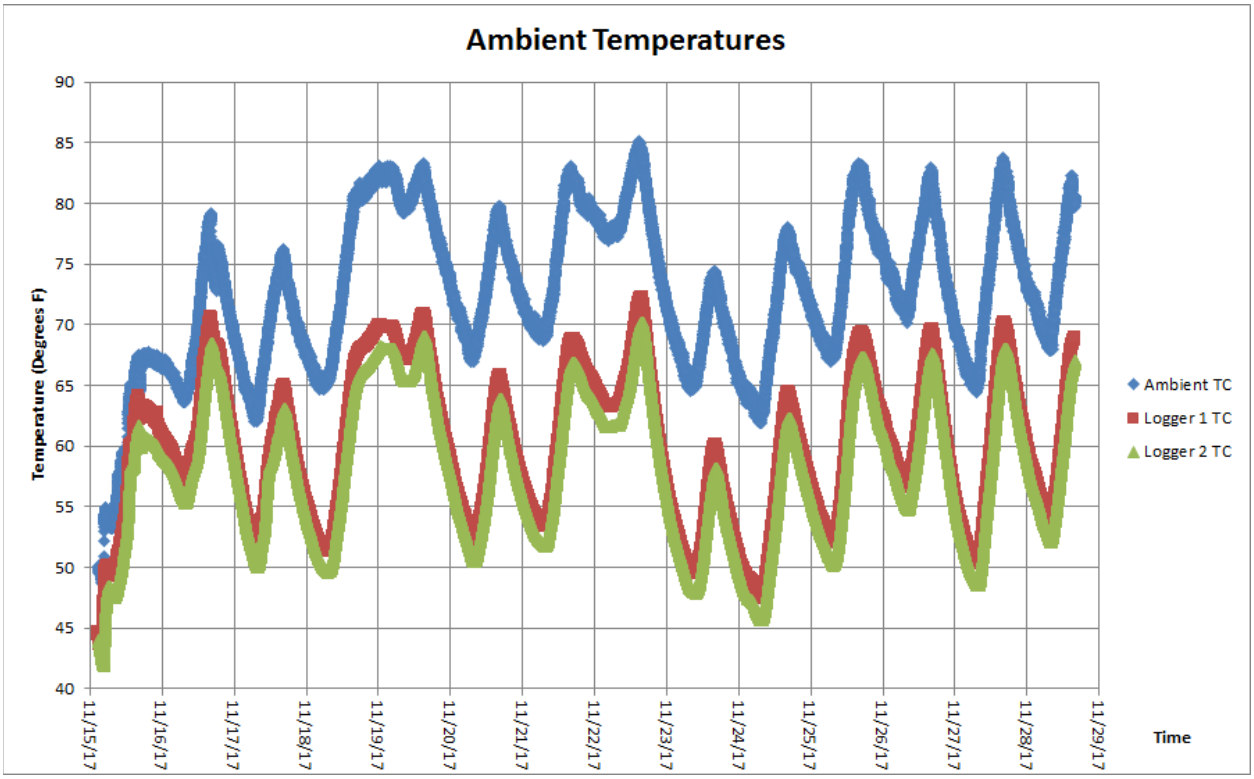

Figure 2.4. Ambient temperatures in decontamination bay

2.4 Outdoor Ambient Temperatures

North Anna Nuclear Power Station outdoor ambient temperature data was provided by Dominion Energy.

2.5 Nearby Airport Weather Data

Wind data on the ISFSI was not available so the wind speeds used for modeling were from Louisa County’s Freeman Field Airport, which is located about 17 kilometers (10.5 miles), 250° southwest from the North Anna Nuclear Power Station. This is close enough to provide a good approximation for the intents and purposes of this study. The data set used was from the National Oceanic and Atmospheric Administration (NOAA) Local Climatological Data set for this weather station, WBAN:03715. The automated weather station is positioned according to FAA guidelines (FAA 2017).

This page is intentionally left blank.

3. TN-32B LOADING AND DRYING PROCESS

The TN-32B Demo cask was cycled through a loading process that is typical to any cask of a similar design. The only differences would be any added time to insert thermocouples through the lid and into the assemblies and minor differences in the order of lid closure. These differences do not amount to a substantial change from a thermal modeling perspective. The entire cask loading process can be broken down into six parts for the purposes of this report.

3.1 Loading

The loading process previously described encompasses the time where the cask is in the spent fuel pool and assemblies are moved into the cask. The cask is in the pool for a significant amount of time and the pool water is actively cooled by plant systems. The cask structures and fuel are likely to be very near the pool temperature; however, no temperature measurements are available.

3.2 Movement and Drying Preparation

After loading, the lid is placed and the cask is moved to the decontamination bay. During this period, the cask continues to be filled with water for shielding and cooling. For the TN-32B, the water is not recirculated and is heated by the decay heat of the fuel. A time to boil limit is specified in the Final Safety Analysis Report (FSAR) and Technical Specifications where the cask must be drained or put back into the pool. The draining and drying equipment are hooked up after the cask move. In the case of the demonstration project cask there is some additional time spent with water in the cask because the thermocouple lances are installed at this point in the experiment.

3.3 Drain

The water inside the cask is drained while helium is pumped in as a cover gas. The helium provides an inert environment and assists in cooling.

3.4 Blowdown

The blowdown phase is designed to remove large amounts of residual water from the cask. The cask is successively pressurized, then the drain port is opened, and water blown out of the cask through a sight glass. This procedure may be conducted many times until the operator does not see any more liquid water exiting the cask.

3.5 Vacuum Drying

The vacuum drying process is commonly used to provide a dry environment for spent fuel storage. In general, the cask atmosphere is pumped down in successive stages to achieve near vacuum pressures. This low-pressure environment coupled with heating from the fuel promotes vaporization of any residual water in the cask. After a given time the vacuum pumps will be shut off and the cask will be sealed. If the internal pressure remains under three torr for 30 minutes, it is declared dry. Any pressure rise is assumed to be additional water vaporizing and more time with vacuum pumps would be necessary if the pressure rises above three torr within 30 minutes. In this experiment the vacuum drying time was relatively typical at approximately 8.5 hours.

3.6 Backfill

After drying, the cask is backfilled with helium to its technical specification pressure (2.2 atm [1672 torr] in this case). The helium provides an inert environment that is also conducive to heat transfer. For the transient analysis using COBRA-SFS this will be the end of the analysis sequence. For the transient analysis with STAR-CCM+ the simulation continues beyond the backfill.

3.7 Timeline for Process Steps in the High-Burnup Demonstration

The modeling process requires as inputs the durations of steps described in the previous sections. For the TN-32B loading at North Anna a timeline is provided in Table 3.1.

Table 3.1. Timing of events during high-burnup demonstration[a]

Activity	Date	Time
Cask out of pool	14 Nov 17	21:25
Cask set in decontamination bay		21:56
Begin draining cask	15 Nov 17	17:22
Finish draining cask		18:05
Begin blowdowns		22:00
Finish blowdowns	16 Nov 17	00:30
Begin vacuum drying		00:35
Complete dryness test		07:40
Initial helium backfill		09:00
Begin final helium backfill		09:35
Backfill complete		10:54
Move cask to truck bay	30 Nov 17	09:30
Begin transporting cask to ISFSI		10:33
Cask set on storage pad		11:24

[a] Waldrop, K. 2019, DRAFT Final Report. *High Burnup Dry Storage Research Project Cask Loading and Initial Results*. Electric Power Research Institute, Palo Alto, CA.

4. COBRA-SFS LOADING AND DRYING TRANSIENT MODEL

The modeling approach and tools used in this analysis are consistent with what was demonstrated in the steady-state data comparisons using the TN-32B Demo cask (Fort, et al. 2019) except where they were modified specifically for transient analysis. COBRA-SFS has significant advantages that make it well suited for transient analysis. Primarily, the model size and solution method allow for timely solutions to practical transients. The small size of the model and finite difference solution method allows for fast solutions on relatively low-powered hardware. For transient analysis the solution is fully implicit in time. Practically this allows for very large time steps. The primary limitation on time step size is the interval that model parameters might need to be changed and the interval that output data is desired by the user. Because run times were practical on the available hardware, there was no need for extensive time step optimization in this work. All COBRA-SFS solutions used 100-second time steps to simulate about 15 hours of experimental time. When including the calculation of an initial condition, the COBRA-SFS simulation took approximately 3.5 hours to complete on a desktop computer.

One limitation of COBRA-SFS in transient modeling is the inability to change fluid types during a calculation. Because the code uses an energy balance calculated from enthalpy, it is very difficult to simulate the change from water to helium. It may be difficult for the solver to model the radical changes in fluid flow that would result from altering the density and reach convergence at a given time step. To avoid this problem, the COBRA-SFS analysis starts when the drain process ends and finishes when vacuum drying ends. There are still limitations in being able to model an unknown and variable quantity of water vapor in helium.

4.1 Boundary Conditions

The boundary conditions during the transient are very important for accurate simulation. Clearly this is true with any analysis, but with a steady-state analysis, any misestimation of the boundary temperature will have a corresponding effect on the temperatures of interest. With a transient solution, any error in estimating the boundary temperature will have compounding effects on the temperature solution as it is propagated through time. In this case, a small under estimation of the temperature throughout the transient could have a very large impact on the fuel temperature estimates at the end of the analysis.

Early attempts at using a natural convection correlation were not successful in predicting the temperature through time. This is likely due to the same issues that were present in the steady-state TN-32B demonstration cask analysis (Fort, et al. 2019). In that case, the work platform and small size of the decontamination bay is thought to have impeded the flow around the cask. Additionally, the rollup doors that separate the decontamination bay from the outside as well as the reactor auxiliary building were opened multiple times. In steady-state analysis, these variations would be smoothed out by using an average boundary temperature. There is no data on the environmental conditions during the test that can readily be applied to the simulation. Because of this lack of data, surface temperature data from before and after vacuum drying was interpolated to provide an estimation of surface temperature through time across the 160 in. fuel region of the model. The surface temperature rises by around 10°C throughout the transient. This relatively small change allows for the surface temperature to be updated roughly once per hour over the course of the simulation. The boundary temperature profile at select times is shown in Figure 4.1 where “Y” is the basket region length.

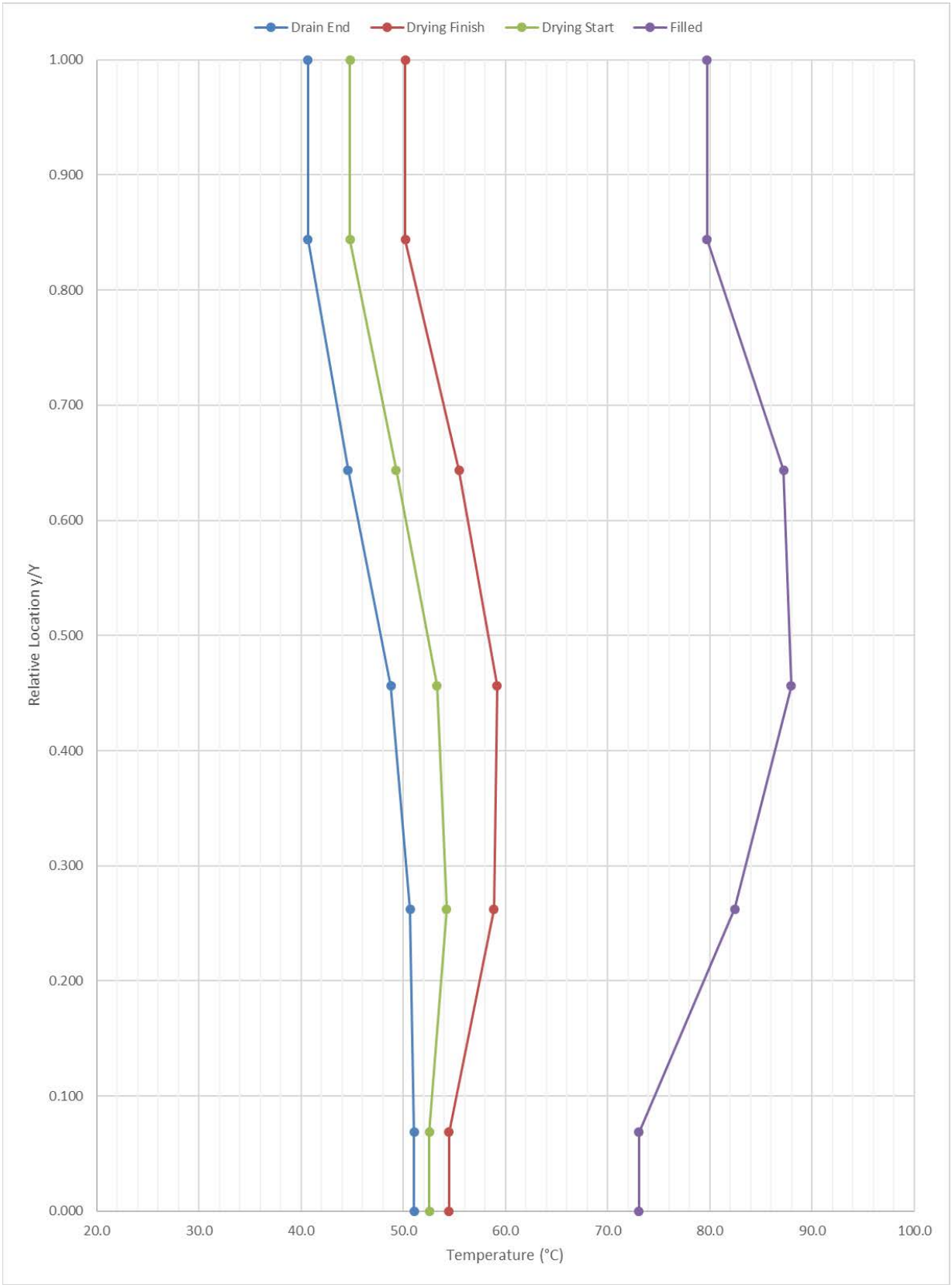

Figure 4.1. Selected boundary conditions for COBRA-SFS

4.2 Initial Conditions

Like the boundary conditions, initial conditions can have a profound impact on the temperature solution. In this case, the fuel temperature increases non-linearly meaning small differences in initial condition can grow large toward the end of the transient. To define the initial condition in this model, the power level and boundary conditions were adjusted until the temperatures achieved reasonable agreement with the data in a steady-state case. After time zero in the transient simulation, the power and boundary conditions were reset to match the external conditions of the cask. Because data were available for the surface condition and thermocouples at various locations, this is a reasonable method for initializing the temperatures over the entire cask. There are potential weaknesses in that there were no available data on other cask component temperatures.

The accuracy of this method relies on the assumption of a consistent radial temperature gradient. In general steady-state cask analysis, the validity of this is apparent on inspection. The only heat generation source is in the center of the cask and the interior is a closed fluid system. However, when the cask is submerged in the spent fuel pool the interior fluid system is no longer closed. This could potentially result in either an isothermal or other unusual temperature gradient in the cask wall between the outer and inner surfaces. This type of temperature gradient would begin to normalize as the cask is drained and staged for vacuum drying and there is no indication of excessive gradients in general.

4.3 Fluid Properties

The vacuum drying process is a common terminology and standard industry practice. However, “vacuum” may be a misnomer. In spent fuel casks, the gas pressure during the process rarely approaches a vacuum state and is better characterized as a very low pressure. The dryness test consists of holding the cask below three torr for 30 minutes. For the High-Burnup Demo cask, the dryness pressure at the end of the 30 minutes was measured at 0.97 torr (EPRI 2019).

In terms of modeling, normal fluid conduction is still present in the system. However, the low density (pressure) means that there will be little to no heat transfer through convection. In COBRA-SFS, it is very difficult to model very low-pressure gasses and achieve convergence in the fluid solution. To simulate the lack of convection, the best method is to turn off the gravity term and change the fluid heat transfer correlations to force a Nusselt number of unity which equates to a pure conduction system.

In addition to the helium in the system, there is going to be residual water driven to the vapor phase by the vacuum drying process. To account for this additional species, the thermal conductivity of steam was used in the fluid properties of the COBRA-SFS model. This is a simplification because the fluid system would be a helium-water mixture that evolves through time. In the model the fluid properties are consistent through time. The steam property choice is likely conservative although it is not a dominant effect on clad temperature. The relatively small influence of fluid properties is expected because there is no convection modeled and the cask is designed to remove heat through solid conduction. There are no concerns with water vapor acting as a participating radiation media at this temperature due to the partial pressures and length scales present in the cask (Incropera and DeWitt, 2002.).

4.4 Basket-Rail Gap

When steady-state temperature predictions were compared with data (Fort, et al. 2019), it was determined that the gaps between the basket and rail of the cask were a critical parameter for accurate solutions. Due to thermal expansion the gap likely closes to a dimension that is much smaller than the dimension specified in the Updated Final Safety Analysis Report (UFSAR) (2012). In the case of the loading and transient, there will undoubtedly be a temperature change and corresponding dimension change through time.

For a completely accurate model of this behavior, it would be necessary to have an accurate measurement of the starting gap dimensions so that a component temperature distribution through time could be used to iteratively calculate thermal expansion at each time step. Even if the necessary data were available, this approach would be extremely time intensive and impractical with the current codes and methods.

In this analysis, the gap size is assumed to be directly related to the thermal expansion of aluminum and linear through time. If the final size is assumed to be 0.10” as postulated in Fort, et al. (2019), then an assumed nominal temperature rise of 200°F is used to calculate the initial gap size and closure rate over the 15 hour simulation. In this case, the gap is assumed to close from 0.18” to 0.1” at a rate of approximately 0.005 in./hr. The starting gap size was chosen by back-calculating from the assumed 0.1” final gap size and updated once per hour throughout the solution. There are limitations to this approach because it is unlikely that the gap closure behavior is completely linear through time. There is also a practical limit to the rate at which the gap size can be updated because of input limitations for COBRA-SFS.

4.5 Time Step Selection

There is no inherent limitation on time step size in COBRA-SFS. For this analysis, 100-second time steps were considered appropriate for data analysis and provided reasonable run times for the entire solution. Changing solution parameters requires stopping the solution, writing a restart file, and then restarting with the new inputs. Generating the new input files can be a time-consuming process and file management would also become challenging. For this reason, roughly 1-hour intervals are used to update boundary conditions and gap size. This is appropriate for the relatively slow change in those parameters and the overall thermal response of the cask and fuel.

5. COBRA-SFS TRANSIENT RESULTS

This section describes the COBRA-SFS transient results. These consist of comparisons of overall temperature and thermocouple plots.

5.1 Overall Temperature Comparisons

Figure 5.1 shows the calculated peak cladding temperature (PCT) through time for each thermocouple from the Assembly 14 lance. This figure gives a general understanding of the temperature behavior in the cask vs. in the model. The PCT is always expected to be ~2-5°C greater than the thermocouple measurements, because the thermocouples are measuring guide tube temperatures. Time zero is at the end of drain down. Time 54000 s (15 h) is during the first helium backfill. The starting temperature of each thermocouple is not strongly influenced by its elevation and each point along the lance is within a ~15°C temperature range. The typical steady-state temperature profile of the TN-32B (Fort, et al. 2019) is influenced by the power profile of the fuel, heat transfer through the ends of the cask, and convection. In the transient data, the pool water in the cask is a dominant factor that drives component temperatures toward the bulk water temperature. After the cask is drained, the measured temperatures separate and move toward a typical axial profile (Figure 5.2 -5.8). Qualitative inspection shows the heat-up to be linear overall with minor inflections at different points in time. The smooth inflection of the PCT plot is due to the simplified and idealized nature of the model. The COBRA-SFS method described in Section 4 neglects the effect of blowdown and the different variations of the vacuum drying procedure. There is no data available that can definitively explain why each variation is occurring. Possibilities include component thermal expansion, the introduction of cold helium during blowdowns, and the dynamic nature of water vaporization.

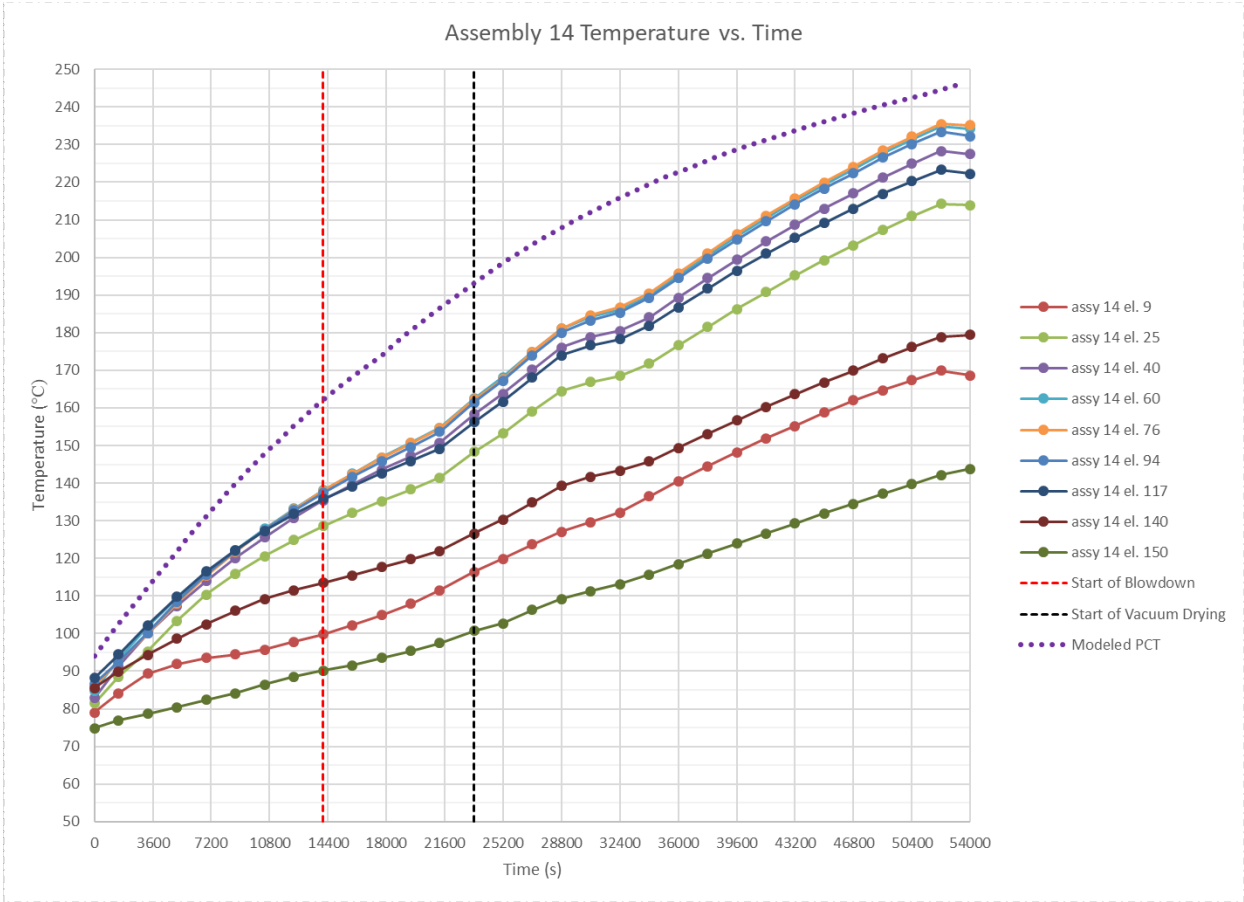

Figure 5.1. Assembly 14 lance thermocouples plotted with calculated PCT through time (elevations in inches)

5.2 Thermocouple Plot Comparisons with Data

Figures 5.2 - 5.8 show how the COBRA-SFS simulation compares to the thermocouple data through time. Overall, the simulation can match the data within 15°C along the axial center of the cask and within 20°C at the upper and lower extents of the thermocouple lance.

This simulation uses power profiles that are calculated highly accurately by Oak Ridge National Laboratory (ORNL) using ORIGEN (Gauld, et al. 2009). The model temperature predictions show this very consistently in the small dips near the locations where the fuel hardware affects burnup in reactor. This effect is expected because the model has no convective heat transfer and is axially discretized, both overall and in the power distribution specifically. Real temperatures are not expected to have the small axial temperature variations seen in the model. However, since there are only nine thermocouples in each lance, this cannot be determined definitively from the data.

For most of the transient simulation, the simulated temperatures are higher than the measured temperatures. However, this margin is not consistent in time and the simulation begins to “accelerate” away from the data and then fall back toward the end of the simulation. While there are many possible explanations for this behavior, it is difficult to conclusively determine the cause based off of the available data. There are three explanations that are readily apparent. The basket-rail gap discussed in Section 4.4 may not be matching ideally with the model. The steam properties being used for the fluid may not be matching the fluid conditions in the cask. Finally, any inaccuracy in the initial/boundary conditions may

be affecting comparisons even in the late stages of the simulation. Any of these could lead to the behavior seen, as could any combination of all three.

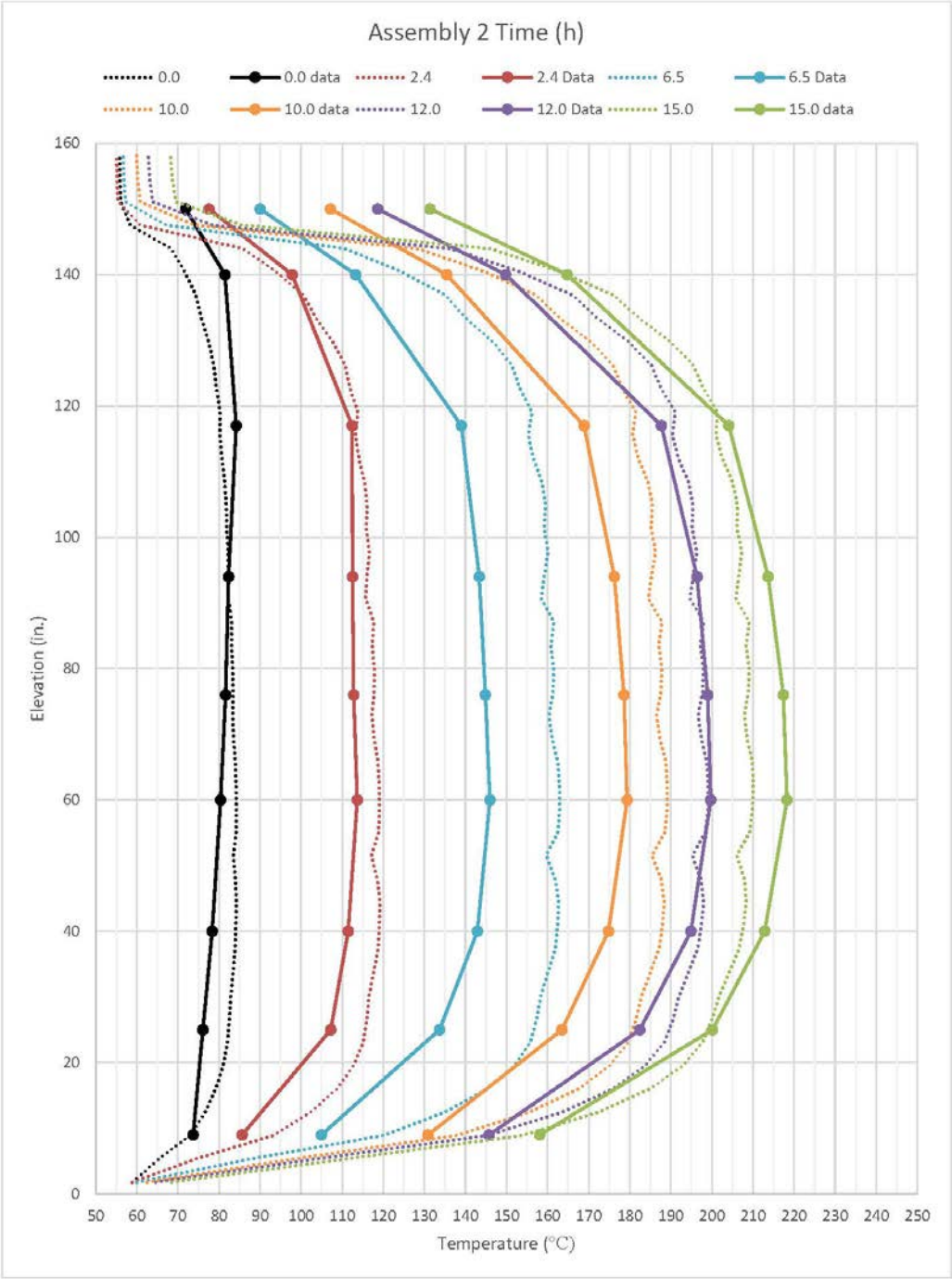

Figure 5.2. COBRA-SFS simulation compared to thermocouple data through time, Assembly 2

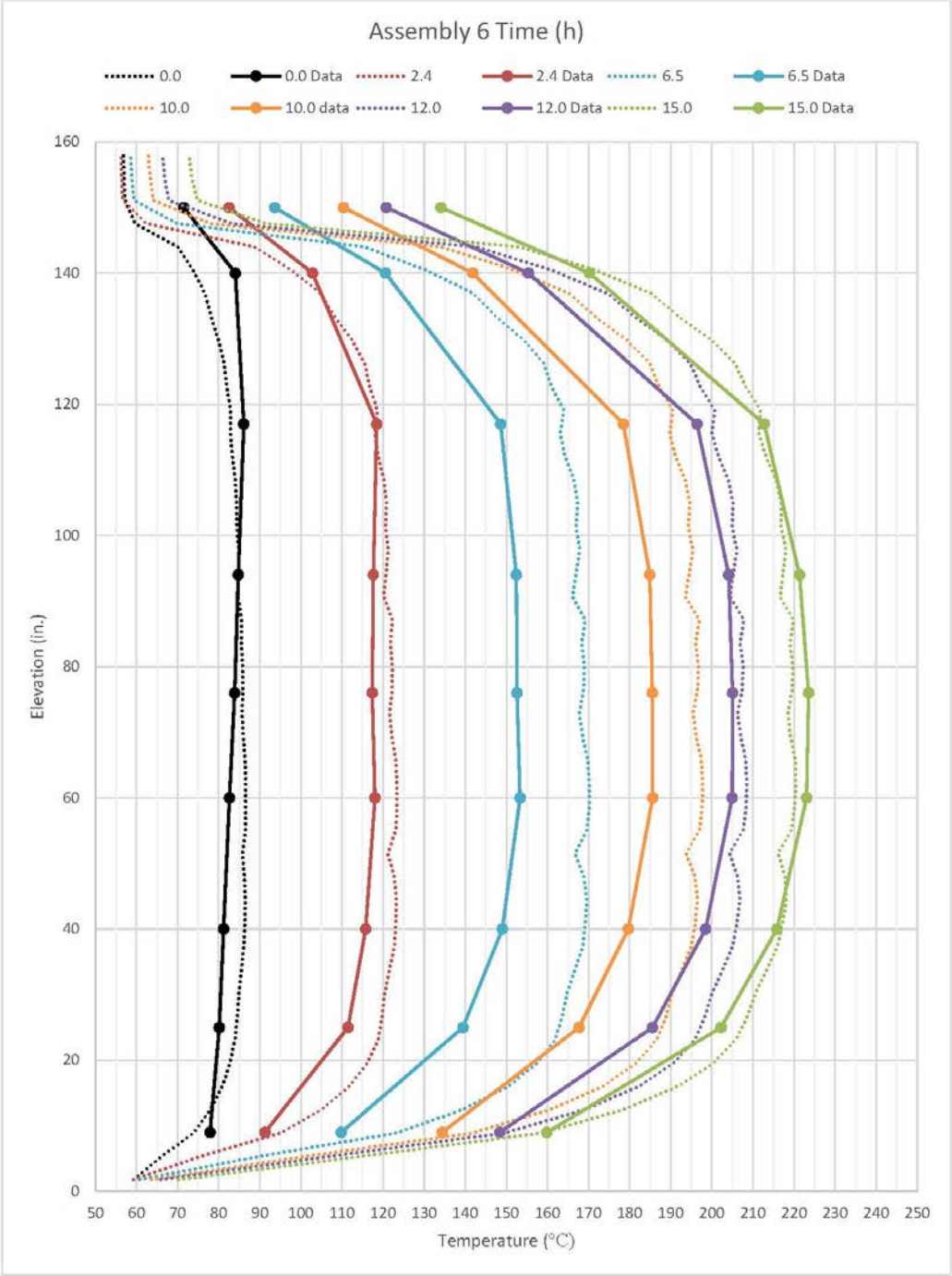

Figure 5.3. COBRA-SFS simulation compared to thermocouple data through time, Assembly 6

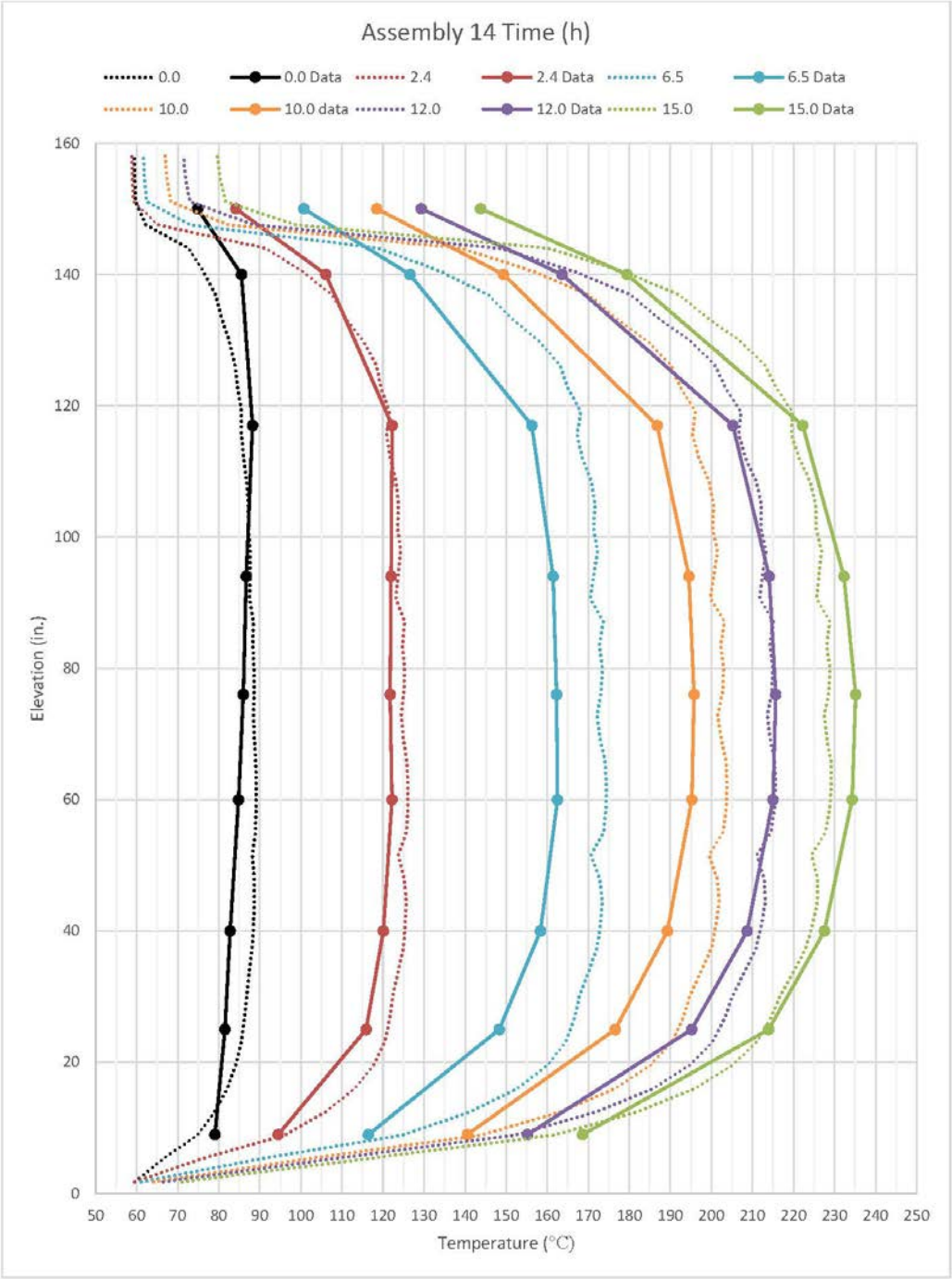

Figure 5.4. COBRA-SFS simulation compared to thermocouple data through time, Assembly 14

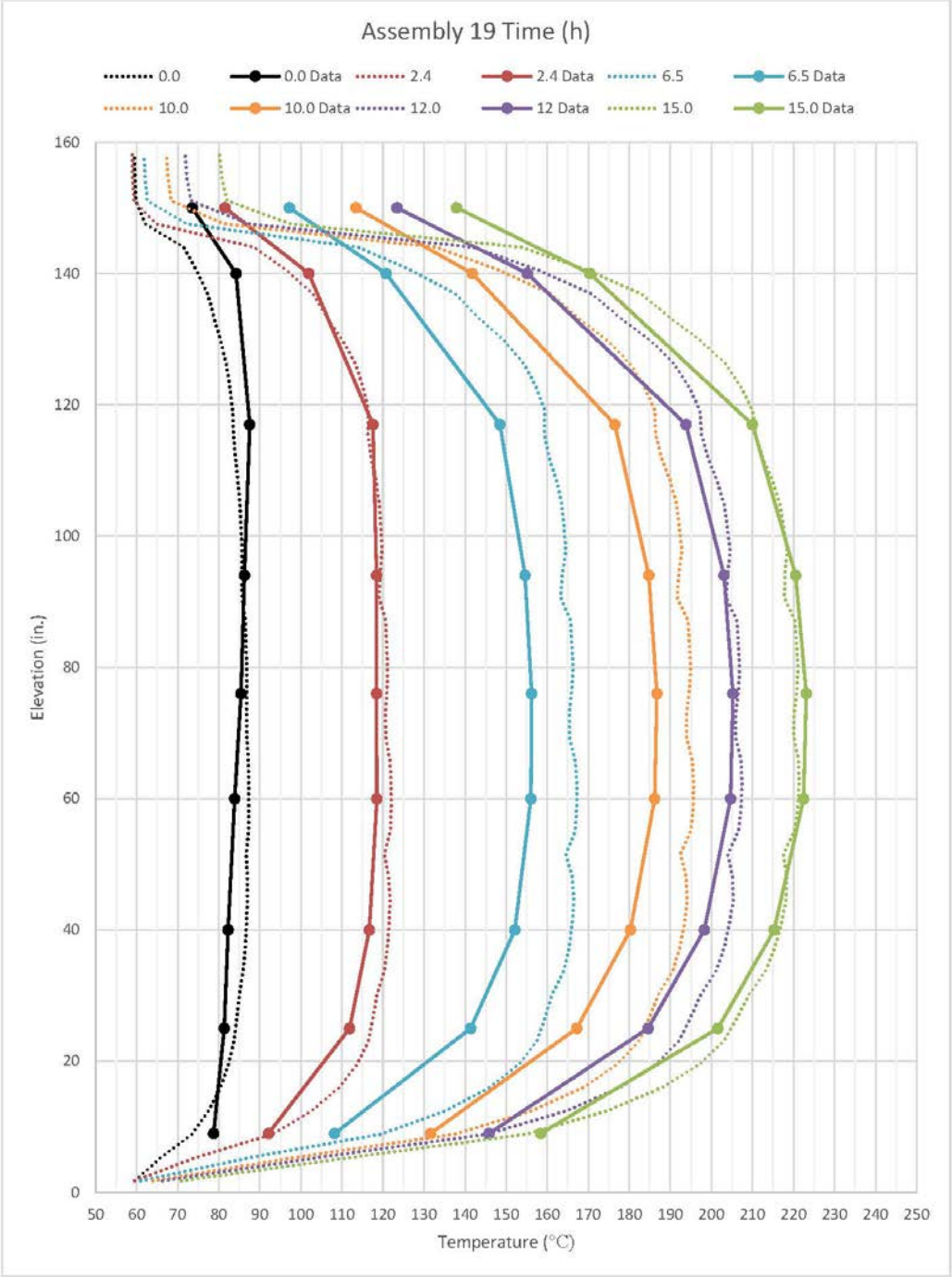

Figure 5.5. COBRA-SFS simulation compared to thermocouple data through time, Assembly 19

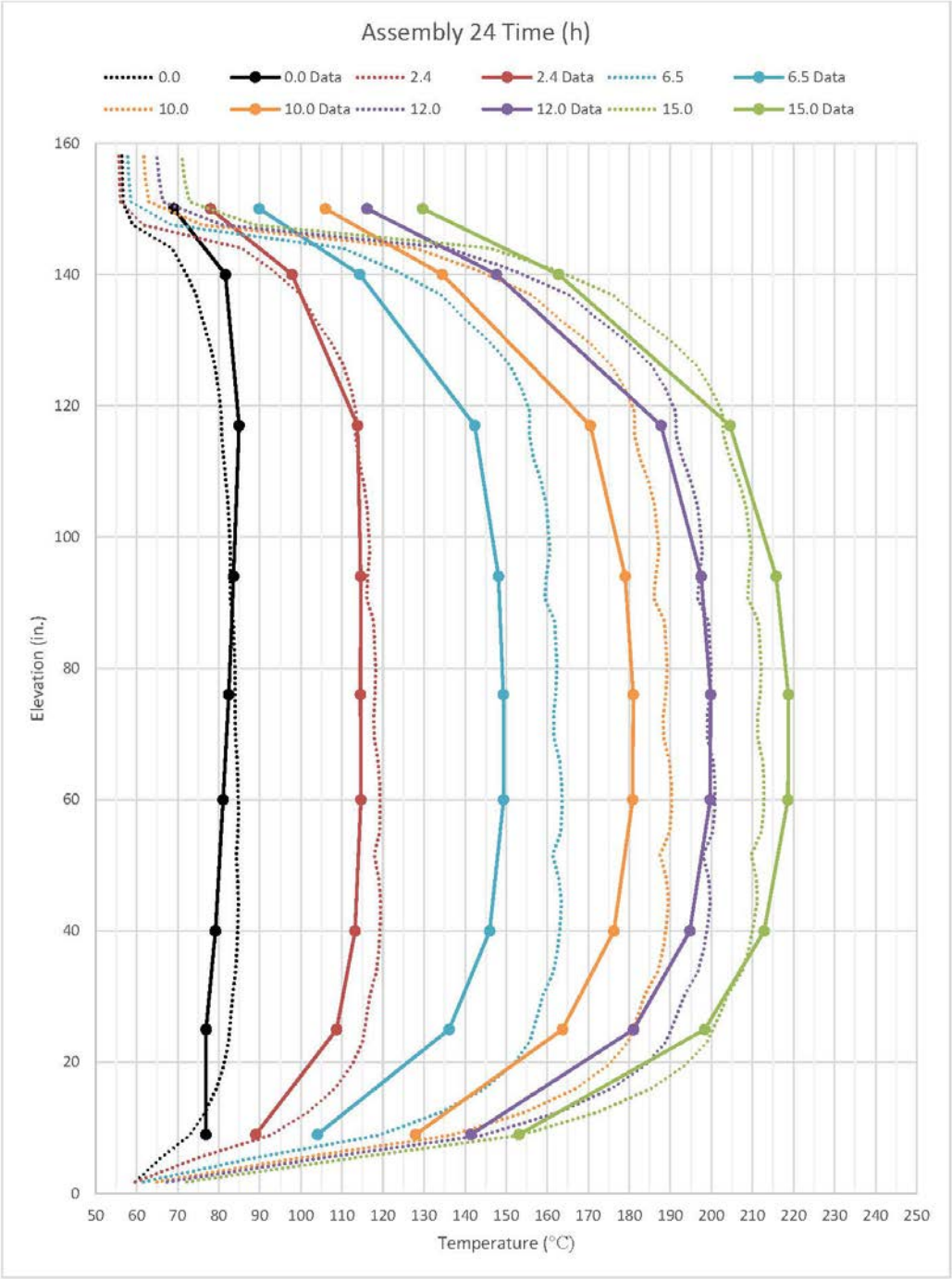

Figure 5.6. COBRA-SFS simulation compared to thermocouple data through time, Assembly 24

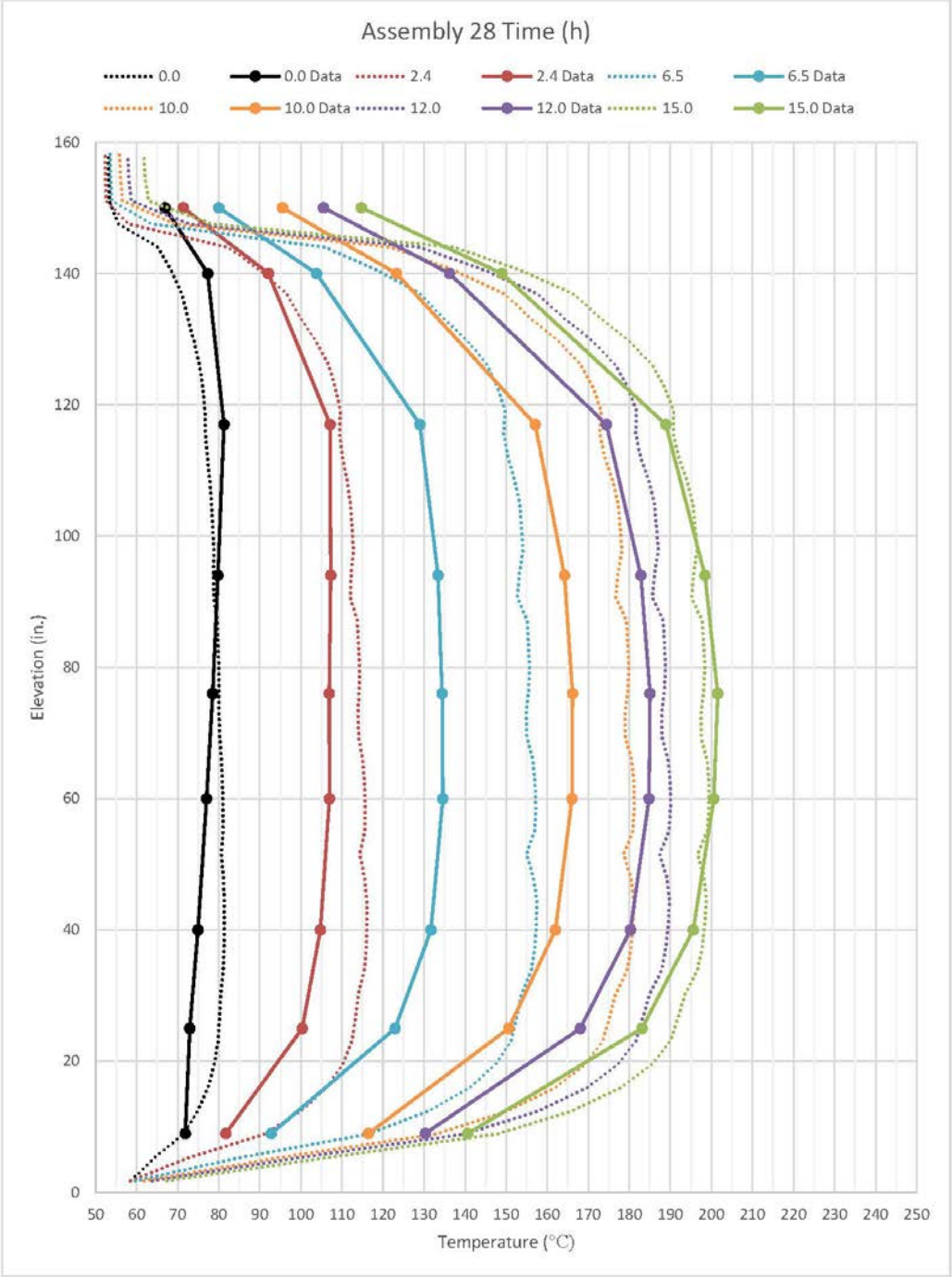

Figure 5.7. COBRA-SFS simulation compared to thermocouple data through time, Assembly 28

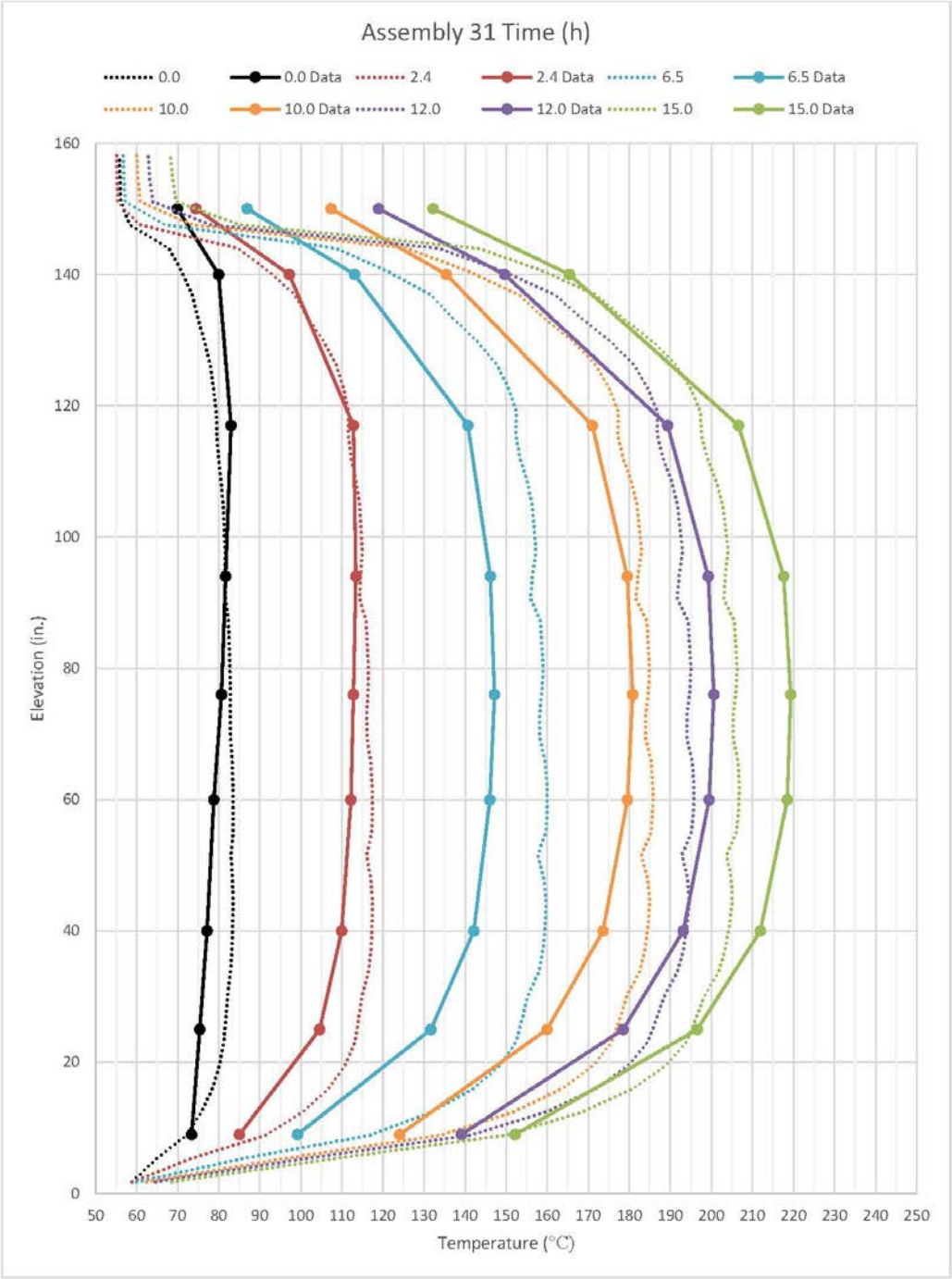

Figure 5.8. COBRA-SFS simulation compared to thermocouple data through time, Assembly 31

This page is intentionally left blank.

6. STAR-CCM+ LOADING AND DRYING TRANSIENT MODEL

Two different STAR-CCM+ models were used to simulate the vacuum drying process of the demonstration cask. The first model was a straight-forward adaptation of the model used in the Demo Round Robin exercise (Fort, et al. 2019). That model does not explicitly model the fuel rods and assembly hardware. Instead it uses a porous media representation of the fuel region. For comparison, a second STAR-CCM+ model was developed that models the fuel rods and hardware separately from the fluid, thereby eliminating the need for the porous media approximation.

The STAR-CCM+ models both require more computational resources than the COBRA-SFS model. The time steps were smaller, typically 10 seconds for both the porous and detailed STAR-CCM+ models. The porous model was run in parallel on a single, 24-core compute node of the PNNL institutional computer and the vacuum drying portion of the transient took approximately 12 hours to complete. The detailed model was run on six 24-core nodes of the same computer and the same 8.5-hour vacuum drying transient required approximately 32 hours of wall clock time.

The STAR-CCM+ model transients begin with the cask removal from the pool. Four distinct stages are modeled:

1. From when the cask is removed from the pool to when it is drained of water.
2. From when the cask is drained to when the blowdowns with helium are completed.
3. From the end of the blowdowns to the completion of vacuum drying.
4. From the beginning of backfill and into the thermal soak.

Timing and duration of each stage is shown in Table 6.1 and described below. Only a part of the final stage was modeled.

Table 6.1. Stages in modeling drying and thermal soak transient with STAR-CCM+

Stage	Condition	Event	Date	Time	Duration
1	Water filled	Cask out of pool	14Nov17	21:25	20 hrs
		Begin draining cask	15Nov17	17:22	
2	Helium filled	Draining complete		18:05	6.5 hrs
		Finish blowdowns	16Nov17	00:30	
3	Steam filled	Begin vacuum dry		00:35	8.5 hrs
		Begin backfill		09:00	
4	Helium filled	Begin backfill		09:00	13 days 9 hrs
		Final seal leak test	29Nov17	15:58	

6.1 STAR-CCM+ Porous Media Model

In the porous media representation of the cask fuel regions, fuel rods and fuel assembly hardware are treated together with the surrounding fluid as a continuum. Individual cells in this model region have a solid-fluid fraction (porosity) with separate solid and fluid properties, but the ability to represent each is limited in this arrangement. The porous media approach presents a problem when trying to model the changeout of fluids from liquid water to helium or when the cask is backfilled with cooler helium following vacuum drying. There is no way to maintain the current temperature of the fuel when changing to a different fluid at a different temperature. The fluid temperature must be assumed the same as the fuel during these transitions. Arguably, the impact of this approximation may be small.

This model is essentially the same model used in the steady-state analysis in Fort et al. (2019). In that case a steady-state solution was appropriate after the two-week thermal soak in the decontamination bay. In this case, the transient behavior is of interest. For the STAR-CCM+ models, it is possible to change the fluid in the cask model by initializing the next stage in the transient simulation with the temperature fields from the previous stage. For the porous model the temperature in each fluid cell is assumed to be unchanged from the prior stage in the calculation.

6.1.1 Boundary Conditions

In addition to thermal radiation to the environment, convective heat transfer correlations were used to solve for heat transfer from the cask exterior and base. These boundary conditions are described in Fort, et al. (2019). The ambient temperature for the porous model simulations was maintained constant at 23.9°C (75°F).

6.1.2 Initial Conditions

Initial conditions changed with each stage in the simulation (Table 6.1). For Stage 1, the cask and fill water are initially at the pool temperature, which was assumed to be 37.8°C (100°F). The draining process at the end of that stage takes less than an hour and is not modeled. Instead, the change in cask fill medium from water to helium is assumed to occur instantaneously.

Temperatures for the solids are carried into the start of the simulation of Stage 2. The initial temperature of the helium is set to that of the water. The temperature of the porous fuel and fluid region is also carried over from the first stage. Fluid velocities are set to zero at the start of the simulation. Only natural convection is modeled in this stage, no attempt is made to model helium injection and removal during the blowdowns.

The changeover from blowdowns to vacuum drying in Stage 3 is accomplished without having to reinitialize the simulation. The transition is accomplished by stopping the simulation, turning off the Boussinesq model to disable the buoyant driving force for convection, and changing the gas conductivity to that of steam. With these changes the simulation is continued until the start of helium backfill.

The start of the final stage is accomplished by reversing the changes made for simulating vacuum drying. Fluid thermal conductivities are reset to those of helium and the Boussinesq model is again activated, allowing for natural convection in the fill gas to be modeled. The backfill with helium is assumed to occur instantaneously. All solid and fluid cell temperatures as well as conserved quantities in the simulation are unchanged in the transition to Stage 4.

6.1.3 Fluid Properties

Fluid properties were changed with each stage of the simulation. Water properties were used in Stage 1. Helium properties were used for Stages 2, 3, and 4. Some steam properties were also used in Stage 3. The vacuum drying process used for the TN-32B takes the pressure down in steps and there is no reinjection of helium. Because of this, the fraction of steam in the gas contents grows and, with continuous gas removal, the gas content becomes almost exclusively steam. The assumption made in modeling this process is that the steam fraction is dominant during most of the time devoted to vacuum drying. As a simplified approach, steam properties are assumed at the outset and are maintained unchanged until backfill begins at the start of Stage 4. Furthermore, it is assumed that differences in gas heat capacity or density are negligible relative to the thermal mass of the solids in this system, so these properties are left unchanged as helium. Only the thermal conductivity of the gas is changed. Finally, the gap resistances inside the cask are changed during vacuum drying to correspond to those of gaps filled with steam rather

than helium. In Stage 4, the gas properties (thermal conductivity of the gas and gap resistances) revert to those for helium.

6.1.4 Basket-Rail Gap

For the STAR-CCM+ models, the basket-rail is kept fixed for all stages of the simulation at 0.1 in. This value was postulated in Fort, et al. (2019).

6.2 STAR-CCM+ Detailed Model

As a general-purpose computational fluid dynamics (CFD) package, STAR-CCM+ requires considerable detail to explicitly represent the fuel rods and assembly hardware. In contrast, COBRA-SFS is purpose built for rod bundle geometries and is capable of modeling them with greater efficiency. It is useful to have an independent model for comparison and the STAR-CCM+ models fulfill that purpose. The detailed model developed for this effort provides the additional feature of allowing comparison of fuel cladding temperature details that can be compared directly with the COBRA-SFS model.

A one-eighth section of symmetry model was chosen for computational efficiency. The cask loading map was loaded with as much symmetry as possible with the available assemblies. The section of symmetry chosen is shown in Figure 6.1. It includes the hot assembly and thermocouple lance position. The decay heat load in this section is 3765 W, which applied symmetrically, would represent 98.9% of the 30456 W actual loading.

Figure 6.1. One-eighth section of symmetry selection from the loading map

The geometry and mesh are shown in Figure 6.2. Note that only nozzles are included in addition to the fuel rods. Additional components are not important to represent the small amount of convection in this cask.

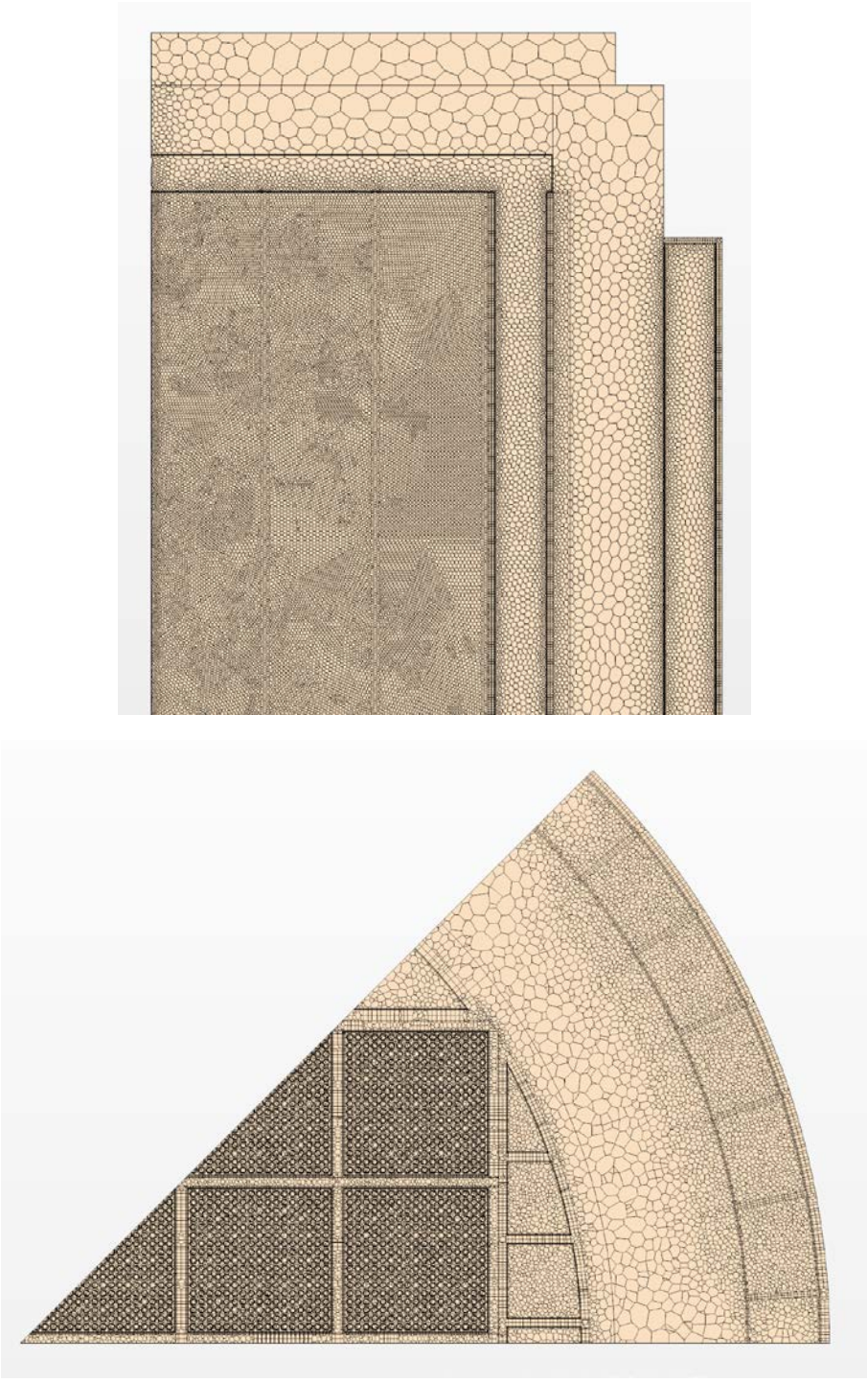

Figure 6.2. Detailed model geometry and mesh

One of the thermocouple lance positions was in an equivalent position in this section of symmetry. These locations are shown in the radial cross-section of the geometry in Figure 6.3.

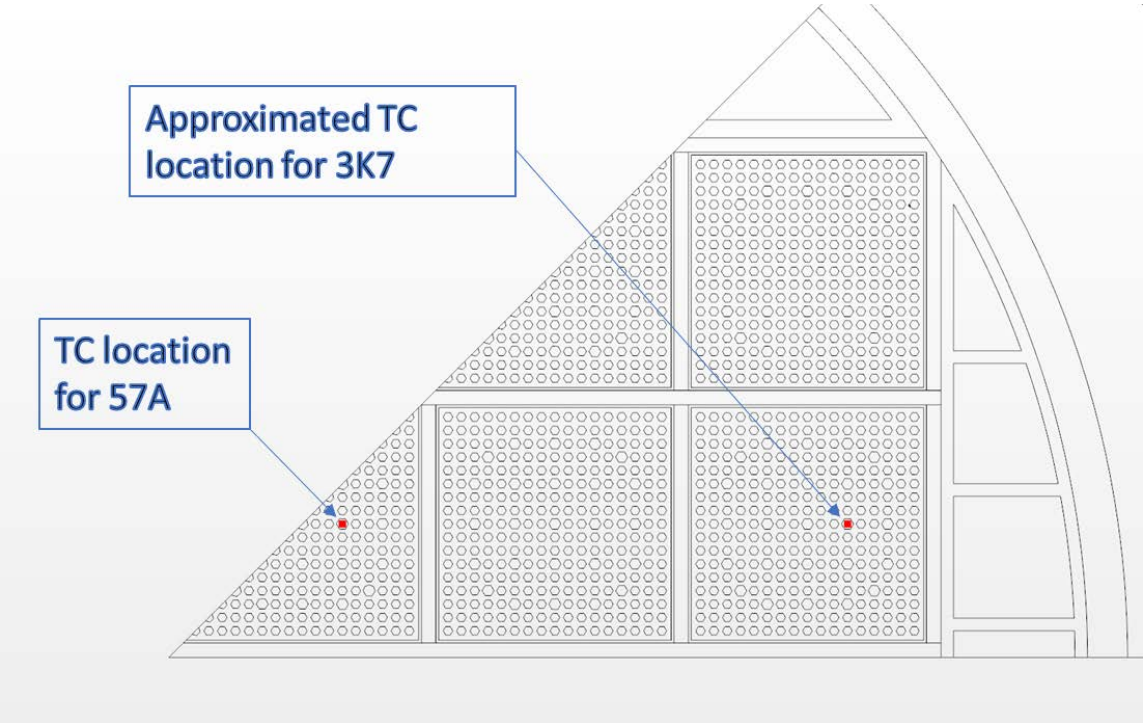

Figure 6.3. Thermocouple positions for in the one-eighth section of symmetry model

6.2.1 Boundary Conditions

Other than at the symmetry boundaries, the model boundary conditions are applied in identical fashion as those in the porous model. Also, the ambient temperature was changed from 15.5°C (60°F) for the early stages of the simulation to 23.9°C (75°F) when vacuum drying began.

6.2.2 Initial Conditions

The initial conditions for the detailed model were applied as in the porous model, except for the helium temperature. At the start of the blowdown simulation and following vacuum drying, the helium backfill is given a temperature of 37.8°C (100°F).

6.2.3 Fluid Properties

For the initial stage in the detailed model simulation the water was treated as having no convection. To approximate the enhancement to heat transfer due to buoyancy induced natural convection, the water thermal conductivity was increased to correspond to a Nusselt number of 3.66, a value that has been justified for use with COBRA-SFS cask applications (Fort, et al. 2019).

Remaining properties were treated identically to those described for the porous model.

6.2.4 Basket-Rail Gap

As with the STAR-CCM+ porous model, the basket-rail gap in the detailed model is kept fixed at the postulated value of 0.1 in. from Fort, et al. (2019) for all stages of the simulation. The thermal conductivity of the fluid filling this gap, and consequently the gap resistance, was changed over the different stages of the simulation.

This page is intentionally left blank.

7. STAR-CCM+ LOADING TRANSIENT RESULTS

Results will be presented first for the porous media model, followed by those for the detailed model.

7.1 STAR-CCM+ Porous Media Model

Results for fuel temperature are presented first, followed by a comparison of predicted cask surface temperatures with measured values. Those surface temperature comparisons are shown in Section 7.1.2.

7.1.1 Fuel Temperatures

Figure 7.1 shows the model results for PCT during blowdown and vacuum drying along with temperature measurements for the hot assembly. The predicted trend is consistent with the measured data, but the modeled temperature maximum falls under the measured peak.

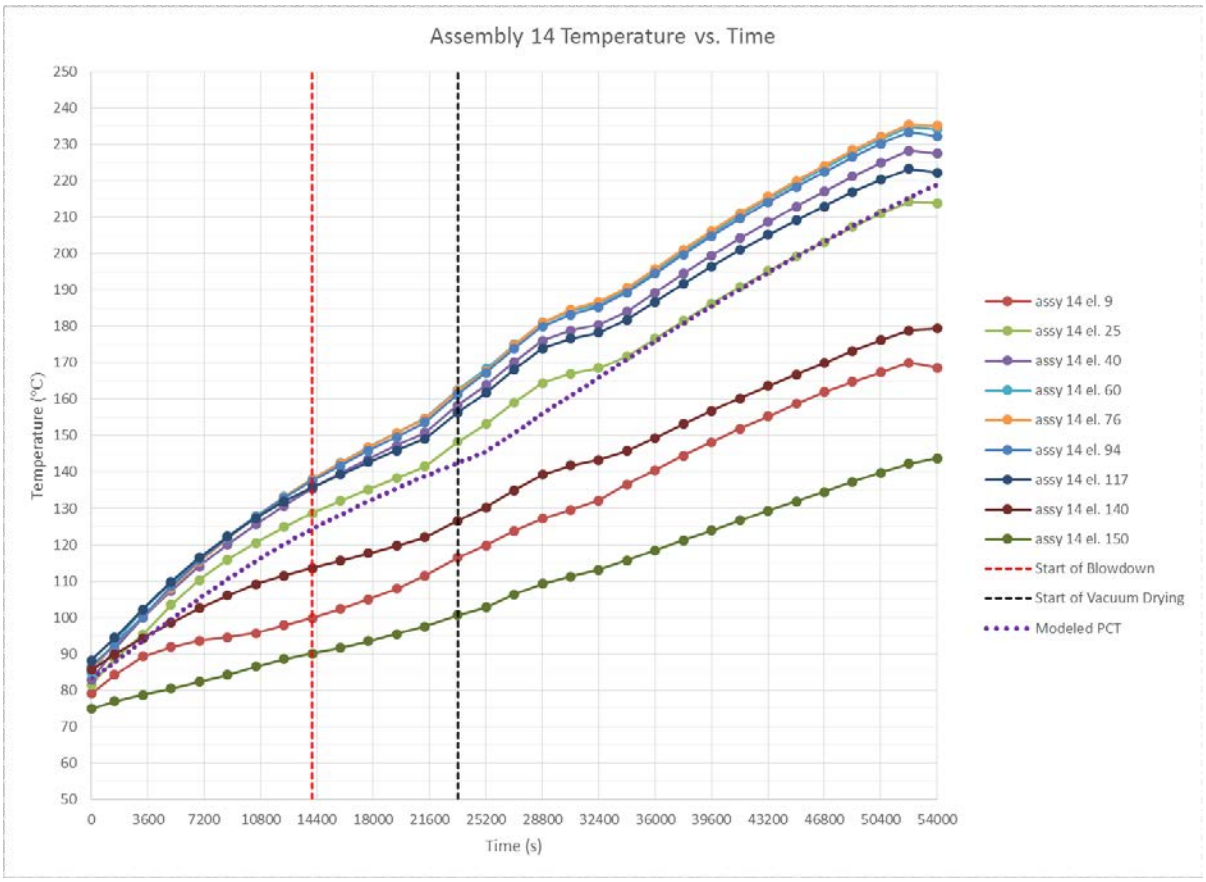

Figure 7.1. Peak cladding temperature during blowdowns and vacuum drying (simulation stages 2 and 3) – porous model (elevation in inches)

Figure 7.2 compares the model predictions for temperatures at the thermocouple lance measurement locations in Assembly 2 with measurements for the vacuum drying part of the transient. Time zero represents the end of the canister draining operation. The 6.5-hour plots are at the end of blowdowns and the 15-hour profiles are at the completion of vacuum drying. The time zero profiles are in very good agreement, except for missing the temperature decrease at the uppermost thermocouple location. The predicted temperatures at the end of blowdowns and vacuum drying are generally underpredicted. At the end of blowdowns this difference is up to 17°C and at the end of vacuum drying the difference is as much as 24°C.

Results for Assembly 14 are shown in Figure 7.3. These show very similar trends as in the outer assembly (Figure 7.2). The absolute temperatures for Assembly 14 are larger as are the differences. They are estimated at 5, 22, and 25°C, respectively, at the beginning of drain, end of blowdowns and completion of drying.

Similar plots are shown in Figures 7.4 and 7.5 for modeled and measured temperature data after vacuum drying. The simulation was run to 174 hours, which is roughly at the middle point of the two-week thermal soak. Temperatures are overpredicted at this point, by up to 15°C for Assembly 2 and approximately 27°C for Assembly 14, except for somewhat greater difference at the uppermost thermocouple position.

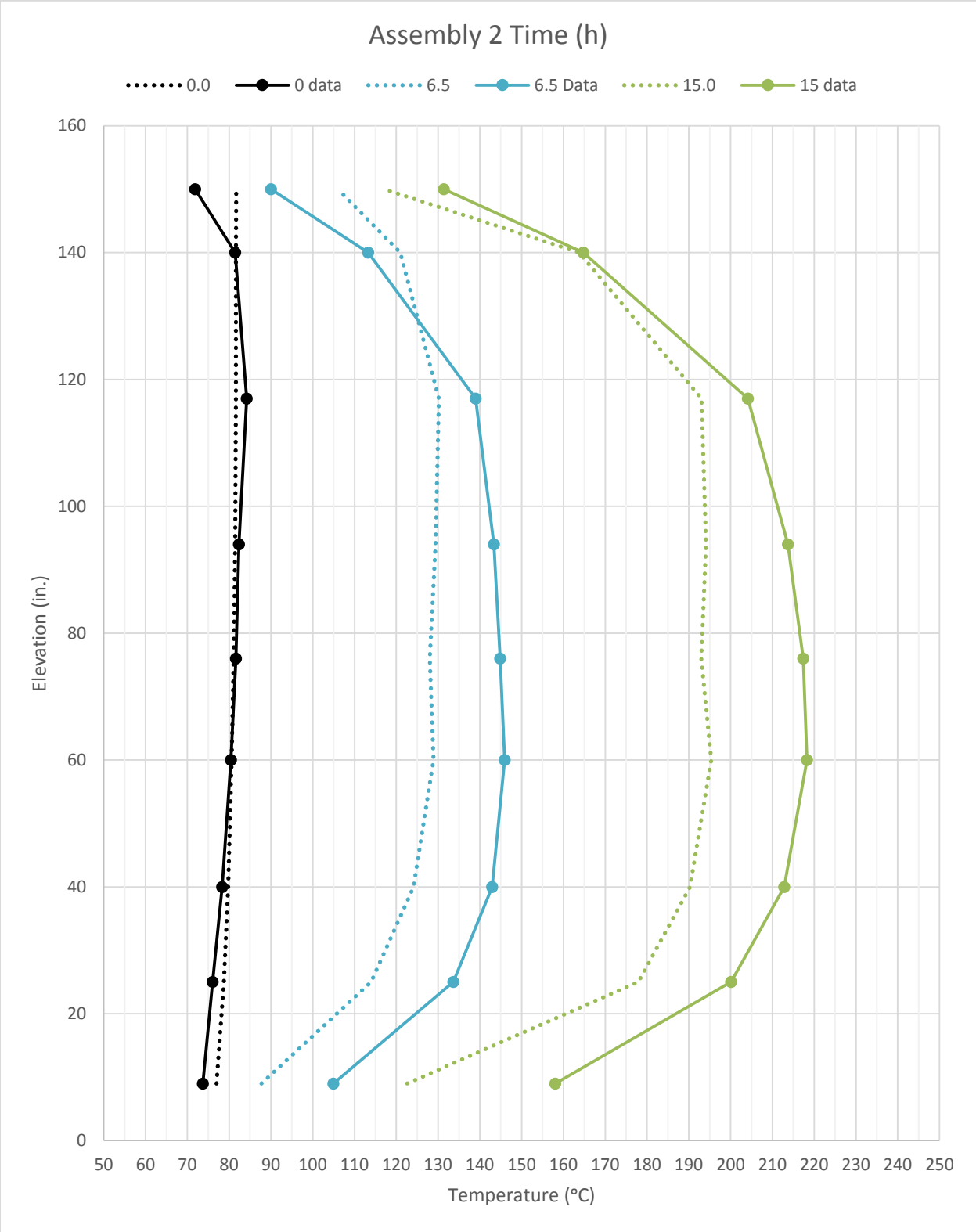

Figure 7.2. Comparison of STAR-CCM+ porous model results with measurements – cask drain through drying – Assembly 2

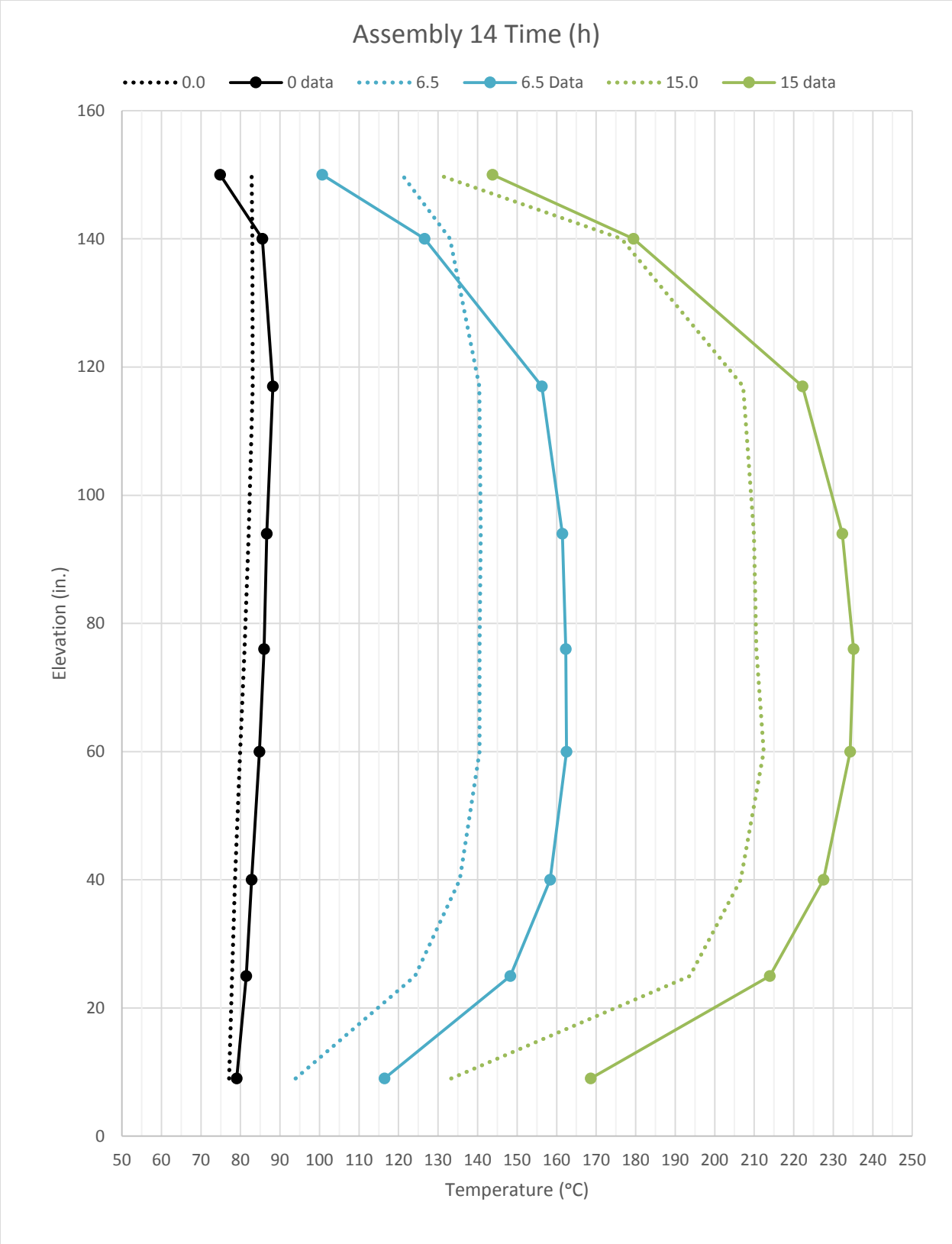

Figure 7.3. Comparison of STAR-CCM+ porous model results with measurements – cask drain through drying – Assembly 14

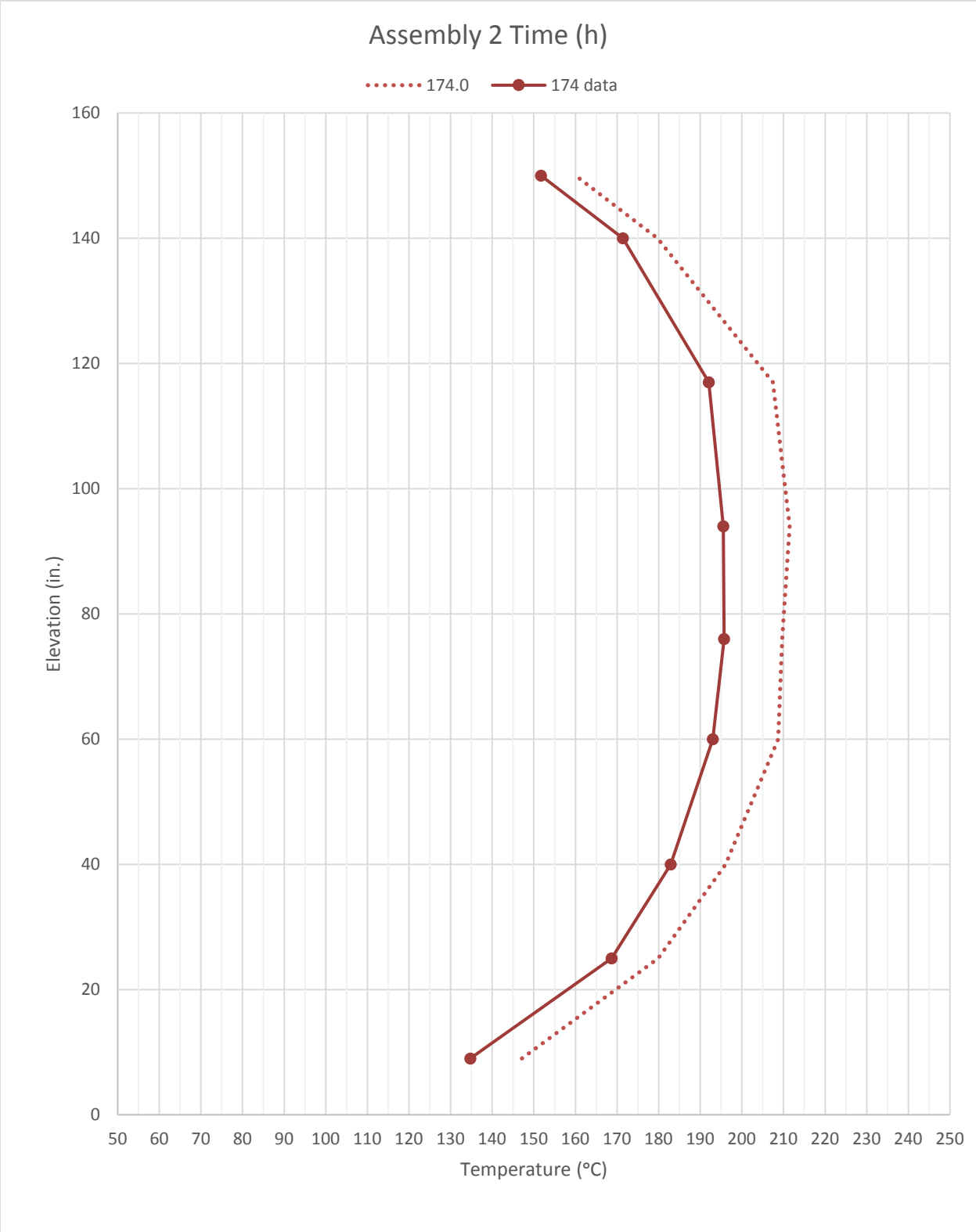

Figure 7.4. Comparison of STAR-CCM+ porous model results with measurements – after completion of drying – Assembly 2

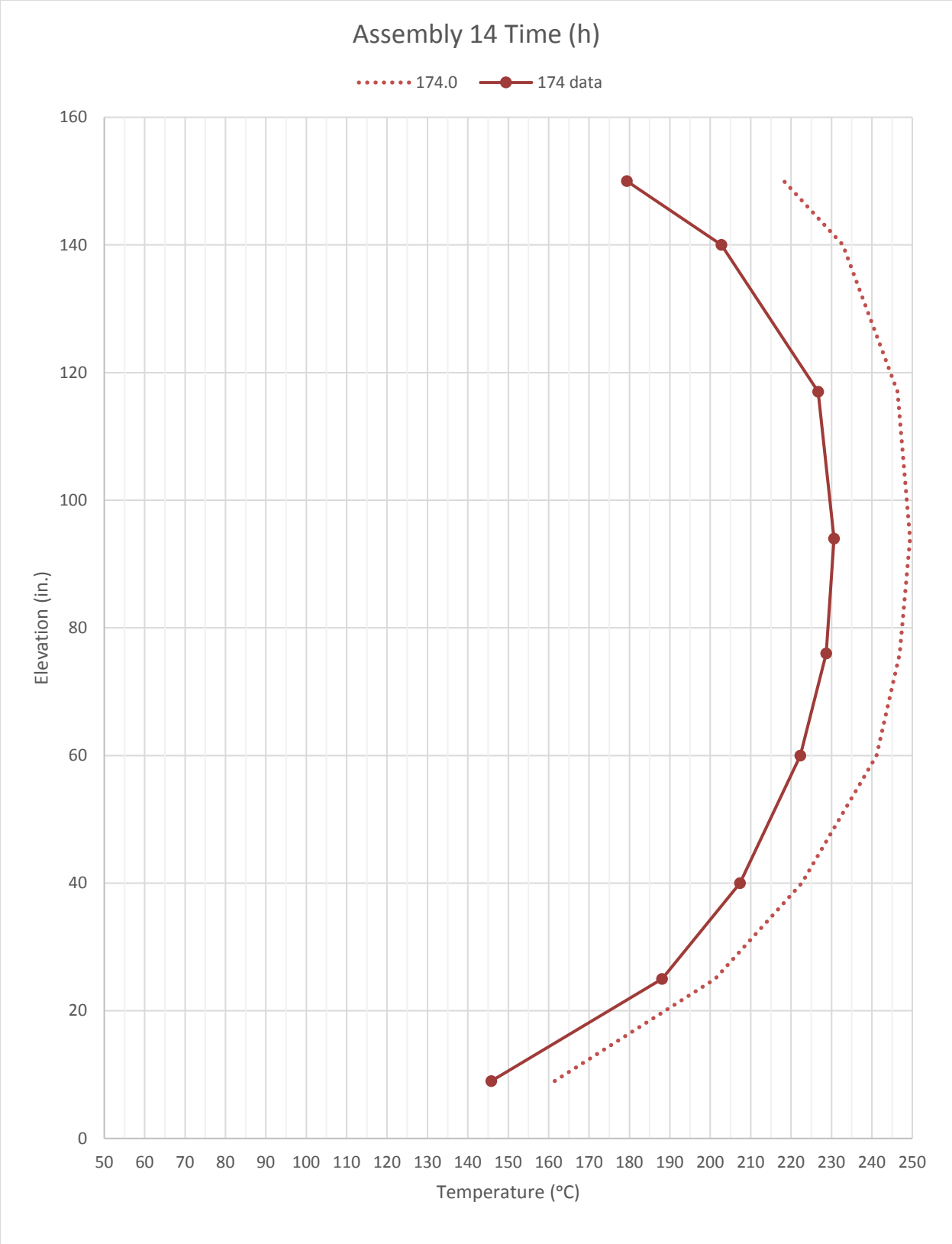

Figure 7.5. Comparison of STAR-CCM+ porous model results with measurements – after completion of drying – Assembly 14

7.1.2 Cask Surface Temperatures

Cask surface temperature measurements are compared with predictions for the STAR-CCM+ porous model in Table 7.1. The measurement data are from the EPRI High-Burnup Demo data website (EPRI, 2019). Measurement locations are shown in Figure 2.3. Agreement is mixed for the first set of comparisons, near the time the cask is drained. Model predictions are within 1°C at the uppermost measurement locations, but the model overpredicts measurements by up to 14°C at the bottom locations.

The second comparison with surface temperature measurements is well into the test. The model results are for 174 hours, which is where the porous simulation was stopped. The surface temperature measurements were taken a day and a half before this point in the transient, but fuel temperatures over this period were uniform by this time (see, for example, Figure 2.2). The agreement is very good at this point, within 1°C at the top and within 5°C at all positions.

Table 7.1. Comparison of cask surface measurements and STAR-CCM+ porous model results (°C)

	Measured[b]			**STAR-CCM+ Porous**		
	11/15/17	15:50		11/15/17	17:22	0 hrs.
	A	**B**	**C**	**A**	**B**	**C**
1	52.2	49.4	50.0		48.9	49.0
2	50.0	49.4	48.9	49.6	49.9	50
3	47.8	46.1	47.8	50.5	50.8	50.8
4	43.3	42.2	43.3	51.5	51.8	51.8
5	38.9	39.4	39.4		53.8	53.8
	11/21/17	10:45		11/22/17	23:22	174 hrs.
	A	**B**	**C**	**A**	**B**	**C**
1	75.6	80.6	80.6		80.1	80.4
2	87.8	87.2	86.7	84.6	84.9	85.2
3	87.8	87.8	87.8	86.8	87.1	87.5
4	82.2	80	81.1	84.2	84.3	84.7
5	73.9	72.8	72.8		77.6	77.8

7.2 STAR-CCM+ Detailed Model

Model results are compared with measurements for fuel temperature first. These are followed by surface temperature comparisons in Section 7.2.2 and gas average temperature results in Section 7.2.3.

[b] From Waldrop, EPRI, 2019, DRAFT.

7.2.1 Fuel Temperatures

Plots of temperature versus time during the simulation are shown first. Figure 7.6 shows the model results for PCT during blowdown and vacuum drying along with temperature measurements for the hot assembly. The predicted trend compares very well with the measurements, though the magnitude eventually falls under the measured peak temperature.

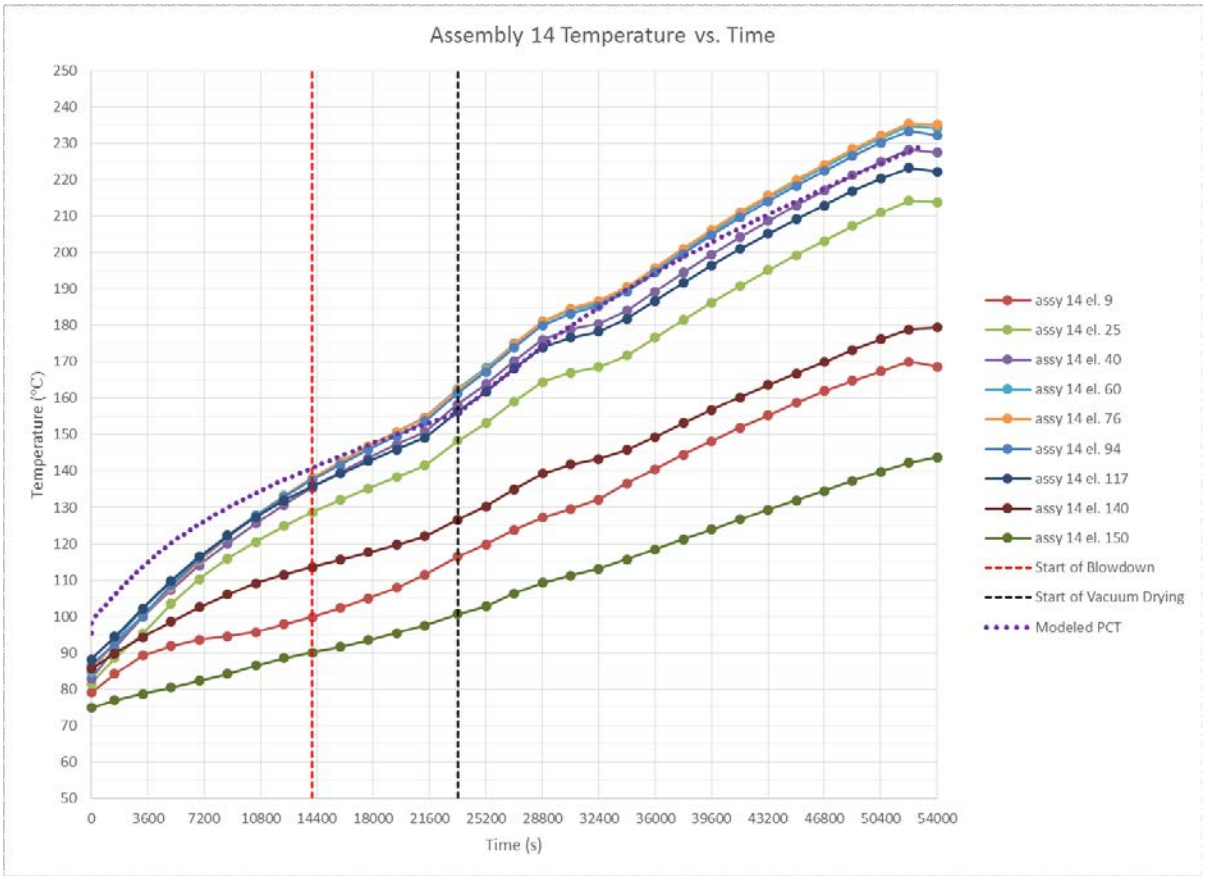

Figure 7.6. Peak cladding temperature during blowdowns and vacuum drying (simulation stages 2 and 3) – detailed model (elevation in inches)

Axial temperature profiles are shown next. Model predictions for temperatures at thermocouple lance measurement locations are compared with measurements for the blowdown and vacuum drying part of the transient in Figures 7.7 and 7.8. The time zero profiles are at the end of canister draining operation. The 6.5-hour plots are at the end of blow downs and the 15-hour profiles are at the completion of vacuum drying. The time zero profiles are less representative than those from the porous model because of the need to run the water-filled transient without convection. The predicted temperatures at the end of blowdowns and vacuum drying are generally underpredicted through most of the profile, by as much as 15°C, but the agreement at the two uppermost measurement locations is very good.

Similar plots are shown for post vacuum drying results in Figures 7.9 and 7.10. The detailed model simulation was not able to be run as far as the porous model. Comparisons are shown for two cases, 19 hours, which is about 4 hours after backfill, and at steady-state conditions, which should be a reasonable comparison for the measurements later in the two-week thermal soak. The comparison at 19 hours for Assembly 2 is very good, differing by less than 2°C except at the uppermost thermocouple location. For the hot assembly the difference at 19 hours is within 10°C at all axial measurement locations.

Measurements are shown at 174 hours, roughly at the middle point of the two-week thermal soak, and at 270 hours, which is near the end. Steady-state temperature results are higher than the measurements over much of the axial profile, but agreement is excellent at the uppermost points in the hot assembly.

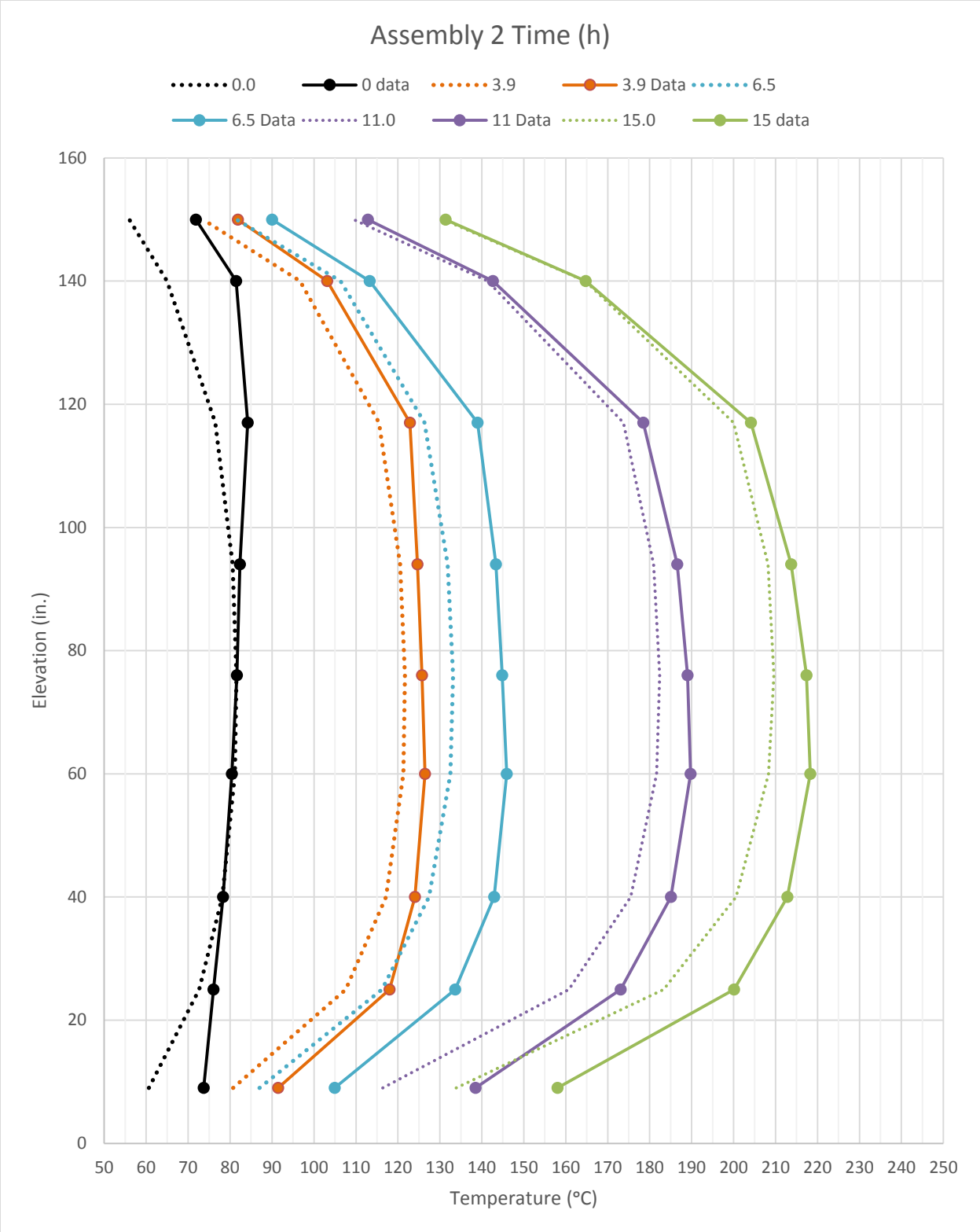

Figure 7.7. Comparison of STAR-CCM+ detailed model results with measurements – cask drain through drying – Assembly 2

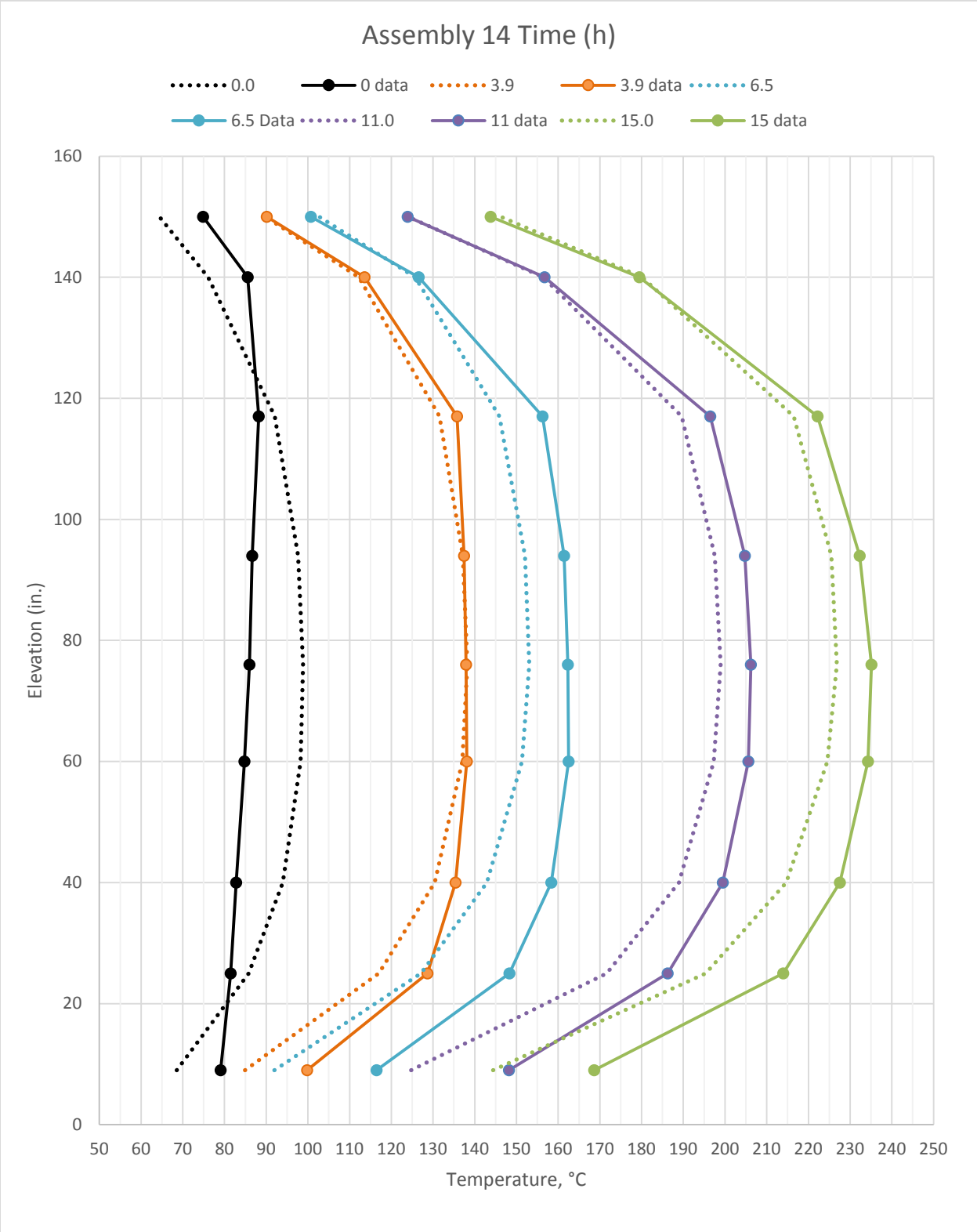

Figure 7.8. Comparison of STAR-CCM+ detailed model results with measurements – cask drain through drying – Assembly 14

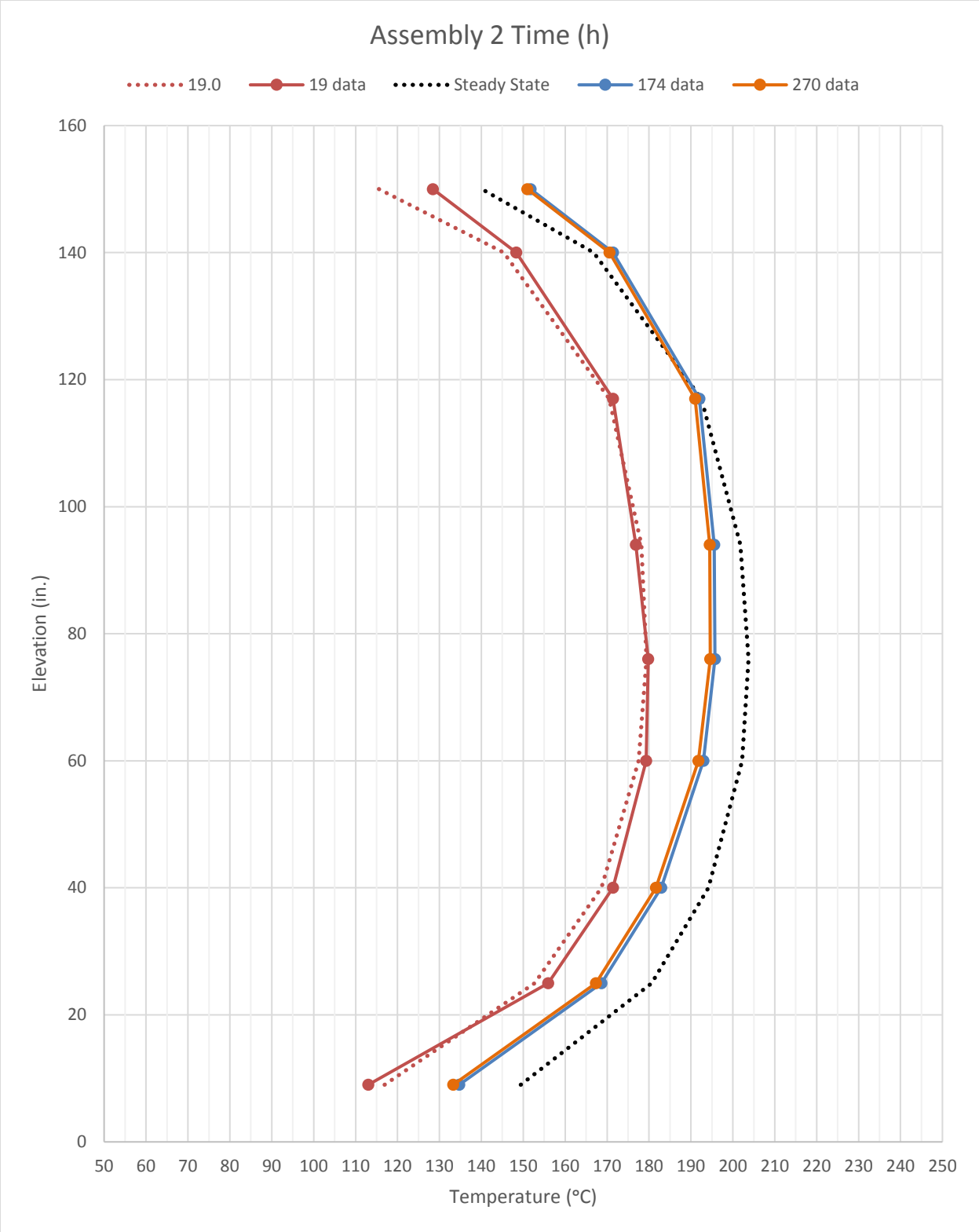

Figure 7.9. Comparison of STAR-CCM+ detailed model results with measurements – after completion of drying – Assembly 2

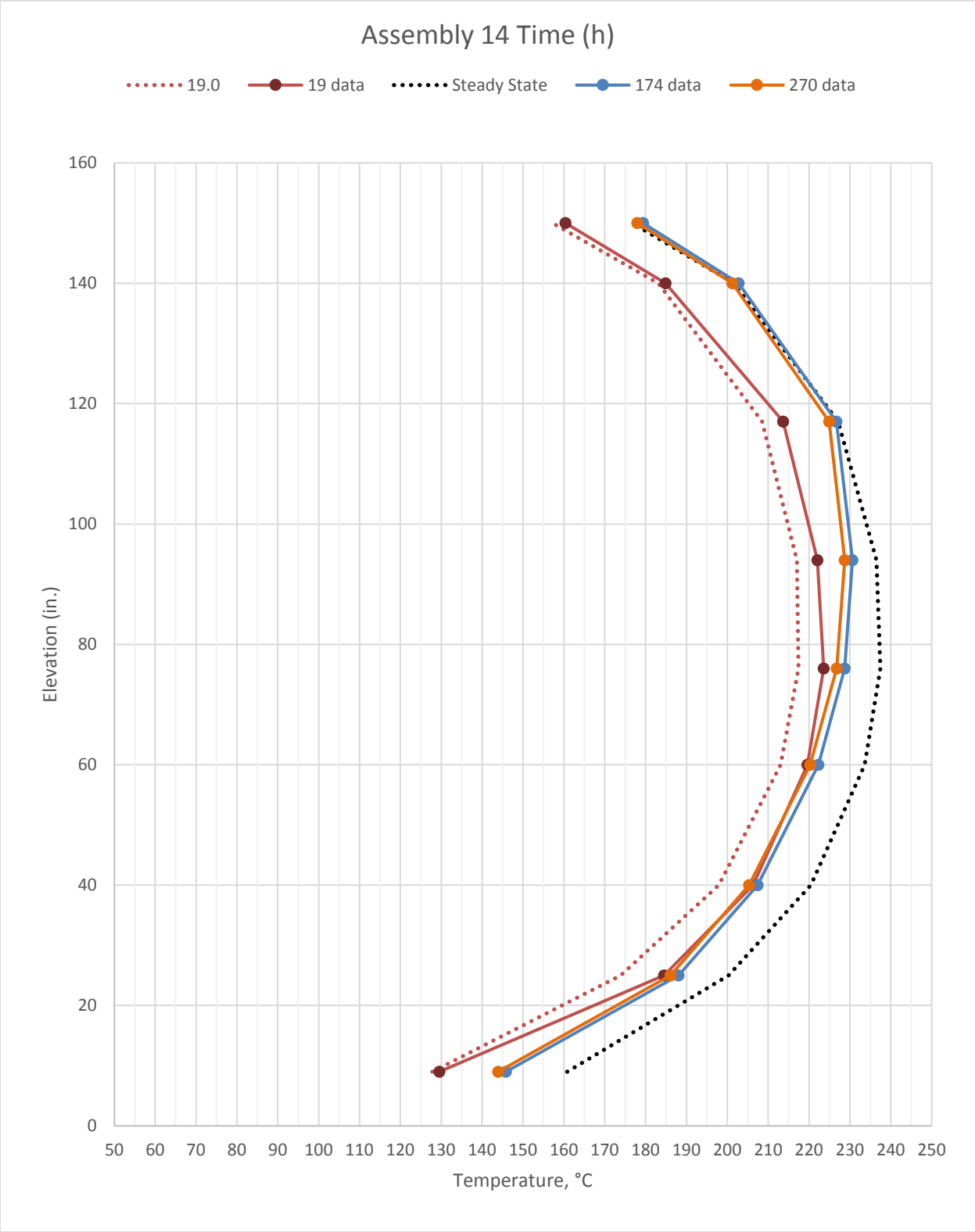

Figure 7.10. Comparison of STAR-CCM+ detailed model results with measurements – after completion of drying – Assembly 14

7.2.2 Cask Surface Temperatures

Cask surface temperature measurements are compared with predictions for the STAR-CCM+ detailed model in Table 7.2. The measurement data are from the EPRI High-Burnup Demo data website (EPRI, 2019). Measurement locations are shown in Figure 2.3. Model comparison for the "C" measurement position is not available with the one-eighth symmetry model. Agreement is good for the first set of comparisons, near the time the cask is drained. Model predictions are higher, but within 5°C at all locations. For the second set of measurements, taken about 5.5 hours after backfill, the model overpredicts the measured values by 7 to 9°C. Finally, the detailed model steady-state solution is compared with measurements near the end of the two-week test and the agreement is very good, within 2 to 3°C at all positions.

7.2.3 Gas Average Temperature

STAR-CCM+ has built-in functions for computing average properties of modeled regions. With the detailed model of the TN-32B it was therefore easy to compute volume average gas temperatures for the fill gas. The detailed model simulation was run long enough to compare results with the surface temperature measurements made at 14:35 on 11/16/17. This was 5 ½ hours after the initial helium backfill. The volume average temperature of the gas at this point was 137°C (279°F). The first gas sample was taken within one hour of this, at 15:21.

Average gas temperature was also computed for the steady state solution. This case represents the cask condition at equilibrium. The volume average gas temperature was 165°C (328°F).

Table 7.2. Comparison of cask surface measurements and STAR-CCM+ detailed model results

	Measured[c]			STAR-CCM+ Detailed		
	11/15/17	15:50		11/15/17	18:05	0 hrs.
	A	**B**	**C**	**A**	**B**	**C**
1	52.2	49.4	50.0		45.1	
2	50.0	49.4	48.9	48.3	48.4	
3	47.8	46.1	47.8	49.7	49.8	NA
4	43.3	42.2	43.3	48.1	48.1	
5	38.9	39.4	39.4		43.6	
	11/16/17	14:35		11/16/17	14:35	20.5 hrs.
	A	**B**	**C**	**A**	**B**	**C**
1	54.4	56.1	56.7		65.6	
2	62.8	61.1	61.7	68.7	68.6	
3	63.9	62.2	62.8	70.4	70.3	NA
4	60.6	58.3	59.4	67.9	67.7	
5	54.4	53.3	53.3		61.4	
	11/28/17	9:00		Steady-state		
	A	**B**	**C**	**A**	**B**	**C**
1	75.6	80	79.4		81.8	
2	87.8	87.8	86.1	86.1	85.9	
3	88.3	88.3	87.2	87.8	87.6	NA
4	81.7	81.7	82.2	84.4	84.1	
5	72.8	72.8	73.3		75.7	

all temps in °C

7.3 Discussion of Results

The porous model benefits from starting with an accurate initial condition. By being able to solve the buoyancy induced convection with water in the cask, the temperature profile is appropriately shifted upward and is flattened by the mixing. The detailed model's initial condition is solved without water convection. This resulted in a higher temperature relative to measurement and a peak temperature that is centrally located in the heated region of the fuel. However, this difference does not appear to be a handicap to the detailed model for any of the time comparisons shown, as results are in all cases represent improvements over the porous model. Cask surface temperatures were reasonably well predicted by both models, but overall the detailed model gave the best agreement with measurements.

[c] From EPRI (2019).

This page is intentionally left blank.

8. ISFSI TRANSIENTS

The TN-32B cask is now located in the North Anna ISFSI. As such it is subject to changing ambient weather conditions. Fuel temperature data is being recorded continuously and is available for study (EPRI, 2019). Of interest here is what influence these ambient weather changes have on fuel temperature and to what extent this response can be simulated with models. The models used in analyses here are the best estimate COBRA-SFS and STAR-CCM+ models of the cask storage configuration. These models were previously used for planning the High Burnup Demonstration test (Fort, et al. 2019). The November 2017 estimates of decay heat were used in the present analyses. The decrease in decay heat for the cases discussed here are modest relative to other uncertainties and therefore can be neglected.

This section of the report describes initial comparisons of models with example weather transients. Two different time periods were selected to form two modeling cases. The two cases modeled feature very different ambient conditions and thermocouple temperature response.

8.1 Case 1: January 5th to January 16th

Case 1 consisted of the ambient conditions from January 5th to January 16th, 2018 outside the North Anna Nuclear Generating Station on the dry cask storage pad. This case was selected because over this time period, the ambient temperatures experienced a significant increase and subsequent decrease. This resulted in a large fluctuation in the thermocouple temperatures inside the cask over a somewhat long period of time.

8.1.1 Ambient Conditions

Figure 8.1 shows the ambient temperatures for this case. For this time period lasting 11 days, the minimum ambient temperature was -15.2°C and the maximum was 20.5°C. The resulting temperature differential is 35.7°C, which is a large change in temperature relative to model and measurement uncertainties. This lends itself well to model testing because temperature changes can be definitively observed and quantified. This change in temperature is expected to be the dominant factor affecting temperatures inside of the cask for this transient scenario.

For two days, January 5th and 6th, the temperatures fluctuated by about 8°C between the high and low. These fluctuations are of sufficiently high frequency as to not impact temperatures inside of the TN-32B cask. This is due to the large thermal inertia characteristic of such storage systems. The average temperature for this period was used to establish a steady-state condition from which to initiate a transient.

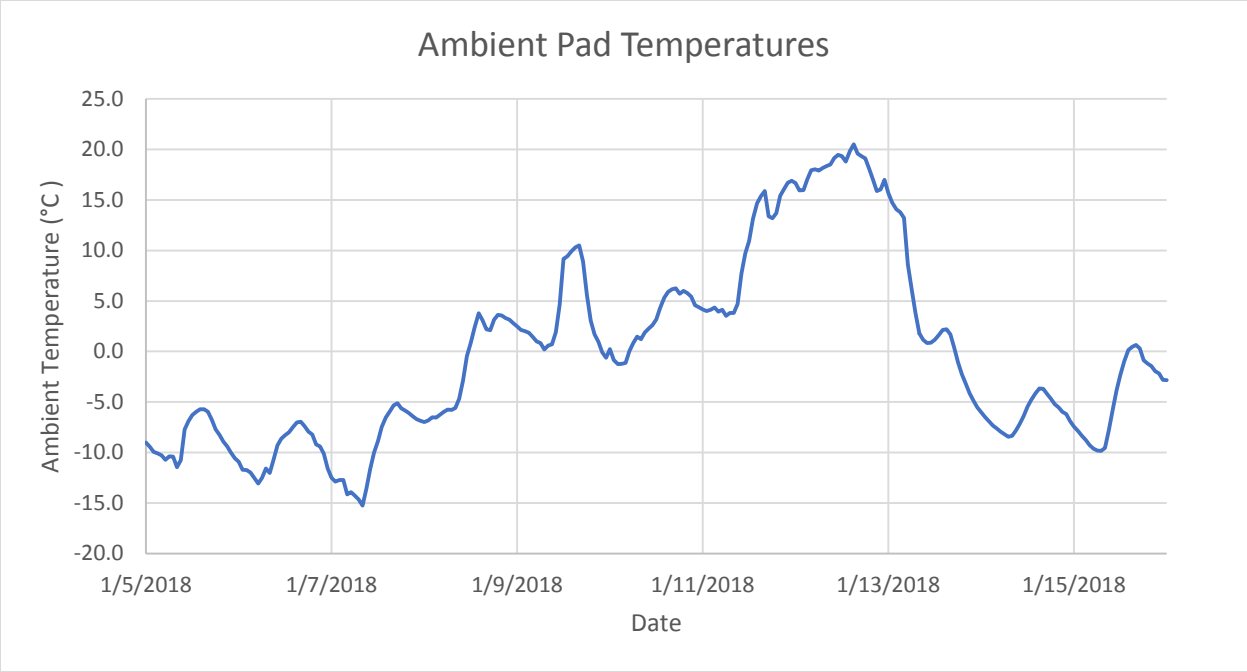

Figure 8.1. Ambient temperatures from Jan. 5th to Jan. 16th

The thermocouple temperatures inside the TN-32B cask are shown in Figure 8.2 and Figure 8.3 for assemblies 14 and 2, respectively. Assembly 14 was selected because it is an interior assembly and has exhibited the hottest PCT (Fort, et al. 2019). Assembly 2 was selected because it is in one of the outermost positions in the basket. The thermocouple temperatures in this location will be cooler. Selecting a hot assembly and a cool assembly provides a representative range of temperatures inside of the cask.

Figure 8.2 shows the measured thermocouple data inside the TN-32B cask sitting on the ISFSI pad with ambient temperatures for the period of January 5th to January 16th. There is a significant increase and subsequent decrease in thermocouple temperatures that coincides with similar changes in ambient temperatures. In the period from January 13th to January 15th it appears that there is a 12 to 24-hour delay in the response of thermocouple temperatures to changes in ambient.

Comparing Figure 8.2 and Figure 8.3, all thermocouple temperature trends are similar between axial levels and assemblies within the cask. The major difference is that Assembly 2 is significantly cooler than Assembly 14. Both profiles have very similar temperature response throughout the transient. The profiles of all the hottest thermocouple locations are close together. The hottest location in the cask is about 76 to 117 inches from the bottom of the cask. In this range there only about 0.5°C difference between the measured temperatures at these thermocouple locations.

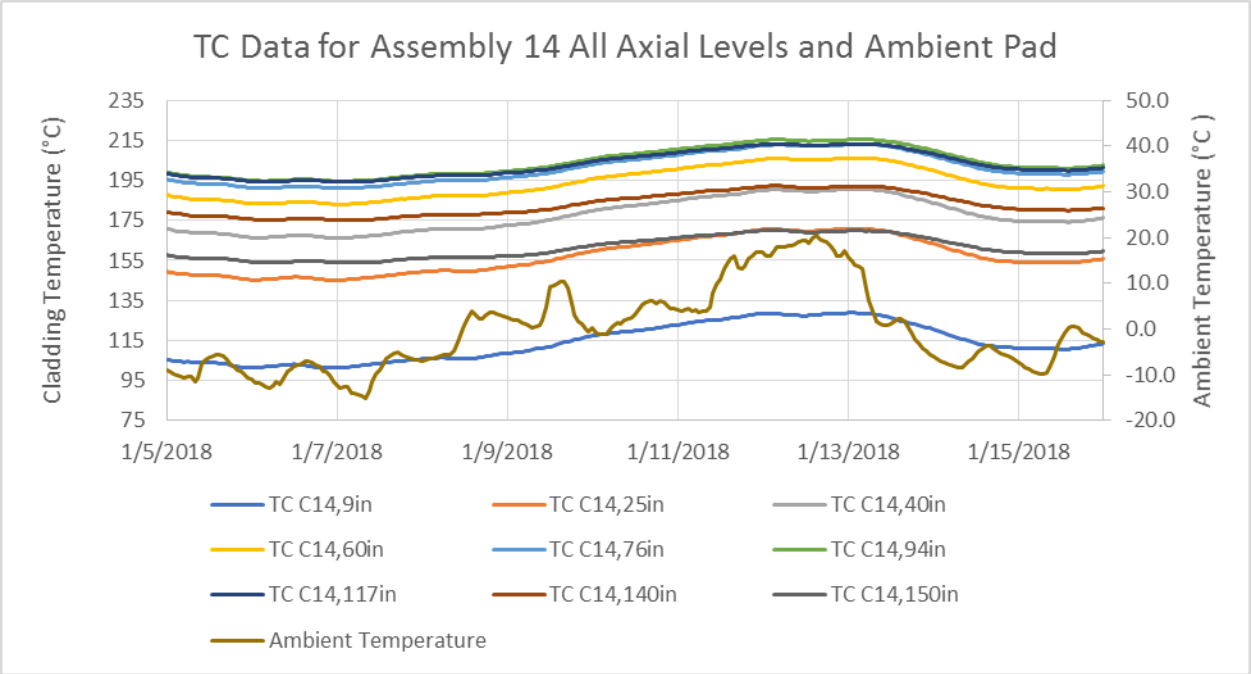

Figure 8.2. Ambient pad temperature and thermocouple data for Assembly 14

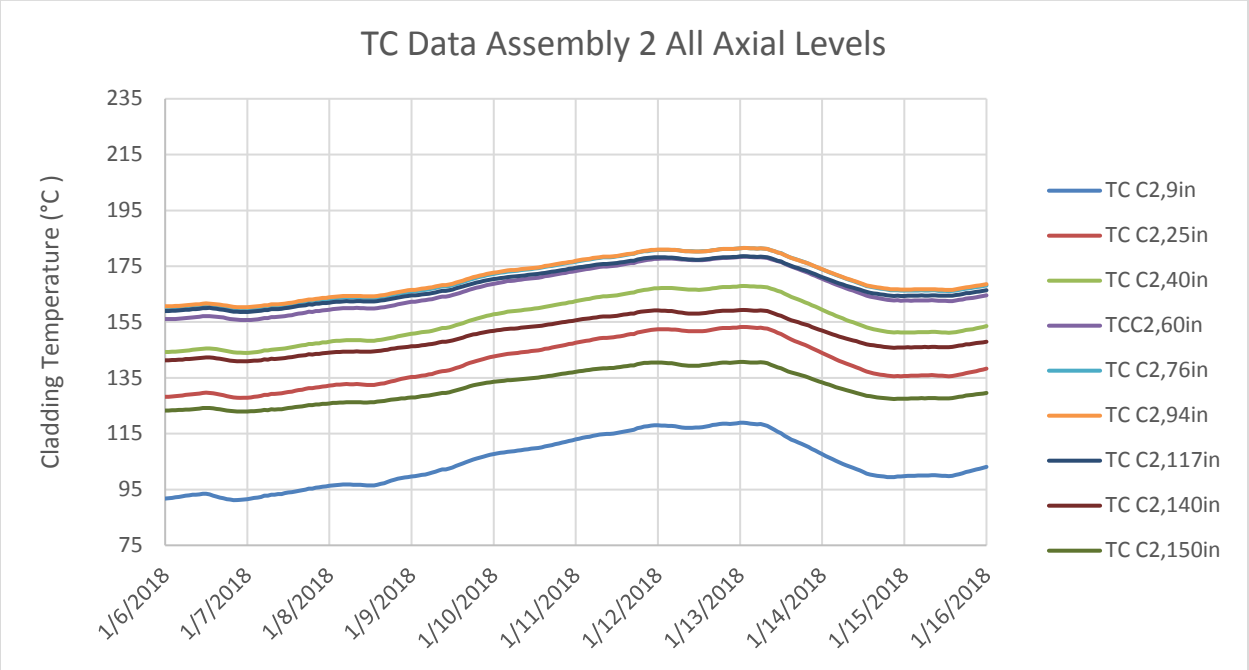

Figure 8.3. Thermocouple data from Assembly 2 Jan 6th to Jan 16th

The maximum and minimum temperatures in thermocouple data over the transient period are summarized in Table 8.1. Axial levels at 76 and 25 inches above the bottom of the cask were selected for comparison. The level 76 inches above the bottom is approximately in the middle of the cask. This will yield higher temperatures. The thermocouple at 25 inches above the bottom of the cask was selected because it is a cooler part of the cask. Selecting these two axial locations provides a representative range of temperatures inside of the cask and will be presented throughout this section.

The biggest difference in temperature change inside of the cask was between the bottom and middle of the cask. The temperature difference between the maximum and minimum near the bottom of the cask (25 inches) was between 25.4°C and 25.7°C for the two assemblies presented here. Near the middle of the cask (assembly 14) at 76 inches from the bottom, the temperature difference was about 21.9°C. The temperature change in the middle of the cask was about 3°C less than at the bottom of the cask. The bottom of the cask is closer to the ambient boundary, so the bottom of the cask is more influenced by the ambient conditions.

Table 8.1. Summary of thermocouple and ambient temperature differences

	C14,76 (°C)	C2,76 (°C)	C14,25 (°C)	C2,25 (°C)	Ambient (°C)
Max	213.0	181.6	170.8	153.2	20.5
Min	190.9	159.7	145.1	127.8	-15.2
Diff	22.1	21.9	25.7	25.4	35.7

8.1.2 COBRA-SFS Model Results

The ambient temperature history for Case 1 was implemented in the boundary condition in the COBRA-SFS transient model. The simulation results are presented in Figure 8.4 and Figure 8.5. Although the COBRA-SFS temperatures are higher than the thermocouple measured temperatures, the timing of the temperature rise in the COBRA model results matches the initial rise in temperature and subsequent fall in the latter half of the transient. From Figure 8.4 and Figure 8.5, it is obvious that the temperature changes from the COBRA-SFS model do not match the changes in the measured temperatures.

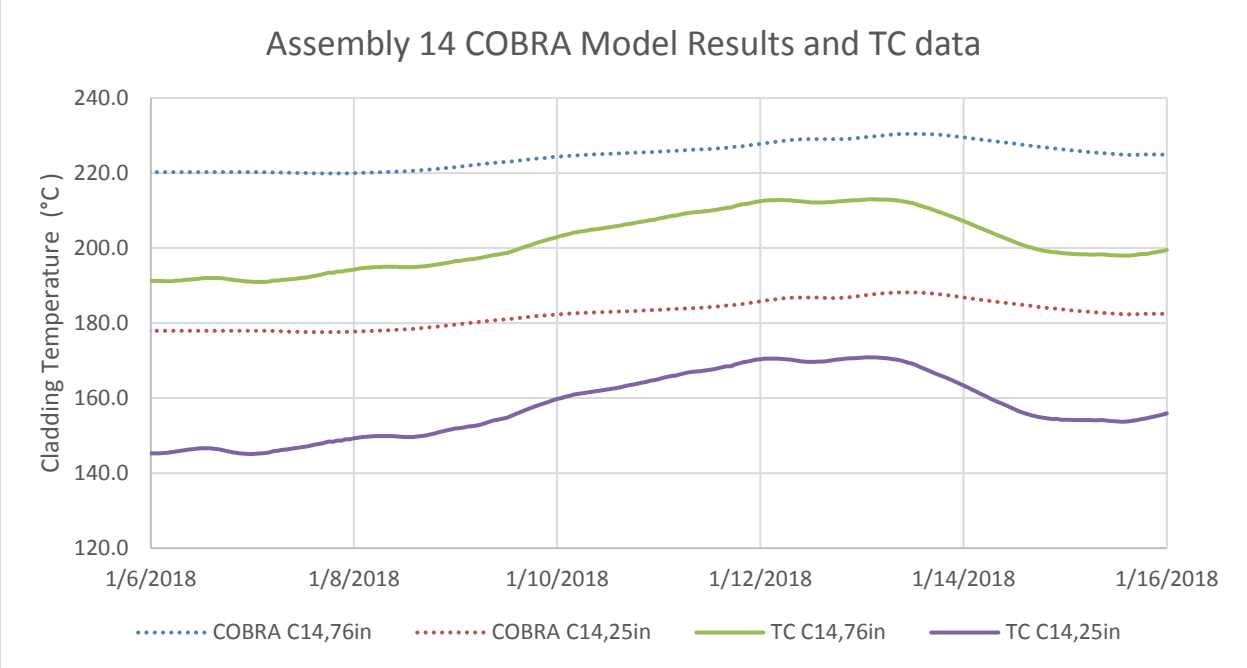

Figure 8.4. COBRA-SFS model Assembly 14 cladding temperature results for Jan. 6th to Jan. 17th

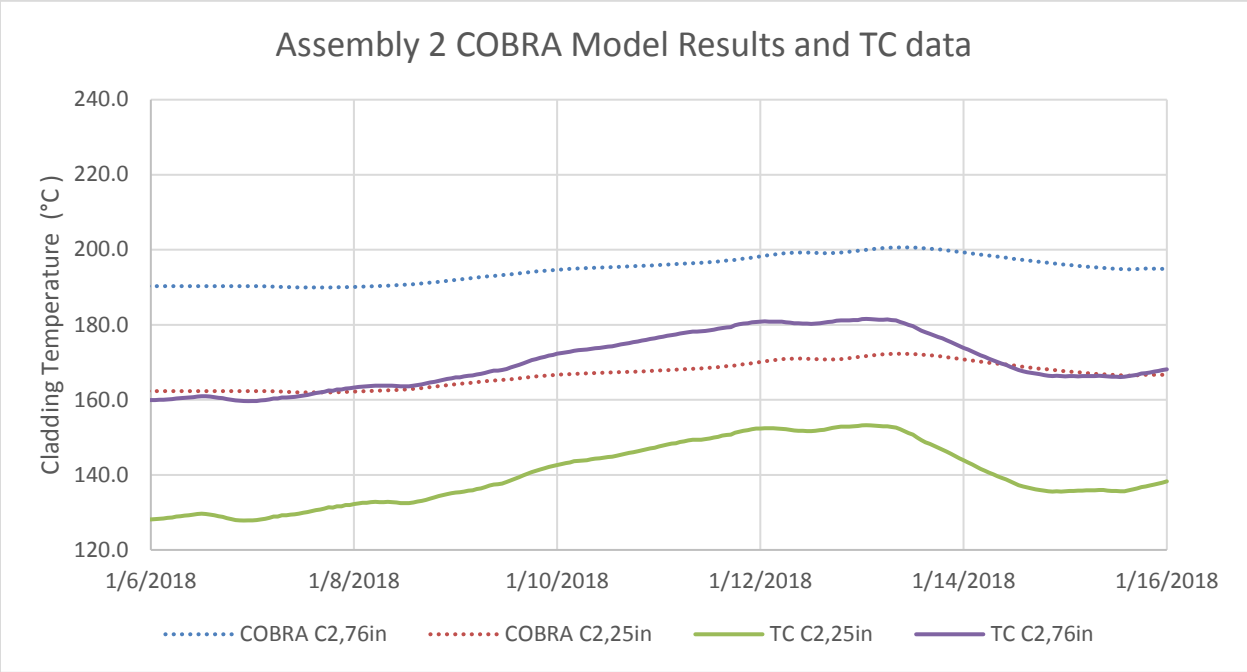

Figure 8.5. COBRA-SFS model Assembly 2 cladding temperature results for Jan. 6th to Jan. 17th

Table 8.2 summarizes the modeled maximum and minimum temperatures for the selected assemblies and axial locations. The differences between the maximum and minimum temperatures were approximately 10°C. In Table 8.1, the differences in measured maximum and minimum thermocouple temperatures were between 22.1°C and 25.4°C. This is a greater change in temperature over the transient period than in the COBRA-SFS model. This may suggest the COBRA-SFS model is not as responsive to ambient temperature as the actual TN32B system sitting on the ISFSI pad, which could be due to other environmental factors that were not considered in the COBRA-SFS model.

Table 8.2. Summary of temperature differences for the COBRA-SFS model

	C14,76 (°C)	C2,76 (°C)	C14,25 (°C)	C2,25 (°C)
Max	230.4	200.6	188.2	172.3
Min	219.9	189.9	177.6	162.0
Diff	10.5	10.7	10.6	10.3

8.1.3 STAR-CCM+ Model Results

Figure 8.6 and Figure 8.7 show the STAR-CCM+ model results for assemblies 14 and 2. As expected, the transient results here are similar to previous COBRA-SFS model results, although the STAR-CCM+ model appears to match the thermocouple data slightly better. The STAR-CCM+ model captures the initial rise in temperatures well but seems to not do quite as well toward the end of the transient. The temperature change from January 13th to January 15th is slower and the magnitude is less in the STAR-CCM+ model than in the measured thermocouple. The difference between this model and the thermocouple data increases toward the end of the transient. Overall, there is a significant difference in

magnitude between the STAR-CCM+ model results and the thermocouple data. These findings are consistent with the previous COBRA-SFS model as well.

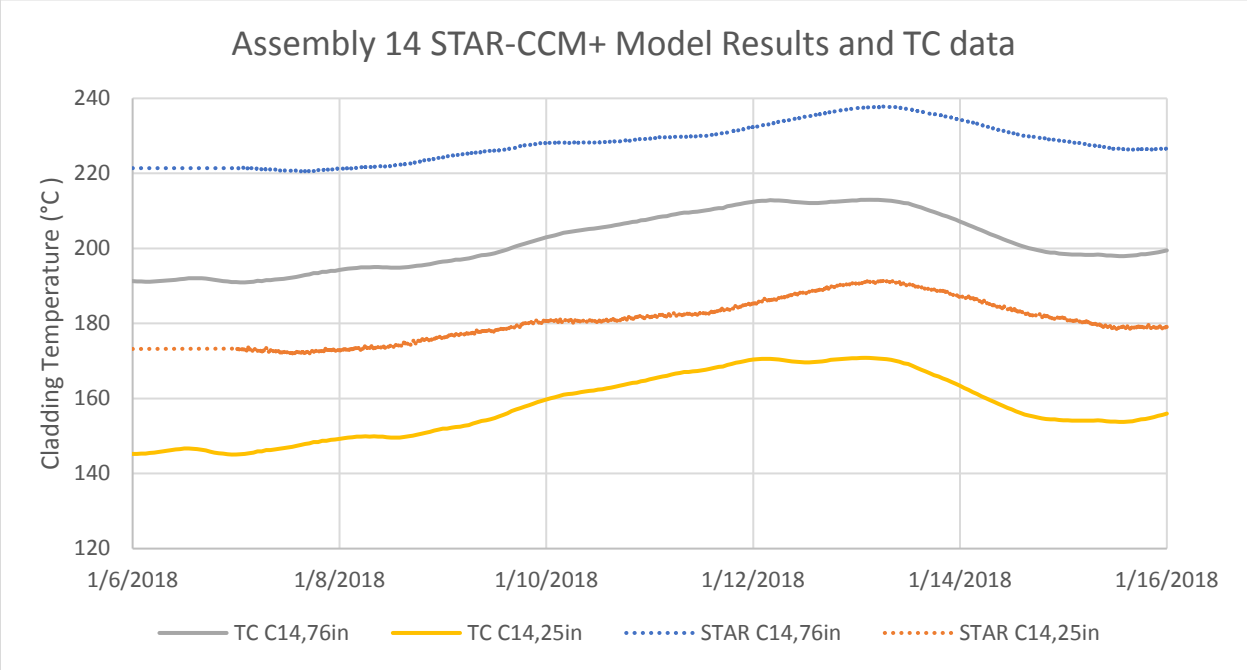

Figure 8.6. STAR-CCM+ model results with thermocouple data for Assembly 14

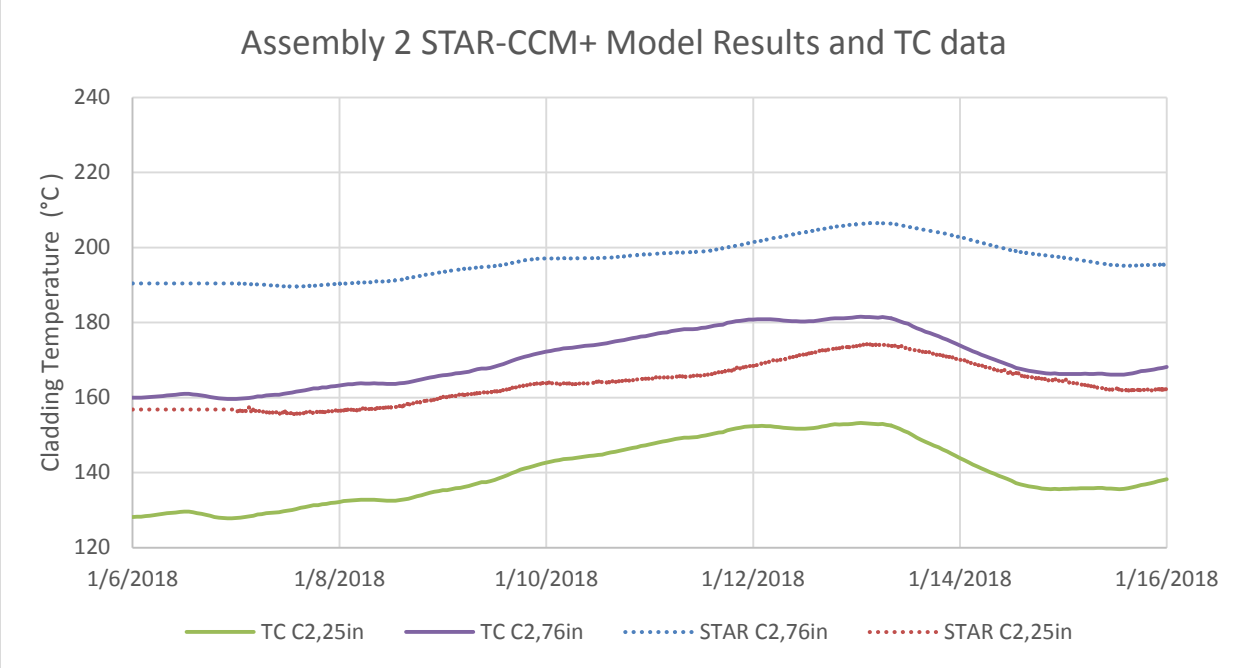

Figure 8.7. STAR-CCM+ model results with thermocouple data for Assembly 2

Table 8.3 summarizes the maximum and minimum temperatures through the transient. The difference between the maximum and the minimum for the selected assemblies was 17.0°C to 19.7°C. This is closer to the measured thermocouple maximum and minimum temperature differentials of 22.1°C to 25.7°C for

the selected assemblies and axial levels. The STAR-CCM+ model appears to be more responsive to the ambient temperature changes than the COBRA-SFS model.

Table 8.3. Summary of STAR-CCM+ maximum and minimum temperatures through the transient period

	C14,76 (°C)	C2,76 (°C)	C14,25 (°C)	C2,25 (°C)
Max	237.9	206.6	191.5	174.6
Min	220.4	189.6	171.8	155.4
Diff	17.5	17.0	19.7	19.2

8.1.4 Model Comparison

The STAR-CCM+ model uses the same inputs as the COBRA-SFS model, so they should be directly comparable. Figure 8.8 and Figure 8.9 compare the COBRA-SFS model results with the STAR-CCM+ results for two axial levels in two different assemblies. At 76 inches above the bottom of the cask the two models are very similar. At this axial level the temperatures for the initial steady-state and end of the transient are almost identical. In the middle of the transient from January 12th to January 14th there is a bit of a discrepancy in temperatures between the two models. The STAR-CCM+ model peaks higher than in the COBRA-SFS model. For the axial level at 25 inches above the bottom of the cask the STAR-CCM+ modeled temperatures start lower and then peak higher than the COBRA-SFS model. The difference between maximum and minimum temperatures for the COBRA-SFS model was from 10.3°C to 10.7°C in the selected assemblies and axial levels (Table 8.2). The STAR-CCM+ model resulted in 17.0°C to 19.7°C difference between maximum and minimum temperatures (Table 8.3). These temperature differences are summarized in Table 8.4. The temperature response for the STAR-CCM+ model is somewhat better than the COBRA-SFS model.

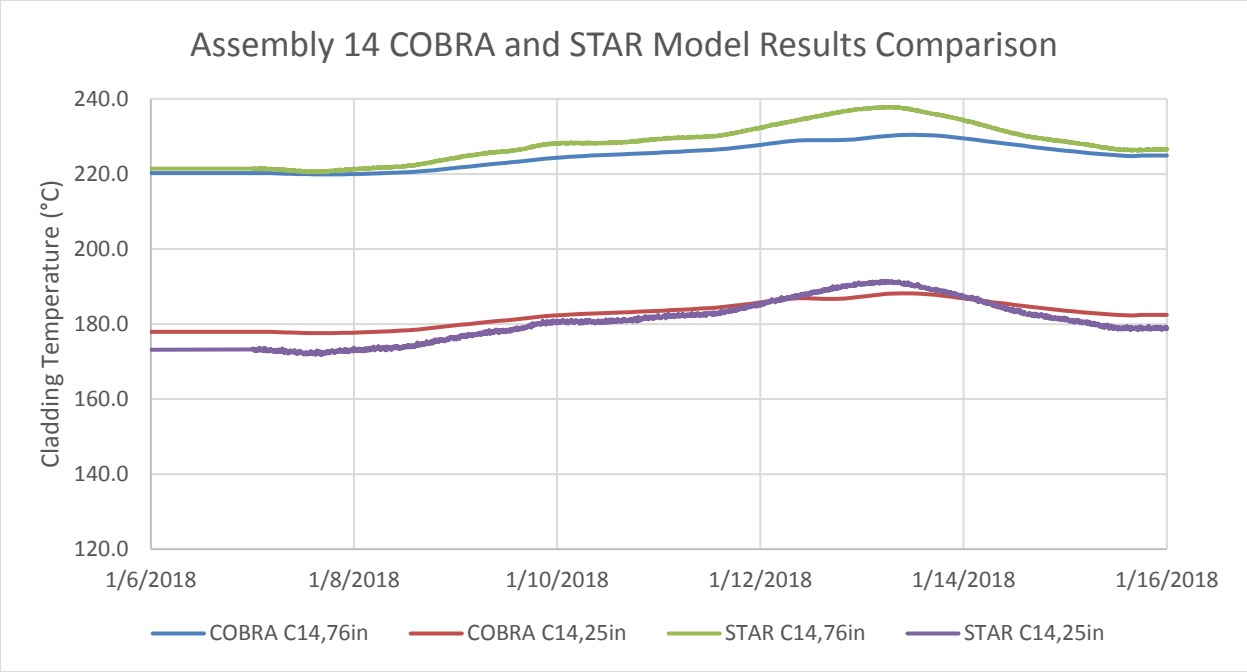

Figure 8.8. COBRA-SFS and STAR-CCM+ model comparison for Assembly 14

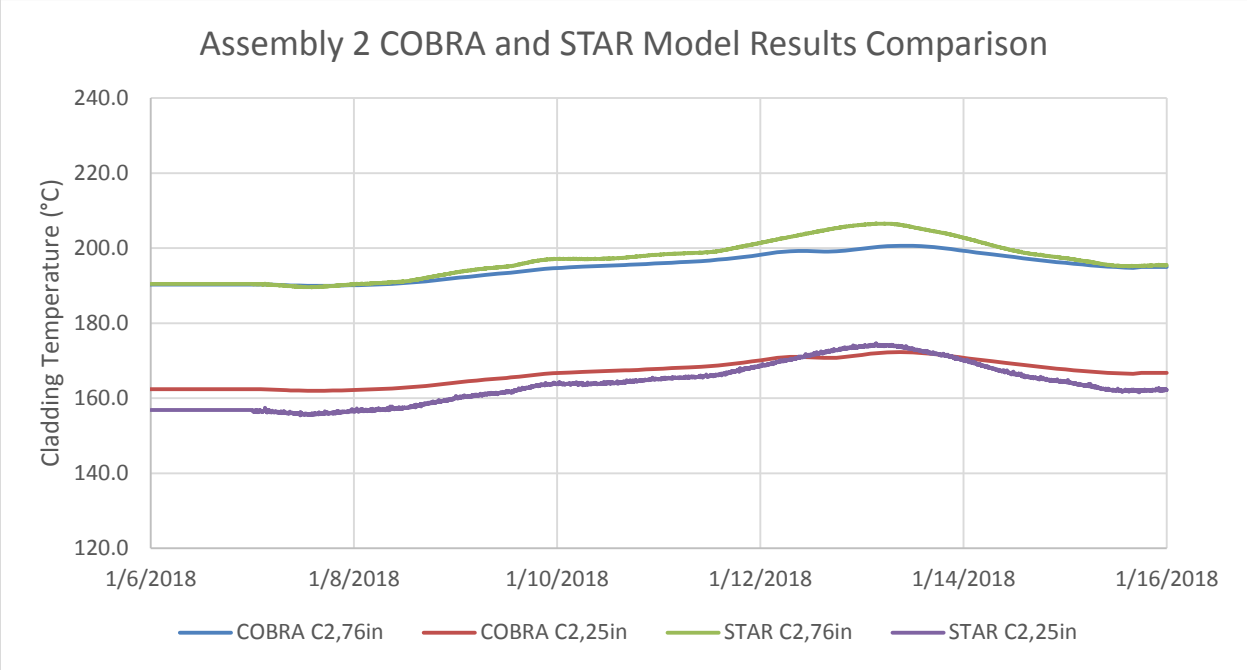

Figure 8.9. COBRA-SFS and STAR-CCM+ model comparison for Assembly 2

Table 8.4 Difference in cladding temperatures between the COBRA-SFS and STAR-CCM+ model

	C14,76		
	COBRA (°C)	STAR (°C)	Diff Between Models (°C)
Max	230.4	237.9	7.5
Min	219.9	220.4	0.5
Diff	10.5	17.5	7.0

	C2,76		
	COBRA (°C)	STAR (°C)	Diff Between Models (°C)
Max	200.6	206.6	6.0
Min	189.9	189.6	-0.3
Diff	10.7	17.0	6.3

	C14,25		
	COBRA (°C)	STAR (°C)	Diff Between Models (°C)
Max	188.2	191.5	3.3
Min	177.6	171.8	-5.8
Diff	10.6	19.7	9.1

	C2,25		
	COBRA (°C)	STAR (°C)	Diff Between Models (°C)
Max	172.3	174.6	2.3
Min	162.0	155.4	-6.6
Diff	10.3	19.2	8.9

8.1.5 Discussion

After examining the modeling results and comparing them to the measured thermocouple data, both the COBRA-SFS and STAR-CCM+ models are capturing the general behavior of the cask and measured thermocouple temperatures. The difference in the maximum and minimum for selected assemblies and axial levels was between 21.9°C and 25.8°C for the thermocouple temperatures. The difference for the COBRA-SFS and STAR-CCM+ models were 10.3°C to 10.7°C and 17.0°C to 19.7°C, respectively. The modeled temperatures were not as responsive as the measured thermocouple temperatures.

Toward the end of the transient both models deviate from the measured thermocouple data. The measured temperatures decrease at a faster rate than the modeled temperature. The models seem to match the initial thermocouple temperature changes well. This inconsistency is likely due to wind effects, which were not initially modeled. Figure 8.10 shows ambient temperature and estimated wind speed on the pad (see Section 2.5). From approximately January 12th to January 15th there appears to be a wind event at about 4 to 5 meters per second. This coincides with the period where the COBRA-SFS and STAR-CCM+ models do not consistently match the measured temperatures. A wind model was developed and implemented to account for these inconsistencies and was applied to Case 2.

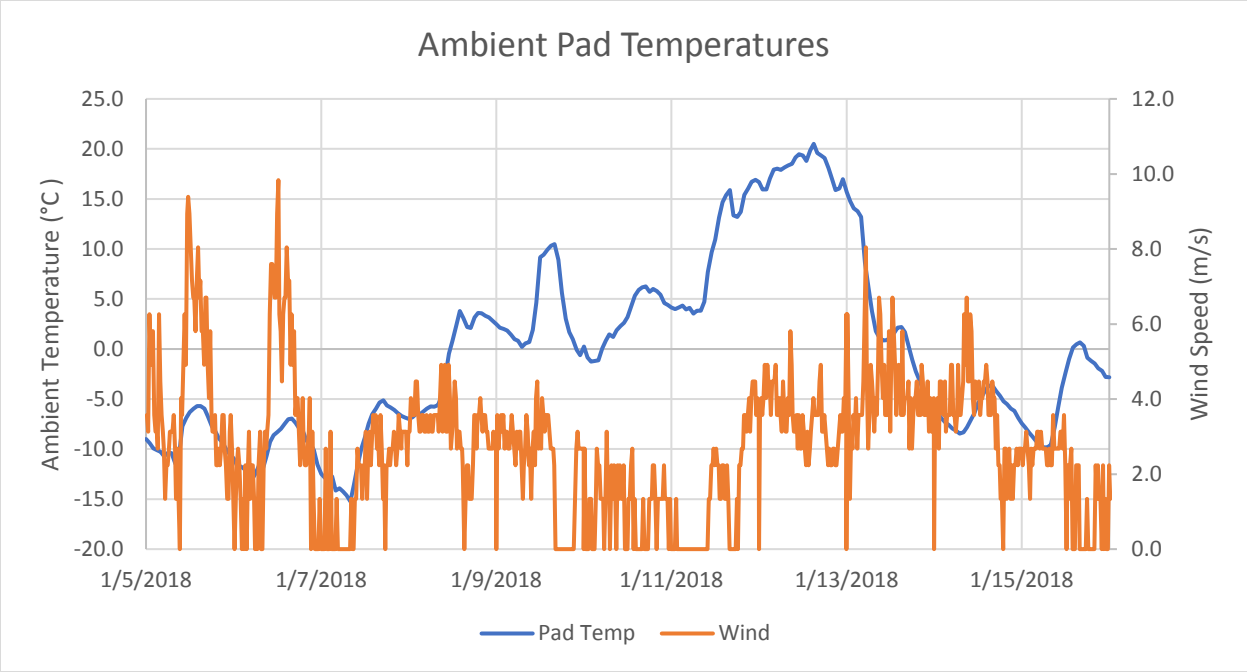

Figure 8.10. Ambient temperatures with wind speed for the transient period

8.2 Case 2: March 1st to March 5th

Case 2 consisted of ambient conditions from March 1st to March 5th, 2018. The conditions in this case were interesting because the ambient temperature appeared to be relatively constant throughout this time period, but the thermocouple measurements exhibited a steep drop in temperature in the 24 hours following March 2nd. Upon further investigation, it was discovered that there was a strong wind present for that 24-hour period. This was the basis for further investigation in Case 2.

8.2.1 Ambient Conditions

The ambient temperatures are presented along with thermocouple temperatures for this case in Figure 8.11. In Figure 8.11 it is easy to see what makes this case unique. The average ambient temperatures decrease a relatively small amount, although there are considerable fluctuations, but there is a much larger drop in thermocouple temperatures over that same 24-hour time period, from March 2nd to March 3rd. In Table 8.5, an 11.4°C difference between maximum and minimum temperatures resulted in a 16.8°C to 19.2°C difference in maximum and minimum thermocouple temperatures for the selected assemblies and axial levels. In the previous case, from January 5th to January 17th, a 35.7°C difference in ambient maximum and minimum temperatures resulted in a 21.9°C to 25.8°C difference between maximum and minimum thermocouple temperatures (Table 8.1). If ambient temperatures were the only factor contributing to the change in thermocouple temperatures it is expected that the change in ambient temperatures for these two cases will result in consistent changes in thermocouple temperatures. But when making this comparison between the two cases the resulting thermocouple changes are not similar. After finding this anomaly other ambient conditions were considered.

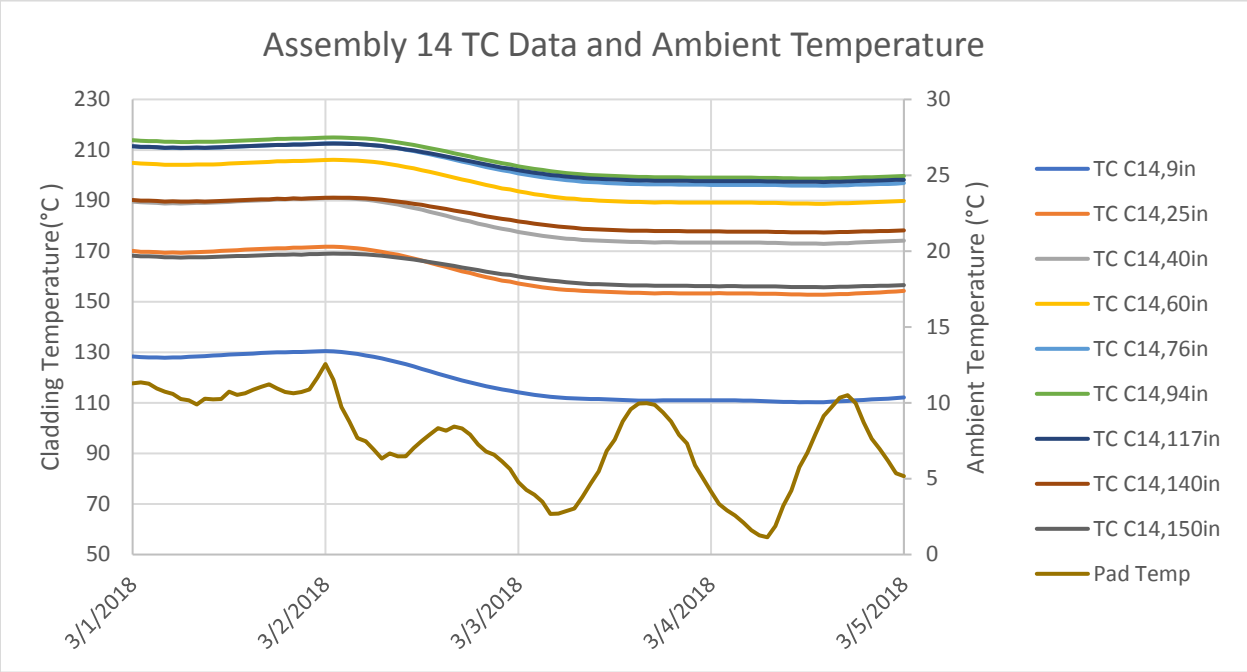

Figure 8.11. Ambient temperatures and thermocouple data for Mar. 1st to Mar. 5th

Table 8.5. Summary of thermocouple and ambient temperature differences

	C14,76 (°C)	C2,76 (°C)	C14,25 (°C)	C2,25 (°C)	Ambient (°C)
Max	212.7	181.3	171.7	153.7	12.6
Min	195.9	164.0	152.8	134.5	1.1
Diff	16.8	17.3	18.9	19.2	11.5

Further investigation into the ambient conditions for this transient period revealed a significant wind event. In Figure 8.12 it is clear a significant wind event coincides with a steep drop in in thermocouple temperatures inside the cask. The peak wind speed reached 16.1 m/s between March 2nd and March 3rd, 2018. A 16.1 m/s wind is very fast (36 mph) and could have a significant effect on the heat rejection ability of the storage cask. The average wind speed between March 2nd and March 3rd is 10.1 m/s (22.6 mph) followed by an average wind speed of 5.1 m/s (11.4 mph). For the initial "steady-state" period from February 26th to March 2nd the average wind speed was 2.0 m/s (4.5 mph). These are dramatic changes in wind speed in three distinct periods throughout the transient. The differences in wind speed could have a significant effect on temperatures inside of the cask.

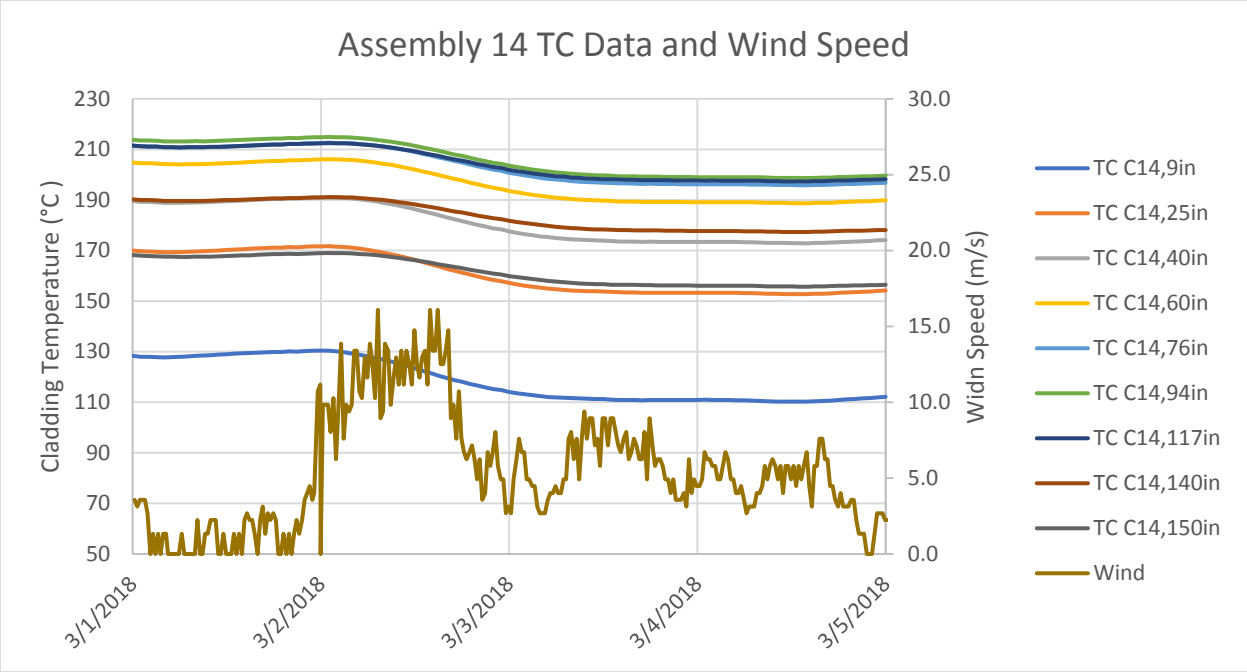

Figure 8.12. Thermocouple temperature from Assembly 14 and estimated pad wind speed

8.2.2 Wind Modeling

After considering the ambient conditions in this case it was determined that a boundary model that includes the effects of wind, or more specifically forced convective heat transfer, is required to accurately model the thermocouple temperatures. In the current models, heat transfer at the boundary of the cask and ambient are modeled based on free convection using the Grashof, Prandtl, and Nusselt number (Michener et al. 2017). The Grashof number is (Incropera et al. 2002)

$$\mathrm{Gr_L} = \frac{g\beta(T_s - T_\infty)L^3}{\nu}. \quad (1)$$

With the Prandtl number and a few other coefficients dependent on the model parameters the Nusselt number can be determined (Incropera et al. 2002)

$$\mathrm{Nu_L} = C(\mathrm{GrPr})^n. \quad (2)$$

From this, the overall heat transfer coefficient for free convection can be determined (Incropera et al. 2002)

$$h = \frac{\mathrm{Nu}k}{D}. \quad (3)$$

This model works very well for situations in which there is no wind or in safety analyses. However, in this case the objective is to model real-world transient conditions with wind. As seen earlier, free convection alone cannot accurately model the behavior of the TN-32B cask.

8.2.2.1 Assumptions/Simplifications

In order to model the effects of wind on heat transfer on the TN-32B cask, the following assumptions were made:

- The free, forced, or combined free and forced heat transfer is represented by a heat transfer coefficient dependent on ambient wind conditions;

- The cask is a long cylinder with the same diameter for its entire length (only applies to determining the heat transfer coefficient);
- The top of the cask is a flat plate;
- Wind conditions on the pad at North Anna Nuclear Power Generation Station are well represented by the Louisa Country Freeman Airfield where the wind data was collected (NOAA 2019);
- There are no obstructions, other storage casks, or anything else that could disrupt the wind flowing around the cask; and
- The wind direction is perpendicular to the vertical axis of the cask.

8.2.2.2 Wind Model Description

To adapt the current COBRA-SFS and STAR-CCM+ TN-32B models to incorporate forced convection, a new model for the heat transfer coefficient at the boundary of the ambient and side of the cask needed to be implemented. This new model was created by including the wind speed in the form of the Reynolds number in a forced convection correlation for the Nusselt number. The Reynolds number is defined as (Incropera et al. 2002)

$$\mathrm{Re_L} = \frac{\rho \mathrm{UL}}{\mu}. \tag{4}$$

Where U is the velocity of the wind and L is the diameter of the cask. Since the cask is being treated as a cylinder in cross flow, the diameter of the cask is the same as the length of the "plate" on the top of the cask. The Reynolds number for the side and the top of the cask are the same.

The major difference between how the side of the cask and the top of the cask are modeled is the correlation used for the Nusselt number. For the side of the cask, which is treated as a cylinder in cross flow, Incropera, et al. (2002) gives

$$\mathrm{Nu_L} = 0.3 + \frac{0.62\mathrm{Re_L^{1/2}Pr^{1/3}}}{[1+(0.4/\mathrm{Pr})^{2/3}]^{1/4}}\left[1+\left(\frac{\mathrm{Re_L}}{282000}\right)^{5/8}\right]^{4/5} \tag{5}$$

and for the top of the cask (flow over a flat plate), the Nusselt number is given as

$$\mathrm{Nu_L} = 0.664\mathrm{Re_L^{1/2}Pr^{1/3}}. \tag{6}$$

From the Nusselt number the heat transfer coefficient can be determined and applied to the ambient boundaries of the cask using Equation (6) (Incropera et al. 2002).

$$\mathrm{Nu}_L = \frac{\bar{h}L}{k} \tag{7}$$

This method is appropriate for approximating the heat transfer when forced convection is the dominant mode of heat transfer. But forced convention is not always the dominant mode. In the first part of the transient for this case the wind speeds are relatively calm. This allows solving for the initial condition using a steady state solution. To determine the dominant mode of heat transfer the Richardson number is used

$$\mathrm{Ri} = \frac{\mathrm{Gr_L}}{\mathrm{Re_L^2}} \tag{8}$$

When the Richardson number is in the range of from one to ten, free and forced convection must be considered simultaneously. If the Richardson number is less than one, then forced convection is dominant. If the Richardson number is greater than ten then free convection is dominant (Incropera et al.

2002). The combined heat transfer coefficient is complicated because most of the information is from experimental data and no direct analytical solutions are readily available. In Incropera et al. (2002), an approximation for a combined Nusselt number is suggested for a cylinder in cross flow, given in Equation (9).

$$\mathrm{Nu}^4 = \mathrm{Nu}_{free}^4 + \mathrm{Nu}_{forced}^4 \tag{9}$$

This approximation is less accurate when attempting to determine the overall heat transfer coefficient due to the air flow of free convection being perpendicular to the flow of forced convection. For free convection, the Grashof number used to determine the Nusselt number is determined using the length of the cask. For forced convection, the Nusselt number is determined using the Reynolds number and the diameter of the cask. The length scales used to determine the heat transfer coefficient are different between free and forced convection. In this model, the combined heat transfer coefficient for the side of the cask is given by Equation (10).

$$h^4 = h_{free}^4 + h_{forced}^4 \tag{10}$$

This expression was used for this study but should still be considered an approximation. Further investigation into the effects of perpendicular forced and free convection flow may be necessary for future studies.

The top of the cask is more straightforward because the length scales used in determining the heat transfer coefficient are the same. The combined Nusselt number for a flat plate suggested by Incropera et al. (2002) was given as

$$\mathrm{Nu}^{7/2} = \mathrm{Nu}_{free}^{7/2} + \mathrm{Nu}_{forced}^{7/2}. \tag{11}$$

From there, Equation (3) was used to find the combined heat transfer coefficient. For both COBRA-SFS and STAR-CCM+ models, the boundary between the cask system and the environment is treated as a simple heat transfer connection. The wind dependent heat transfer coefficient provides a simple and effective way of modeling the effects of wind that is easily implemented in COBRA-SFS and STAR-CCM+.

8.2.3 COBRA-SFS Model Results

In order to better explore the effect of wind on the modeled cladding temperatures two COBRA-SFS models were developed. One model included wind effects and the other did not.

8.2.3.1 COBRA-SFS Model with No Wind

Figure 8.13 and Figure 8.14 show the COBRA-SFS model results without wind and the thermocouple data overlaid. The COBRA-SFS results are significantly different than the thermocouple data from inside of the cask. For every instance the COBRA-SFS model gives higher temperatures and apparently insensitive to the apparent transient condition that is occurring. From this it is easy to see that there is a major shortcoming in the model. This continues to enforce the previous hypothesis that there is another factor driving the transients other than ambient temperature change.

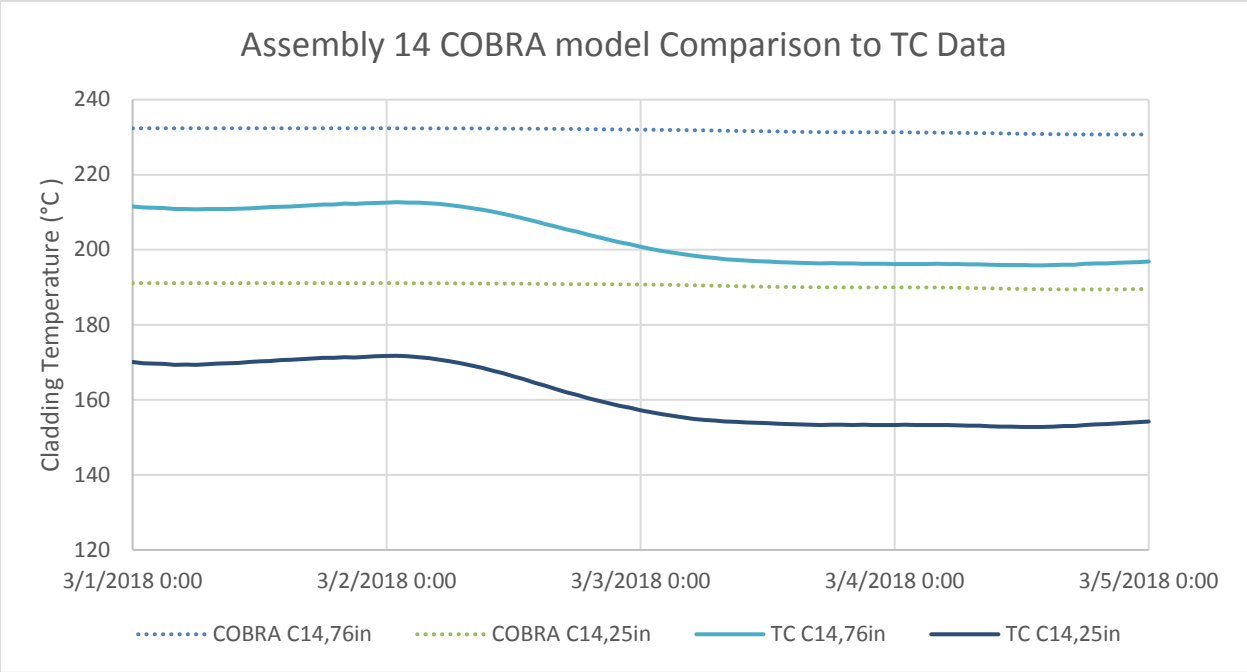

Figure 8.13. COBRA-SFS model without wind and thermocouple data for Assembly 14

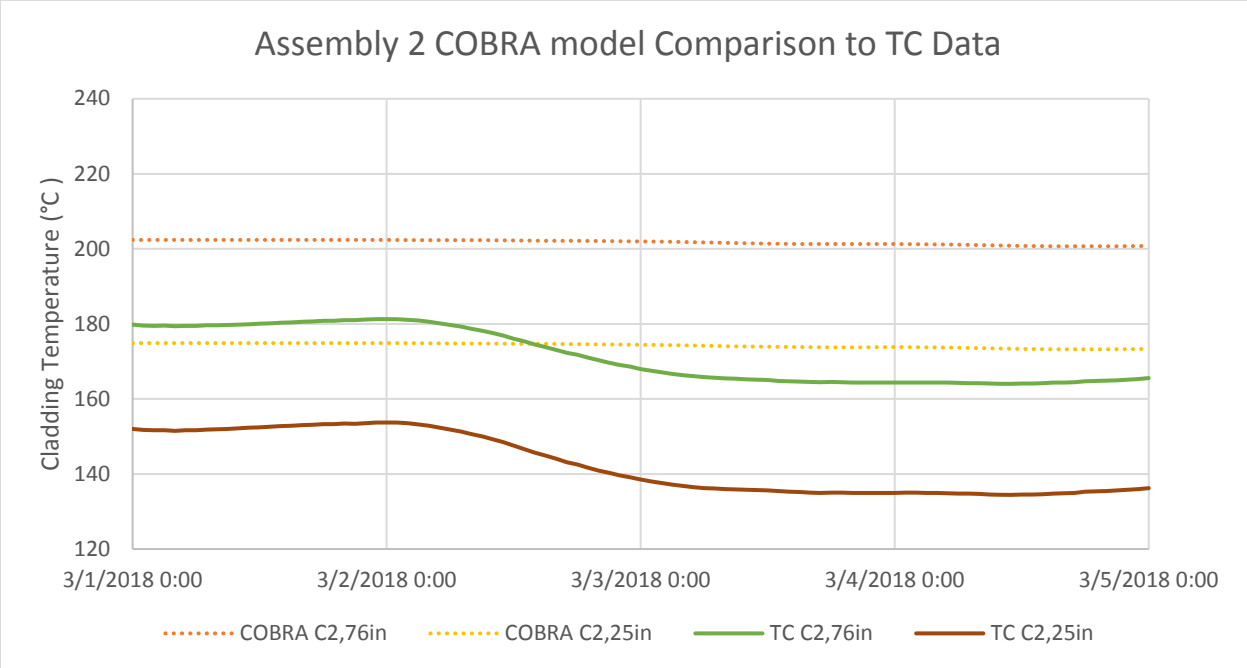

Figure 8.14. COBRA-SFS model without wind and thermocouple data for Assembly 2

Table 8.6 summarizes the temperature differences for the COBRA-SFS model. There is approximately a 1.7°C difference between the maximum and minimum temperatures regardless of assembly and thermocouple position. This is a very different result from the thermocouple data from the same transient

period. Looking back at Table 8.5, the thermocouple temperature differences were between 16.8°C and 19.2°C.

Table 8.6. Summary of differences in temperatures for the COBRA-SFS model without wind

	C14,25 (°C)	C14,76 (°C)	C2,25 (°C)	C2,76 (°C)
Max	191.1	232.4	174.9	202.4
Min	189.4	230.7	173.2	200.7
Diff	1.7	1.7	1.7	1.7

8.2.3.2 COBRA-SFS Model with Wind

The results of the implemented wind model are shown in Figure 8.15 for COBRA-SFS and Figure 8.16 for STAR-CCM+. When we examine these graphs, the COBRA-SFS model better fits with the thermocouple data. The initial steady-state temperatures are cooler and closer to the thermocouple temperature data. Also, the model better reflects the transient changes in temperatures over the previous model where the effects of wind were not considered. These results further support the hypothesis that wind is a significant factor contributing to the temperature changes within the cask.

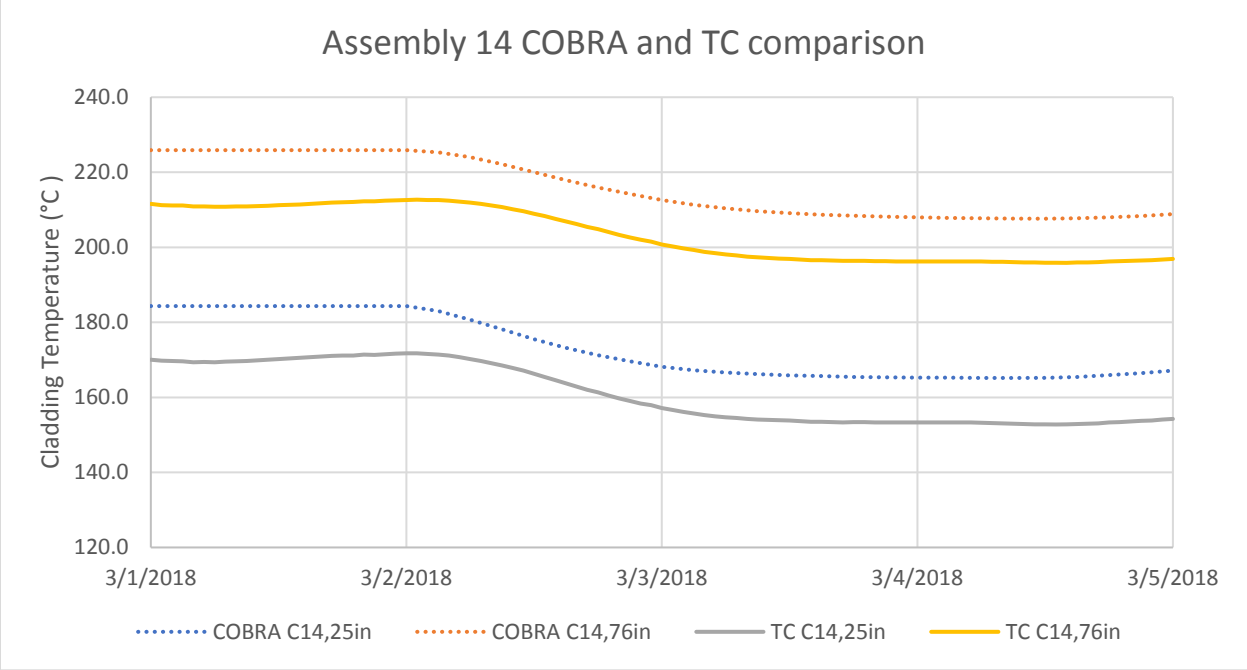

Figure 8.15. COBRA-SFS model with wind and thermocouple results for Assembly 14

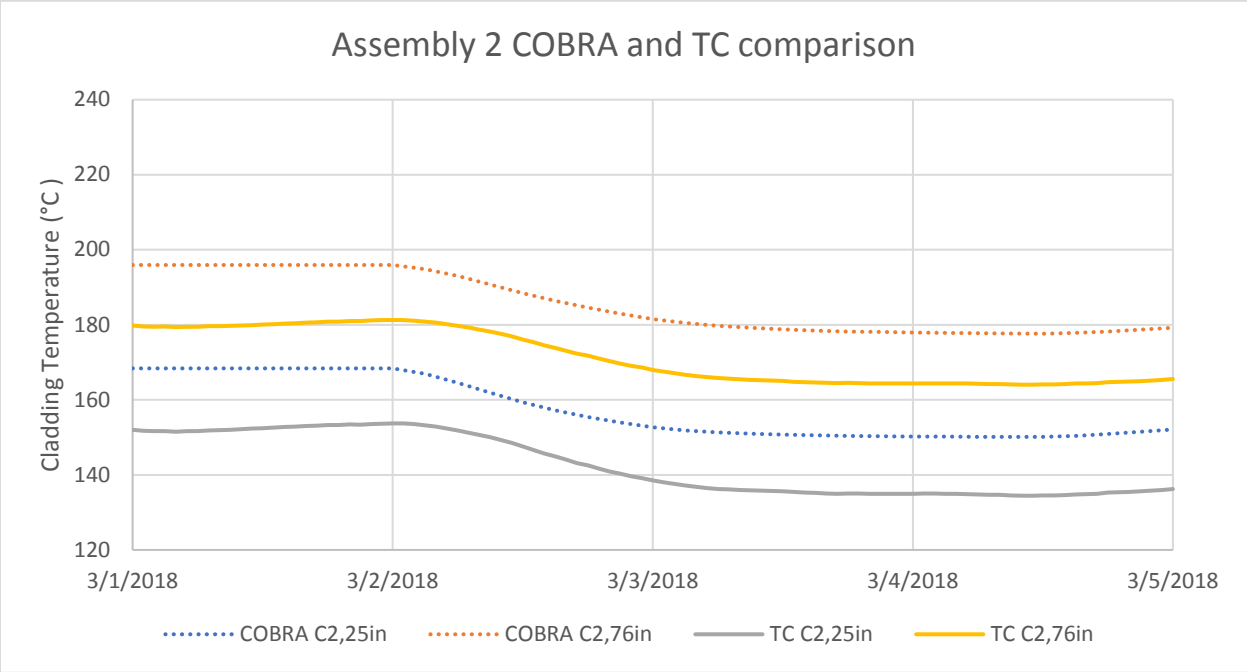

Figure 8.16. COBRA-SFS model with wind and thermocouple results for Assembly 2

Although the temperatures from the COBRA-SFS model remain higher than the thermocouple data for this exercise, the changes in temperature throughout the transient are very similar to the changes in the measured thermocouple data. Table 8.7 summarizes the maximum and minimum temperatures throughout the transient. For this COBRA-SFS model, the difference between the maximum and the minimum were between 18.3°C and 19.1°C which is very close to the 16.8°C and 19.2°C range of the thermocouple data.

Changes in the COBRA-SFS model are more homogenous than in the thermocouple data. The differences between the maximum and minimum temperatures in the COBRA-SFS model are similar regardless of the position inside the cask whereas in the thermocouple data there is a distinct variation between the difference in maximum and minimum temperatures depending on the measurement location. For the COBRA-SFS model temperature in Assembly 14 at 76 inches above the bottom of the cask the temperature change was 18.3°C versus 16.8°C for the thermocouple temperature at the same location. Future investigation into this inconsistency could improve the COBRA-SFS model.

Table 8.7. Summary of COBRA model with wind temperature differences

	C14,76 (°C)	C2,76 (°C)	C14,25 (°C)	C2,25 (°C)
Max	225.9	195.9	184.3	168.4
Min	207.6	177.6	165.2	150.1
Diff	18.3	18.3	19.1	18.3

8.2.4 STAR-CCM+ Model Results

To provide a comparison with the COBRA-SFS models, two STAR-CCM+ models were developed for this case. The results of both no wind and wind models are presented. Running the models in both software packages helps validate the methods employed in this effort.

8.2.4.1 STAR-CCM+ Model with No Wind

Figure 8.17 and Figure 8.18 show the results of the STAR-CCM+ model without wind. Comparing this to the previous COBRA-SFS model in Figure 8.13 and Figure 8.14, these results are very similar. The same pattern where the modeled temperatures are not changing throughout the transient is present here as well. Also, the modeled temperatures are 15°C to 20°C hotter than the thermocouple data. This provides further support that the changes in thermocouple temperature inside of the cask on the ISFSI pad are not just driven by changes in ambient temperature.

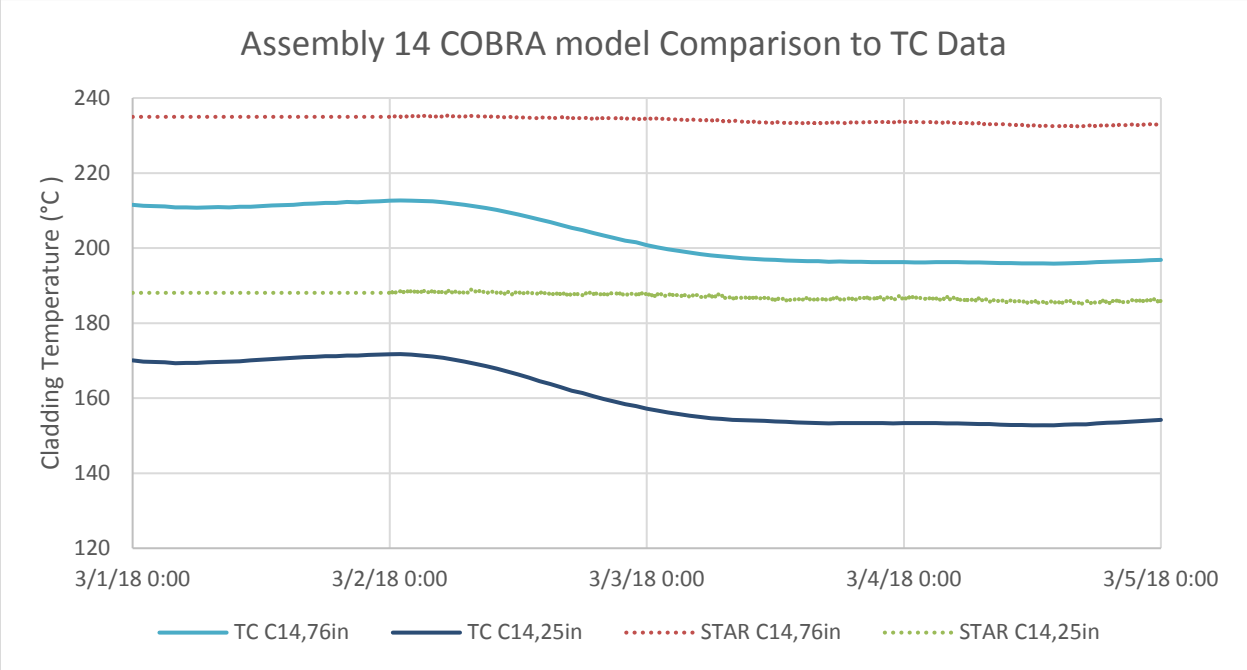

Figure 8.17. STAR-CCM+ model without wind comparison to thermocouple data for Assembly 14

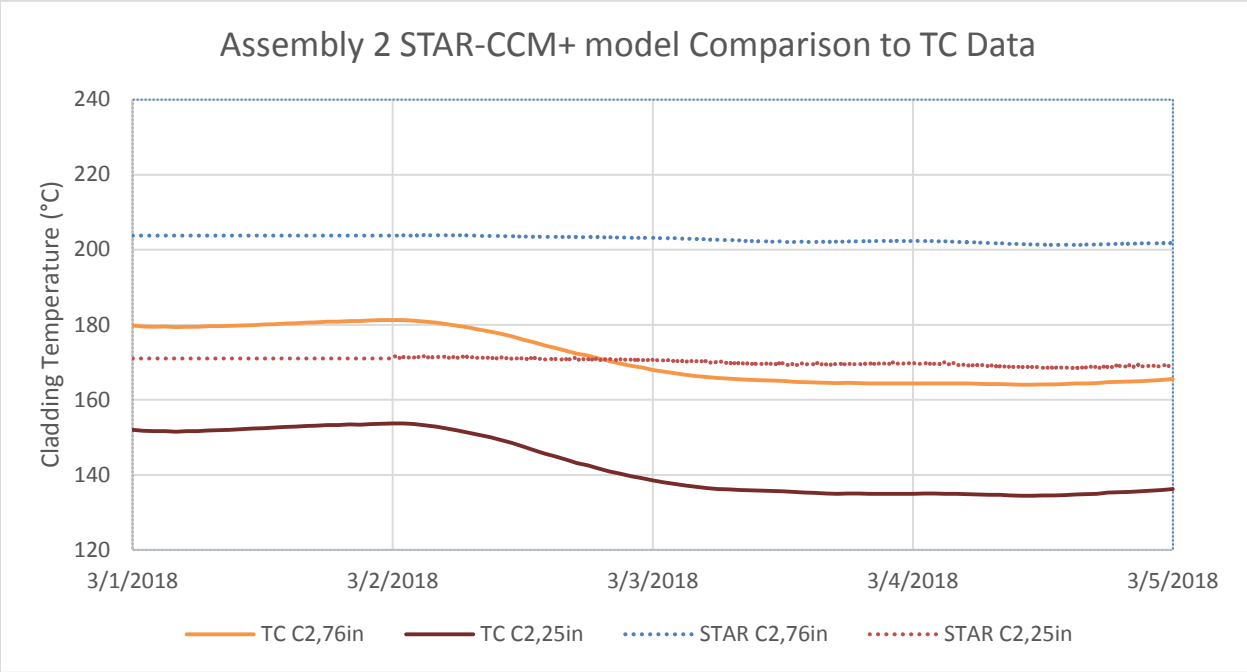

Figure 8.18. STAR-CCM+ model without wind comparison to thermocouple data for Assembly 2

As shown in Table 8.8, the STAR-CCM+ model appears to be a bit more responsive than the COBRA-SFS model (Table 8.6). There is about a 1-2°C greater difference between the maximum and minimum temperatures in this model than in the COBRA-SFS model. Another interesting note is that there is a greater difference between maximum and minimum on the lower "thermocouple" locations with Assembly 14, 25 inches above the bottom of the cask having the highest temperature difference. This pattern is similar to the thermocouple data.

Table 8.8. STAR-CCM+ model without wind differences in temperature throughout transient

	C14,76 (°C)	C2,76 (°C)	C14,25 (°C)	C2,25 (°C)
Max	235.3	203.9	189.0	171.7
Min	232.4	201.3	185.1	168.4
Diff	2.9	2.6	3.9	3.3

8.2.4.2 STAR-CCM+ Model with Wind

Figure 8.19 and Figure 8.20 show the results for the STAR-CCM+ model with wind considered. Including wind effects in the model has had a significant impact on the results of the model. This model with wind is much closer the actual thermocouple data. This provides confirmation to our initial hypothesis that wind has a significant effect on heat transfer out of the cask. The modeled temperatures 25 inches from the bottom for both assemblies appear to better fit the thermocouple data than the modeled temperatures in the middle of the cask.

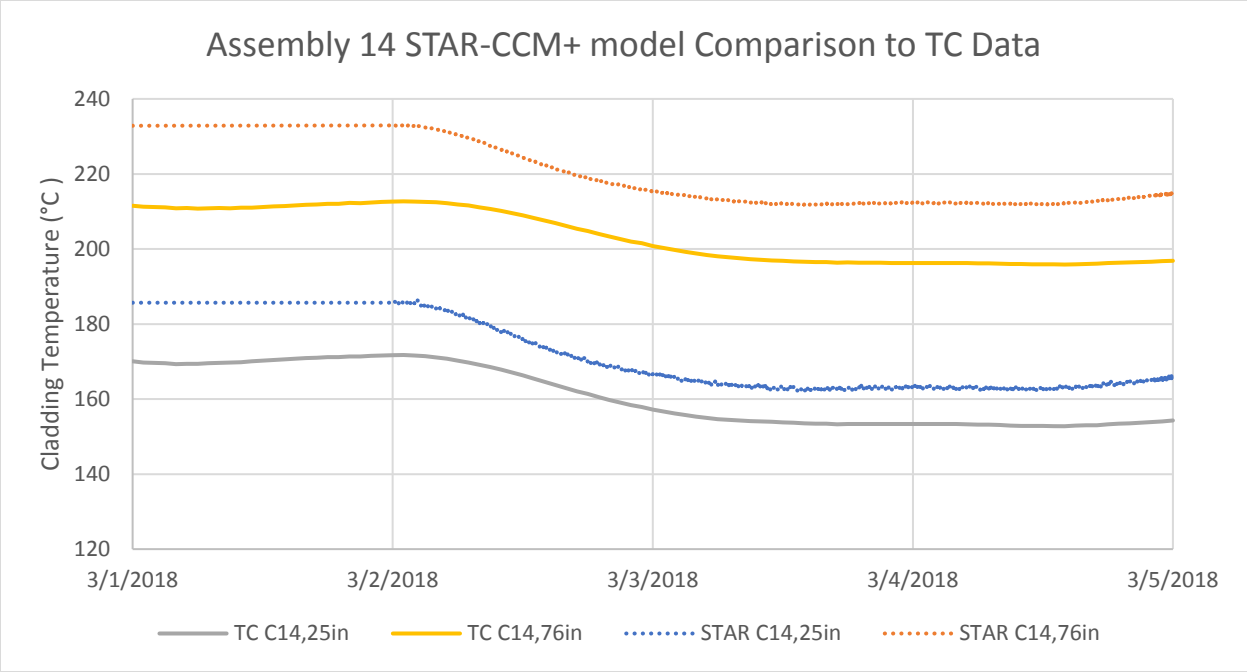

Figure 8.19. STAR-CCM+ model with wind results and thermocouple data for Assembly 14

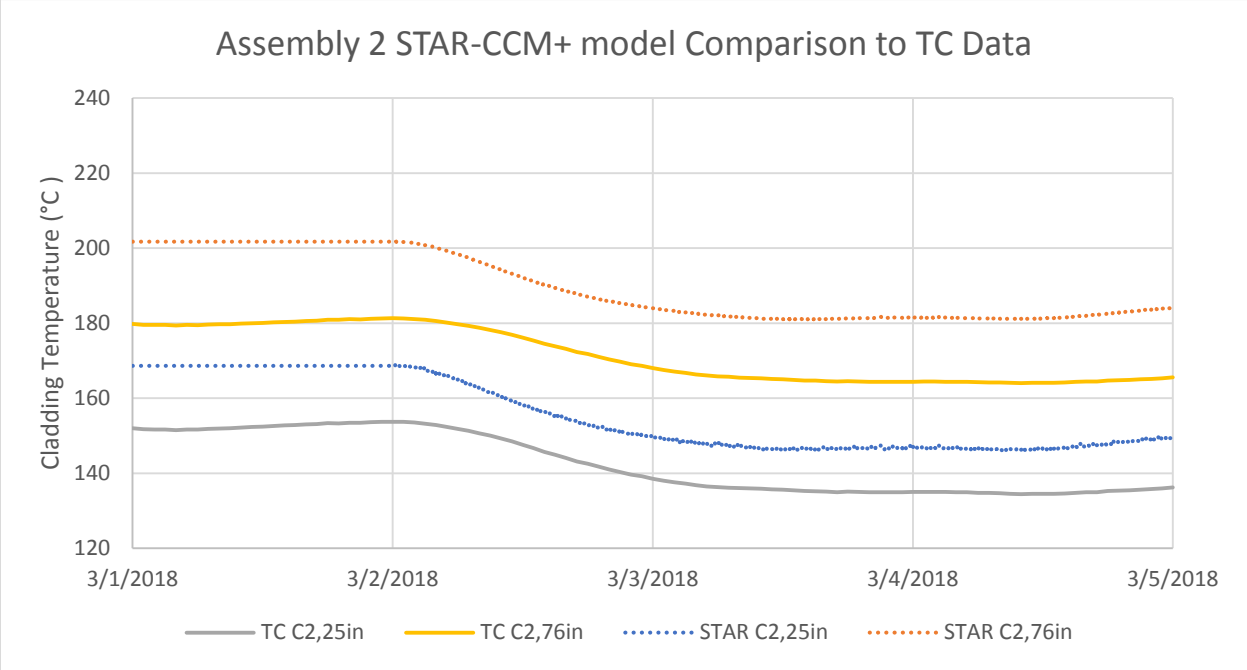

Figure 8.20. STAR-CCM+ model with wind results and thermocouple data for Assembly 2

Table 8.9 summarizes the differences between the maximum and minimum temperatures in the STAR-CCM+ model with wind. In this model the differences between the maximum and minimum are much closer to the difference in maximum and minimums for the thermocouple data. This is a good indication that the model considering the effects of wind is a better predictor of temperatures inside of the cask. The differences in the STAR-CCM+ model ranged from 21.3°C to 23.0°C for the selected assemblies and

axial levels. The thermocouple temperature difference range was 16.9°C to 19.3°C. The STAR-CCM+ model seems to have overshot modeling the temperature changes throughout this transient.

Table 8.9. Summary of differences in temperatures for STAR-CCM+ model with wind

	C14,76 (°C)	C2,76 (°C)	C14,25 (°C)	C2,25 (°C)
Max	233.0	201.8	186.3	169.0
Min	211.7	180.9	162.1	146.0
Diff	21.3	20.9	24.2	23.0

8.2.5 Model Comparison

Figure 8.21 and Figure 8.22 show the COBRA-SFS, and STAR-CCM+ modeled temperatures with wind for this transient period. The COBRA-SFS and STAR-CCM+ models that include wind better matched the thermocouple data and were selected for comparison in this section. The COBRA-SFS and STAR-CCM+ models are very close to each other. In the case of Assembly 2, 25 inches above the bottom of the cask the initial steady-state temperatures are almost identical as well as the first 12 hours of the transient. Through the middle of the transient to the end the temperatures for the COBRA-SFS model are slightly hotter. In the middle of the cask the two models differ more, but by only about 7°C at most.

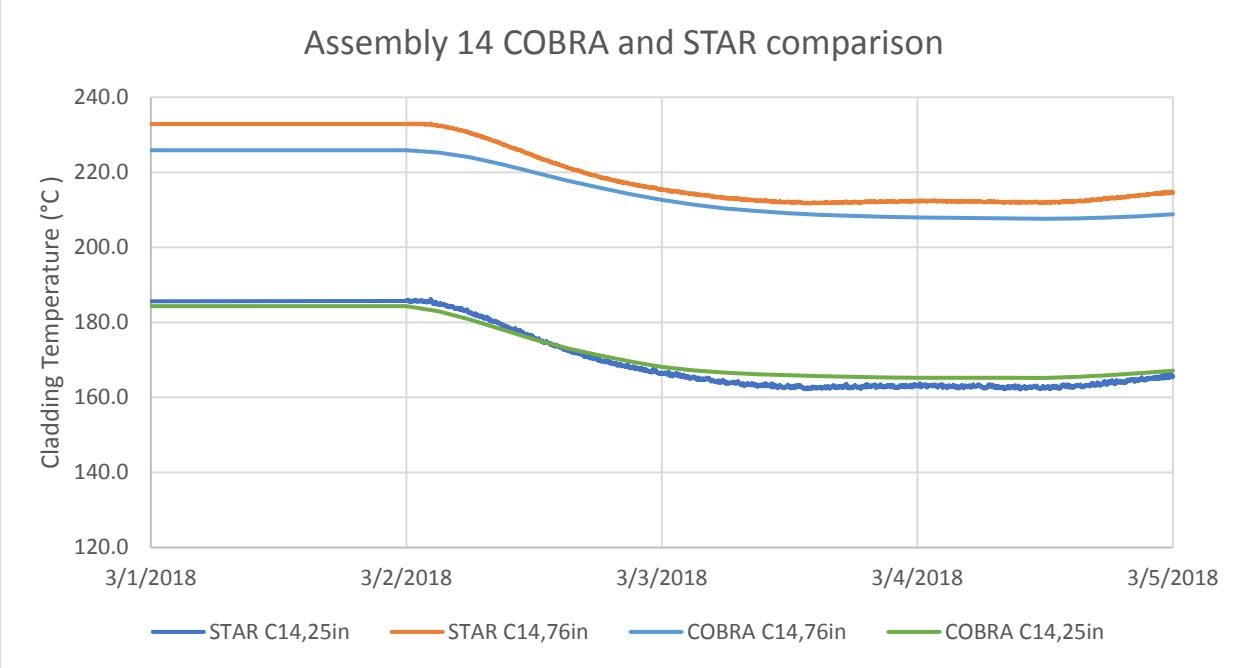

Figure 8.21. Models with wind comparison with thermocouple data for Assembly 14

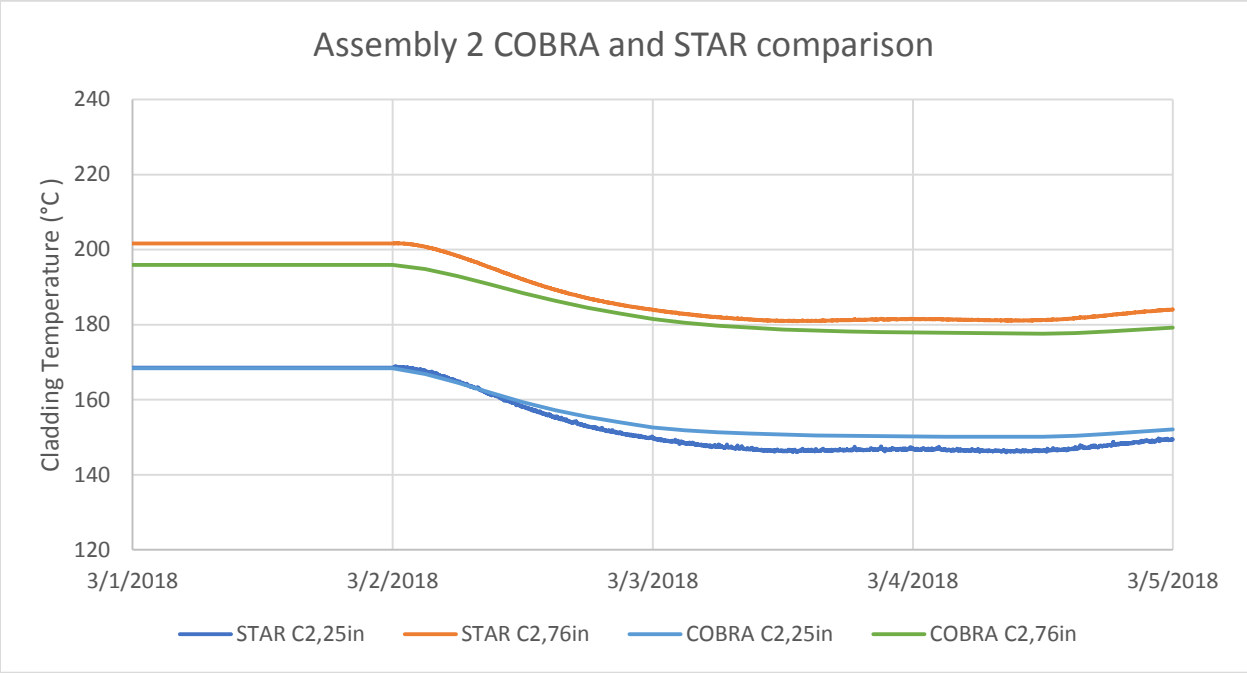

Figure 8.22. Models with wind comparison with thermocouple data for Assembly 2

Table 8.10 summarizes the difference between the maximum and minimum temperatures for both models and the thermocouple data. The COBRA-SFS model and the STAR-CCM+ models showed similar results. The difference between the two models was less than 7.1°C for the maximum and minimum temperatures. The temperature change for the COBRA-SFS model was in the range of the thermocouple data. The STAR-CCM+ temperature change through the transient was greater than the thermocouple data.

Table 8.10. Summary of transient maximums and minimums

	C14,76		
	COBRA (°C)	STAR (°C)	Difference Between Models (°C)
Max	225.9	233.0	7.1
Min	207.6	211.7	4.1
Diff	18.3	21.3	3.0

	C2,76		
	COBRA (°C)	STAR (°C)	Difference Between Models (°C)
Max	195.9	201.8	5.9
Min	177.6	180.9	3.3
Diff	18.3	20.9	2.6

	C14,25		
	COBRA (°C)	STAR (°C)	Difference Between Models (°C)
Max	184.3	186.3	2.0
Min	165.2	162.1	-3.1
Diff	19.1	24.2	5.1

	C2,25		
	COBRA (°C)	STAR (°C)	Difference Between Models (°C)
Max	168.4	169.0	0.6
Min	150.1	146.0	-4.1
Diff	18.3	23.0	4.7

	Thermocouple			
	C14,76 (°C)	C2,76 (°C)	C14,25 (°C)	C2,25 (°C)
Max	212.7	181.3	171.7	153.7
Min	195.9	164.0	152.8	134.5
Diff	16.8	17.3	18.9	19.2

8.3 Further Wind Modeling

The wind models described in the previous section were an initial start and yielded results that were closer to the measured data than when wind was not considered. The wind modeling strategies can be further developed, especially the STAR-CCM+ model. In the STAR-CCM+ model for this study wind was modeled by changing the heat transfer coefficient at the boundary between the side of the cask and the ambient. An interesting and possibly more realistic approach would be to model a flow field around the cask in STAR-CCM+. An external flow model is not possible in COBRA-SFS due to the nature of the program. The external flow method of modeling wind was not utilized in this study due to increased complexity and computational expense over the simpler boundary heat transfer coefficient model. The external flow field could produce more realistic results because it would eliminate a number of simplifications made in the current wind model. Also, the thermal interactions between multiple casks on the pad can be modeled utilizing the external flow field. One situation where thermal interaction between storage casks could be significant is if one cask was sitting in the wind eddy of another cask. Implementing the external flow field model is a next step and could provide solutions to a more diverse set of applications. Assessing the accuracy of such a model would require wind speed and direction data, preferably measured at the ISFSI location.

Another topic of further research is to apply the wind model to different casks. One example would be to apply a wind model of a cask to a canisterized system. These storage systems typically have a large concrete overpack around the canister. This large overpack could hinder the effects from wind but it could have a significant effect on the vents that enable free convection around the inner canister. An external flow field would be required in this case due to the increased complexity of the vented overpack. Applying this wind modeling to other casks would provide a comparison with the TN-32B cask wind modeling presented here.

9. CONCLUSIONS AND RECOMMENDATIONS

The work presented in this report shows that the codes and methods used for simulating the transient response of spent fuel casks can capture the behavior of the fuel over a wide range of conditions. The utility of the codes used in this report has been long established for engineering and safety analysis. However, the relative lack of data on actual vacuum drying operations has limited the development of a best estimate methodology that can be readily applied. The dataset presented in this report is unique and extensive for the field of spent fuel thermal analysis. However, there are still gaps in knowledge that prevent a definitive, readily applicable best estimate methodology from being implemented. The only way to definitively close these gaps will be with tightly controlled and monitored experimental tests from benchtop to full scale. By modeling these experiments it will be possible to isolate the effects and behavior of the unknown parameters that have been discussed in this report. The authors have some specific conclusions and recommendations presented below.

9.1 Conclusions

- The COBRA-SFS models gave very good results compared to measured temperatures in fuel assemblies. The unique aspects of the code allowed for quick solutions on practical computing hardware.
- The STAR-CCM+ detailed models produced results that were nearly as good as COBRA-SFS and demonstrated the feasibility of this approach, when such models are required.
- The STAR-CCM+ porous media model predictions were least accurate and are not generally useful for modeling a vacuum drying transient with changing fluid conditions.
- The STAR-CCM+ porous media and the COBRA-SFS models were successfully applied to predicting fuel temperature response to changes in ambient temperature and wind speeds.

9.2 Recommendations

For improved understanding of modeling thermal response of metal casks to ambient conditions:

- Model wind effects with a well characterized measured wind speed and direction from directly adjacent to the cask
- Compare a detailed external flow model to the current cask model with wind speed corrected convective boundary condition to determine range of applicability of the current model.

To further understand the vacuum drying process and transient cask thermal modeling:

- Model tests with more measurement points in space and time such that well defined and accurate initial and boundary conditions can be used in modeling.
- Characterize the cask fluid environment through the draining blowdown and drying process so that accurate fluid solutions can be implemented
- Characterize gap closure behavior through time and in response to thermal parameters
- Modify the COBRA-SFS code to allow easier user control of model parameters in time.

This page is intentionally left blank.

10. REFERENCES

EPRI. 2014. *High Burnup Dry Storage Cask Research and Development Project – Final Test Plan*. Contract No. DE-NE-0000593, Electric Power Research Institute, Palo Alto, California.

EPRI. 2019. *High Burnup Demo Data. Initial Report – Decon Bay – 11-15-2017 to 11-29-2017*. https://www.epri.com/#/portfolio/2020/research_areas/2/061149?lang=en-US.

FAA. 2017. Order JO 6560.20C, *Sitting Order for Automated Weather Observing Systems*. Retrieved from https://www.faa.gov/documentLibrary/media/Order/6560_20c_ord.pdf.

Fort, JA, DJ Richmond, JM Cuta and SR Suffield. 2019. *Thermal Modeling of the TN-32B Cask for the High Burnup Spent Fuel Data Project*. PNNL-28915, Pacific Northwest National Laboratory, Richland, Washington.

Gauld IC, SM Bowman, and JE Horwedel. 2009. *ORIGEN-ARP: Automatic Rapid Processing for Spent Fuel Depletion, Decay, and Source Term Analysis*. ORNL/TM-2005/39, Oak Ridge National Laboratory, Oak Ridge, Tennessee.

Incropera FP and DP DeWitt. 2002. *Introduction to Heat Transfer*. 4th edition. John Wiley and Sons, New York, New York.

Michener TE, DR Rector, JM Cuta, and HE Adkins, Jr. 2017. *COBRA-SFS: A Thermal-Hydraulic Code for Spent Fuel Storage and Transportation asks, Cycle 4a*. PNNL-24841, Pacific Northwest National Laboratory, Richland, Washington.

NOAA. 2019. Climate Data Online: Dataset Discovery. National Centers for Environmental Information, National Oceanic and Atmospheric Administration. https://www.ncdc.noaa.gov/cdo-web/datasets. Accessed August 13, 2019.

Siemens, PLM. 2019. STAR-CCM+ 14.02 (computer software). Siemens Product Lifecycle Management Software, Inc., Plano, Texas.

UFSAR TN-32. 2012. "Updated Final Safety Analysis Report." Rev. 5, Transnuclear, Inc., Columbia, Maryland.

Waldrop, KP, WA Brookmire, RL Ridder, DD Tomlinson, BJ Vitello, TM Perrone, D MCGEE 2019. *High Burnup Spent Fuel Dry Storage Research Project*. TopFuel Proceedings 2019, Seattle, WA.